THE UNIVERSITY
of EDINBURGH

THE ROLE OF GPR56 IN MAMMALIAN HEMATOPOIESIS

Antonio Maglitto

College of Medicine and Veterinary Medicine

Centre for Inflammation Research

The University of Edinburgh

Doctor of Philosophy

January 2021

The journey is never over. Only travellers come to an end. But even then, they can prolong their voyage in their memories, in recollections, in stories. The end of one journey is simply the start of another. You have to see what you missed the first time, see again what you already saw, see in springtime what you saw in summer, in daylight what you saw at night, see the sun shining where you saw the rain falling, see the crops growing, the fruit ripen, the stone which has moved, the shadow that was not there before. You have to start the journey anew. Always. The traveller sets out once more.

José Saramago

Ever Tried. Ever Failed. No matter. Try again. Fail again. Fail better.

Samuel Beckett

DECLARATION

I declare that this thesis is the result of my own work, it has been written by myself and has not been submitted for any previous degree. The experimental work is almost entirely my own work; the collaborative contributions have been indicated clearly and acknowledged. Due references have been provided on all supporting literatures and resources. This thesis has not been previously submitted, in part or whole, to any university of institution for any degree, diploma, or other qualification.

Signed:

Antonio Maglitto, BSc, MSc

Edinburgh

Date: 30th July 2020

LAY SUMMARY

Blood cells are responsible for many primary functions in the human body, such as fighting external pathogens (white cells) and providing oxygen to tissues (red cells). Constant supplies of blood cells are ensured by blood (hematopoietic) stem cells (HSCs), which are present in the bone marrow during adult life. When required, these HSCs undergo serial divisions to become all mature blood cells.

Sometimes, HSCs are subjected to uncontrolled divisions that change their behaviour and generate blood cancer cells. Unfortunately, current therapies cannot eliminate blood cancer cells. One approach to restore a normal blood system is to replace patient cancer cells with new healthy HSCs that have been generated in the laboratory. This can be achieved only if we understand more about healthy HSCs, such as how and where they are generated. HSCs are made by continuous changes in specific cells during the embryonic stage of development. During this stage, we discovered an important protein, Gpr56, that is required for HSC generation. However, the reasons why Gpr56 is important for HSCs remains unknown.

To understand the role of Gpr56 in HSC development, we investigated what happens to HSC behaviour when the quantity of Gpr56 is altered. When the amount of Gpr56 is increased, we found that more HSCs were generated, whilst in the absence of Gpr56, we found that HSCs preferentially differentiate into white blood cells. We discovered that another similar protein, Gpr97 appears to compensate for the lack of Gpr56. When both proteins are absent, fewer HSCs are generated.

In summary, this thesis demonstrates that Gpr56 is a key protein in HSC development and can be replaced by the very similar Gpr97 protein. Further work to advance understanding of its mechanistic role is warranted and may provide useful insights in the quest to regulate the production of HSCs in normal health and cancer.

ABSTRACT

Haematopoietic stem cells (HSCs) can differentiate into all blood cell types, making HSC transplantation a promising treatment for many blood-related disorders. Allogenic heathy HSCs can be transplanted into patients, although this approach is limited by availability and compatibility of the donor. Moreover, there are no protocols available to generate transplantable HSCs from pluripotent stem cells (PSC), or expand HSCs *ex vivo*, as the molecules involved in HSC ontogeny remain poorly understood. Embryonically, HSCs derive from a subset of aortic endothelial cells that undergo endothelial-to-hematopoietic transition to become HSCs. During this dynamic process, *Gpr56* is the most upregulated receptor in emerging HSCs. The Gpr56 protein is a cell-surface receptor that is likely involved in the regulation of HSC function. However, its role in mammalian haematopoiesis remains unknown.

In this study, we examine the function of Gpr56 during *in vivo* and *in vitro* HSC development. To explore the effect of *Gpr56* loss-of-function, we characterize the functional role of mouse embryonic stem cell (ESC) derived hematopoietic stem and progenitor cells (HSPCs) and *in vivo* mouse HSCs that lack Gpr56. *Gpr56*-deficient HSPCs have a differentiation bias towards myeloid cells and the upregulation of another GPCR, Gpr97 appeared to compensate for Gpr56 deletion. The simultaneous deletion of *Gpr56* and *Gpr97* severely impaired the production of HSPCs, suggesting that both GPCRs are required *in vitro* for HSPC generation. Conversely, *Gpr56* overexpression during human *in vitro* PSC differentiation resulted in an important HSPC expansion. In summary, these data demonstrate that the lack of Gpr56 alters the HSPC differentiation output, while its overexpression enhances human *in vitro* HSPCs generation. This work represents the most comprehensive and current study of Gpr56 in mammalian haematopoiesis and these findings will improve novel strategies to generate *de novo* HSC and/or promote their *ex vivo* expansion.

ACKNOWLEDGEMENTS

I would like to thank my principal supervisor Prof. Elaine Dzierzak for allowing me to be part of this fantastic team inside and outside the lab. The last 4 years have been challenging and rewarding at the same time. Throughout my PhD, I learnt a lot and matured as a scientist and man. I am grateful to my co-supervisor Prof. Adriano Rossi. Thank you for your support and scientific advice. I would like to thank also all the Rossi Lab members to welcome me during their lab meetings. They have been really helpful in providing constructive suggestions. I would like to thank the members of my thesis committee, Prof. Chris Gregory, Prof. Katrin Ottersbach for their guidance and scientific discussions. I would like to express my gratitude to Prof. Lesley Forrester and Prof. Marella de Bruijn for committing their time to examine this thesis. I want to thank our collaborator Forrester Lab for providing part of the reagents and technical advice on how to engineer the cell line and Dr. Emma de Pater for performing *in vivo* zebrafish experiments. I warmly thank Dr. Samanta Mariani for performing the *in vivo* experiments of the project and for her valuable scientific and human help during tough times. Thanks to the present and past lab people in the Dzierzak lab, Chris, Carmen, Eoghan, Fokion, Zhuan, Mari-Liis, Xabi and Roger. I enjoyed sharing my time working with you and having fun all together outside the lab. Thanks for your smiles, your vibes, your help, your support. I hope you guys receive from me more than you gave. I would like to thank all the QMRI people, especially those working at the Flow Facility, Shonna, Mari, and Will for their precious help. Last but not least, a special thanks to Gemma to be by my side and supporting me during this difficult and unprecedented time. Grazie.

Antonio

CONTENTS

1 INTRODUCTION 1

1.1 THE DISCOVERY OF HAEMATOPOIETIC STEM CELLS 1

1.1.1 HEMATOPOIETIC HIERARCHY AND HETEROGENEITY 2

1.2 HEMATOPOIESIS DURING EMBRYONIC DEVELOPMENT 5

1.2.1 EARLY EMBRYONIC HEMATOPOIESIS 5

1.2.2 THE ONSET OF MOUSE HSC DEVELOPMENT 7

1.2.3 TRANSCRIPTION FACTORS INVOLVED IN HEMATOPOIESIS 10

1.2.4 GATA2 ROLE IN HSC GENERATION 11

1.3 THE LONG ROAD TO HSC *DE NOVO* GENERATION 14

1.3.1 GENERATION OF HPCS FROM ESC DIFFERENTIATION 14

1.3.2 REPROGRAMMING PSC AND DIFFERENTIATED CELLS USING TFS 16

1.3.3 DIRECT REPROGRAMMING OF DIFFERENTIATED CELLS 17

1.4 GPR56 IS A NOVEL REGULATOR OF HSC GENERATION 18

1.4.1 GPR56 STRUCTURE AND MOLECULAR FEATURES 19

1.4.2 BIOLOGICAL FUNCTIONS OF GPR56 23

1.4.3 THE RELEVANCE OF GPR56 IN LEUKAEMIA 24

1.4.4 OTHER GPCRS INVOLVED IN HAEMATOPOIESIS 26

1.5 HYPOTHESIS 28

1.6 AIMS 28

2 MATERIALS AND METHODS 29

2.1 MICE AND EMBRYO PRODUCTION 29

2.2 FLOW CYTOMETRY 29

2.3 HEMATOPOIETIC ASSAYS 30

2.4 MOLECULAR ANALYSES 30

2.5 MOUSE ES CELL MAINTENANCE AND DIFFERENTIATION 33

2.6 HUMAN SFCI55 MAINTENANCE AND DIFFERENTIATION 34

2.7 ZEBRAFISH EMBRYOS 35

2.8 MORPHOLINO AND MRNA INJECTIONS 36

2.9 STATISTICAL ANALYSIS 36

3 UNEXPECTED REDUNDANCIES OF GPR56 AND GPR97 DURING HEMATOPOIETIC CELL DEVELOPMENT AND DIFFERENTIATION 39

3.1 INTRODUCTION 39
3.2 RESULTS 42
3.2.1 PHENOTYPIC YOLK SAC HPCS ARE REDUCED IN GPR56 CONDITIONALLY DELETED EMBRYOS 42
3.2.2 HPC AND HSC FUNCTION IS LARGELY UNAFFECTED IN E13.5 *GPR56* CKO FETAL LIVER 45
3.2.3 CLONAL *IN VIVO* TRANSPLANTATION REVEALS A ROLE FOR GPR56 IN SELF-RENEWAL AND MAINTAINING BALANCED AND LYMPHOID-BIASED FETAL LIVER HSCS 51

4 GPR56 IS EXPRESSED IN ESC-DERIVED HEMATOPOIETIC PROGENITOR CELLS 59

4.1.1 *GPR56* KNOCKOUT AFFECTS HEMATOPOIETIC OUTPUT DURING ESC DIFFERENTIATION 63
4.1.2 GPR97 EXPRESSION IS UPREGULATED *IN VITRO* AND *IN VIVO* IN THE ABSENCE OF GPR56 69
4.1.3 SIMULTANEOUS DELETION OF BOTH GPR56 AND GPR97 SEVERELY REDUCES ESC-DERIVED HEMATOPOIESIS 73
4.2 DISCUSSION 77
4.2.1 GPR56 DELETION PROVIDES NEW INSIGHTS INTO THE REGULATION OF MAMMALIAN HEMATOPOIESIS 77
4.2.2 GPR97 INFLUENCES HEMATOPOIETIC DEVELOPMENT IN THE ABSENCE OF GPR56 78
4.2.3 POSITIVE ROLE OF GPR97 OR NEGATIVE ROLE OF GPR56 FOR MYELOID BIAS? 79

5 THE ROLE OF GPR56 GAIN OF FUNCTION IN HUMAN HEMATOPOIESIS 81

5.1 INTRODUCTION 81
5.2 ESTABLISHMENT OF AN INDUCIBLE HUMAN *GPR56* IPSC LINE 83
5.2.1 GENERATION OF THE *HGPR56* REPORTER CASSETTES 83
5.2.2 TARGETING A HUMAN IPSC LINE WITH AN INDUCIBLE *HGPR56* VECTOR 91
5.2.3 FUNCTIONAL ROLE OF GPR56 OVEREXPRESSION IN IPSC-DERIVED HPCS 107
5.3 DISCUSSION 112

6 DISCUSSION AND FUTURE DIRECTIONS 115

6.1 GPR97 AS PUTATIVE RECEPTOR THAT FUNCTIONALLY COMPENSATES FOR GPR56 DELETION 115
6.2 TO UNDERSTAND THE MOLECULAR MECHANISM THAT REGULATES THE INTERPLAY BETWEEN GPR56 AND GPR97 116

6.3 TO STUDY THE REDUCTION OF SELF-RENEWAL IN GPR56$^{-/-}$ HSCS 117
6.4 TO DETERMINE THE SIGNALLING PATHWAYS REGULATED BY GPR56 118
6.5 GPR56 *GAIN-OF-FUNCTION* ENHANCES THE GENERATION OF HPCS 119
6.6 TO CHARACTERIZE THE BIOLOGY OF GPR56-ACTIVATED HPCS 121

7 CONCLUSION 123

8 REFERENCES 125

9 APPENDICES 137

9.1 APPENDIX A 137
9.2 APPENDIX B 138
9.3 APPENDIX C 139
9.4 APPENDIX D 140

LIST OF PUBLICATIONS

Maglitto A., Mariani S.A., Vink C.S., de Pater E., Rodiguez-Seoane C., Paio X., Lukke, M.L., Dzierzak E. *Unexpected redundancy of Gpr56 and Gpr97 during hematopoietic cell development and differentiation* Accepted for publication in Blood Advances

Vink, C. S., Calero-Nieto F. J., Wang X., **Maglitto A.**, Mariani S. A., Jawaid W., Gottgens B.and Dzierzak E. (2020). "*Iterative Single-Cell Analyses Define the Transcriptome of the First Functional Hematopoietic Stem Cells.*" Cell Reports 31(6): 107627.

Porcheri, C., Golan O., Calero-Nieto F. J., Thambyrajah R., Ruiz-Herguido C., Wang X., Catto F., Guillen Y., Sinha R., Gonzalez J., Kinston S. J., Mariani S. A., **Maglitto A.**, Vink C. S., Dzierzak E., Charbord P., Gottgens B., Espinosa L., Sprinzak D. and Bigas A. (2020). "*Notch ligand Dll4 impairs cell recruitment to aortic clusters and limits blood stem cell generation.*" EMBO J 39(8): e104270.

Kauts ML, De Leo B, Rodríguez-Seoane C, Ronn R, Glykofrydis F, **Maglitto A**, Kaimakis P, Basi M, Taylor H, Forrester L, Wilkinson AC, Göttgens B, Saunders P, Dzierzak E. *Rapid Mast Cell Generation from Gata2 Reporter Pluripotent Stem Cells.* Stem Cell Reports. 2018 Oct 9;11(4):1009-1020.

LIST OF TABLES

TABLE 2.1 ANTIBODIES 37

TABLE 2.2 PRIMER LIST 38

LIST OF FIGURES

FIGURE 1.1 REPRESENTATION OF THE CLASSIC HEMATOPOIETIC HIERARCHY 4

FIGURE 1.2 HEMATOPOIESIS IN THE MOUSE EMBRYO 9

FIGURE 1.3 GPR56 PROTEIN STRUCTURE AND MECHANISM OF ACTIVATION 21

FIGURE 3.1 GPR56 IS DOWN-REGULATED IN *VECCRE:LOXGPR56* YS-DERIVED HPS..... 43

FIGURE 3.2 GPR56 DEFICIENCY AFFECTS EARLY HEMATOPOIETIC DEVELOPMENT IN *VEC-CRE* MOUSE EMBRYOS. 44

FIGURE 3.3 FUNCTIONAL ANALYSES OF *VAV-CRE* FL *GPR56* CKO LSK-SLAM POPULATION 46

FIGURE 3.4 ASSESSMENT OF REPOPULATION ACTIVITY OF TRANSPLANTED FL-LSK SLAM POPULATION IN RECIPIENT PB. 48

FIGURE 3.5 REPOPULATION ACTIVITY OF TRANSPLANTED FL-LSK SLAM POPULATION IN OTHER ORGANS. 49

FIGURE 3.6 REPOPULATION ACTIVITY OF TRANSPLANTED FL-LSK SLAM POPULATION IN OTHER ORGANS. 50

FIGURE 3.7 FLOW CYTOMETRY STRATEGY TO ASSESS THE ENGRAFTMENT POTENTIAL OF CLONAL TRANSPLANTED FL LSK-SLAM DONOR CELLS. 53

FIGURE 3.8 ENGRAFTMENT POTENTIAL OF GPR56 CKO *VAV-CRE* CLONAL FL-LSK-SLAM DONOR-CELLS. 54

FIGURE 3.9 REPOPULATION ACTIVITY OF CLONAL TRANSPLANTED FL-LSK SLAM POPULATION IN DIFFERENT ORGANS. 55

FIGURE 3.10 REPOPULATION ACTIVITY OF CLONAL TRANSPLANTED FL-LSK SLAM POPULATION IN DIFFERENT ORGANS. 56

FIGURE 3.11 BLOOD LINEAGE ANALYSES OF GPR56 CKO FL-HSCS..... 57

FIGURE 4.1 GPR56 IS EXPRESSED DURING ESC HEMATOPOIETIC DIFFERENTIATION. 62

FIGURE 4.2 *GPR56* GENE AND ISOFORMS AS TAKEN FROM ENSEMBL GENOME BROWSER. 65

FIGURE 4.3 GENERATION OF *GPR56*-DELETED G2V ESCS 66

FIGURE 4.4 OUTPUT OF GPR56-KO DERIVED HEMATOPOIETIC AND PROGENITOR CELLS IN THE PRIMITIVE WAVE (DAY 6) OF *IN VITRO* HEMATOPOIESIS. 67

FIGURE 4.5 DAY 10 ESC-DERIVED HEMATOPOIETIC CELL PRODUCTION AND PROGENITOR OUTPUT IN THE ABSENCE OF GPR56. 68

FIGURE 4.6 *IN VIVO* EXPERIMENTS TO ASSESS GPR97 REDUNDANT FUNCTION IN ZEBRAFISH 71

FIGURE 4.7 *GPR97* UPREGULATION IN MOUSE ESCS AND EMBRYONIC TISSUES 72

FIGURE 4.8 GENERATION OF *GPR56:GPR97* DOUBLE DELETED *G2V* ESCS. 74

FIGURE 4.9 *IN VITRO* FUNCTIONAL ANALYSES OF $G2V.56^{KO}97^{KO}$ ESCS 75

FIGURE 4.10 DECREASED PRODUCTION OF HPCS IN THE ABSENCE OF *GPR56* AND *GPR97* 76

FIGURE 5.1 GENERATION OF THREE *MCHERRY-GPR56* CASSETTES. 86

FIGURE 5.2 VALIDATION OF THE *MCHERRY-P2A-HIS-HGPR56* CASSETTE. 89

FIGURE 5.3 GPR56 IS PROPERLY EXPRESSED IN THE CELL MEMBRANE. 90

FIGURE 5.4 SCHEMATIC ILLUSTRATION OF THE *TET-ON* INDUCIBLE SYSTEM. 93

FIGURE 5.5 SCHEME OF THE *ALL-IN-ONE-TET-ON* DONOR VECTORS. 93

FIGURE 5.6 PREPARATION OF THE DONOR VECTOR AND AMPLICONS. 98

FIGURE 5.7 SCREENING OF *AAVS1-TET-ON-HGPR56/HIS/CA* TRANSFORMED BACTERIA. 99

FIGURE 5.8 DIRECTIONALLY SCREENING TO ESTABLISH THE CORRECT CASSETTE'S ORIENTATION. 100

FIGURE 5.9 WORKFLOW TO ESTABLISH THE *I55GPR56CA* IPSC LINE. 103

FIGURE 5.10 SCREENING OF VIABLE SFCI55-AFTER NEOMYCIN SELECTION 104

FIGURE 5.11 ASSESSMENT OF SUCCESSFUL *TET-ON-AAVS1-HGPR56CA* TARGETING. .. 105

FIGURE 5.12 EVALUATION OF *HGPR56* TRANSCRIPT'S EXPRESSION WITHIN THE *MCHERRY* POPULATIONS. 106

FIGURE 5.13 *IN VITRO* FUNCTIONAL ANALYSIS OF *I55GPR56CA* LINE. 109

FIGURE 5.14 *IN VITRO* DOX-DERIVED HPCS ARISE FROM A NON MCHERRY-REPORTER EXPRESSING I*55GPR56CA* SUBFRACTION. 111

LIST OF ABBREVIATIONS AND ACRONYMS

3-a-DOG	3-a-acetoxydihyl-drodeoxygedunin	**iPSC**	induced pluripotent stem cell
7TM	7 transmembrane domain	**IT**	intermediate
AAVS1	adeno associated virus site 1	**KD**	knock down
AGM	aorta gonad mesonephros	**KO**	knock out
aGPCR	adhesion G-protein coupled receptor	**LDA**	limiting diluting assay
AML	acute myeoid leukemia	**LSC**	leukemic stem cell
ATAC	assay for transposase-accessible chromatin	**LT**	long term
BFPP	bilateral frontoparietal polymicroglia	**MEF**	mouse embryonic fibroblast
BM	bone marrow	**MO**	morpholino oligomer
BMP	bone morphogenic protein	**MPP**	multipotent progenitor
CCR5	chemokine receptor type 5	**NFAT**	nuclear factor of activated T-cells
CFU-C	colony forming unit in culture	**NPC**	neural progenitor cell
CFU-S	colony forming unit in spleen	**NTF**	n-terminus fragment
cKO	conditional konck out	**OPC**	oligodendrocyte cell
CLP	common lymphoid progenitor	**ORF**	open reading frame
CMP	common myeloid progenitor	**p2a**	2A peptide
Col3a	collagen IIIA	**PCR**	polymerase chain reaction
CR	complete remission	**PMN**	polymorpho nuclear cells
CTF	c-terminus fragment	**RE**	restriction enzyme
DBS	double strand break	**RT-qPCR**	quantitative reverse transcription pcr
DEG	differentially expressed gene	**rtTA**	reverse tetracycline transactivator
Dox	doxycycline	**SCF**	stem cell factor
E	day	**SP**	signal peptide
E.coli	escherichia coli	**SRE**	serum responsive element
EB	embryoid body	**SRF**	serum responsive factor
EC	endothelial cell	**ST**	short term
ECD	extracellular domain	**Tet**	tetracycline
EHT	endotelial-to-hematopoietic transition	**TetA**	tetracycline resistant gene
EI	embryoid body induction	**TetO**	tetracycline operator
EMP	erythroid myeloid progenitor	**TetR**	tetracycline repressor
EPO	erythropoietin	**TF**	transcription factor
ER	endoplasmic reticulum	**TG2**	transglutaminase2
ESC	embryonic stem cell	**TPO**	thrombopoietin
EV	empty vector	**TRE**	tetracycline responsive element
FACS	fluorescence-activated cell sorting	**UT**	untransfected
FBS	foetal bovine serum	**VEC**	vascular endothelial cadherin
FL	foetal liver	**VEGF**	vascular endothelial growth factor
Flk1	foetal liver kinase	**WT**	wild type
G2V	gata2venus	**YS**	yolk sac
GAIN	GPCR autoproteolysis inducing domain	**ZFN**	zinc finger nucleases
GDP	guanosine diphosphate		
GFP	green fluorescent protein		
GOI	gene of interest		
GPCR	G-protein coupled receptor		
GTP	guanosine triphosphate		
GVHD	graft-versus-host disease		
HA	homology arms		
HDR	homology directed repair		
HE	hemogenic endothelium		
HEC	hemogenic endothelial cell		
his	histidine		
HLA	human leukocyte antigen		
HM	hematopoietic maturation		
HPC	hematopoietic progenitors		
hPSC	human pluripotent stem cell		
HR	homology recombination		
HS	hematopoietic specification		
HS/PC	hematopoietic stem and progenitor cell		
HSC	hematopoietic stem cells		
IAHC	intra aortic hematopoietic cluster		
ICD	intra cellular domain		
IL-3	interleukin-3		
IL-6	interleukin-6		

1 INTRODUCTION

1.1 The discovery of haematopoietic stem cells

The discovery of hematopoietic stem cells (HSCs) occurred with the unfortunate advent of atomic weapons during the second world war. In the first half of the 20th century the scientific community focused its interest on how to protect normal tissues from damages caused by ionizing radiation, attesting that the bone marrow (BM) is one of the most radio sensitive tissues. In mice, scientists found that the injection of whole normal adult bone marrow was able to protect lethally irradiated recipients. Surprisingly, the recipient mice entirely restored a healthy hematopoietic system, suggesting the existence of multipotent cells within the BM cell population: the HSCs.

The unknown entity of these cells prompted scientists to seek HSCs and characterize their biological features (Jacobson, Simmons et al. 1951, Lorenz, Uphoff et al. 1951, Ford, Hamerton et al. 1956). The first step was to quantitatively characterize HSCs. This aim was addressed performing a limiting diluting transplantation assay (LDA) (McCulloch and Till 1960). This experimental assay estimated the frequency of HSCs in the BM by defining the minimal number of BM cells that repopulate the hosts. The experiments demonstrated that in the adult BM the HSCs are rare. Interestingly, 10 days after the BM transplantation into myeloablated mice, some macroscopic cell "clusters" appeared on the surface of the host spleens. These cell formations are called spleen colony-forming units (CFU-S) and their number was directly related to the number of transplanted HSCs (Till and Mc 1961). In addition, cytological analyses on

CFU-S composition revealed novel HSC qualitative features. Each CFU-S cluster consisted of a mixture of lymphoid and myeloid hematopoietic differentiated cells, which derived from a single parental clone (Wu, Till et al. 1967). Notably, this ability was maintained after serial transplantations, indicating the so called "self-renewal" capacity.

These milestone experiments established two HSC fundamental features: differentiation and self-renewal capacities. That means that, when serially transplanted into recipients, these rare HSCs hold the potential to clonally differentiate in all the mature blood cell types while preserving their initial pool. These observations structured the hematopoiesis as a stepwise process where few multipotent cells differentiate unidirectionally towards all mature blood cells.

1.1.1 Hematopoietic hierarchy and heterogeneity

The presence of HSCs in the BM prompted scientists to develop strategies to isolate HSCs and understand the relation with the hematopoietic progeny. Using a combination of cell surface markers, pioneer studies employed fluorescent activated cell sorting (FACS) to purify HSCs and their progeny (Spangrude, Heimfeld et al. 1988, Ikuta, Kina et al. 1990, Ikuta and Weissman 1992, Morrison, Wandycz et al. 1997). Based on the cell surface markers and *in vivo* functional assays, the HSCs can be divided into long term (LT) and short term (ST) HSCs. LT-HSCs possess a permanent reconstitution capacity (> 3-4 months), while ST-HSCs repopulate the recipients for 8-12 weeks only (Morrison, Wandycz et al. 1997). These ST-HSCs differentiate into multipotent progenitors (MPPs), with reduced self-renewal ability (Yang, Bryder et al. 2005) and can further differentiate into common myeloid (CMPs) and common lymphoid progenitors (CLPs). CMPs have myeloid restricted potential and generate erythrocytes, megakaryocytes and granulocytes-macrophage cells. Conversely, the CLP progenitors have the capacity to generate all the lymphoid mature cells. To describe the connection between HSCs and their progeny, the Weissman group established the classical tree-like branch hematopoietic hierarchical model (Morrison, Uchida et al. 1995, Kondo, Weissman et al. 1997, Morrison, Wandycz et al. 1997, Akashi, Traver et al. 2000, Manz, Miyamoto et al. 2002) (**Figure 1.1**). According to this model, HSCs sit on top of hematopoietic hierarchy and

differentiate first to multipotent progenitors (MPPs), then towards single lineage restricted progenitors (unipotent) and finally, to terminally differentiated mature blood cells.

Although the surface markers define HSCs as a homogenous population, *in vivo* functional analyses revealed that they are heterogeneous. LDA and clonal transplantation assays attested the existence of myeloid-biased, lymphoid-biased and balanced BM HSCs (Muller-Sieburg, Cho et al. 2002, Dykstra, Kent et al. 2007). Using similar approaches, other groups identified platelets-biased HSCs (Sanjuan-Pla, Macaulay et al. 2013) and intermediate (IT) HSCs (Benveniste, Frelin et al. 2010, Yamamoto, Morita et al. 2013). The advent of single cell omics and lineage tracing approaches confirmed the presence of heterogenous BM HSCs with distinct features. The Jacobsen laboratory found platelet-biased HSCs that co-express cKit and the platelet/megakaryocyte marker von Willebrand Factor (vWF+) (Carrelha, Meng et al. 2018). These HSCs can exclusively replenish megakaryocytes-platelets without differentiating into hematopoietic intermediates. In another study, Crisan and colleagues demonstrated the presence of two genetically distinct subpopulations of BM-HSCs that respond differently to BMP signalling: HSC BMP-activated and non-BMP activated, (Crisan, Kartalaei et al. 2015). The concept of heterogeneity can be extended also to the MPPs. MPPs derive from HSCs and are a heterogeneous population that consist of MPP1, MPP2, MPP3 and MPP4 (Pietras, Reynaud et al. 2015). The subpopulations differ for transcriptomic profile, cell cycle activity and abundance in the bone marrow (Wilson, Laurenti et al. 2008). MPP1s have molecular features closely associated with ST-HSCs, whereas MPP4s is primed to segregate into downstream progenitors (Pietras, Reynaud et al. 2015). However, the biological mechanisms by which a single HSC differentiates into MPPs is still under investigation.

The origin of HSC heterogeneity is likely to be found at embryonic level (reviewed in (Crisan and Dzierzak 2016). During embryonic development there are several intrinsic and extrinsic factors that contribute to the onset of definitive HSCs. A better knowledge of those molecular signals will be crucial to develop new protocols for *in vitro* generation of *bona-fide* HSCs to be used as therapy for blood-related diseases.

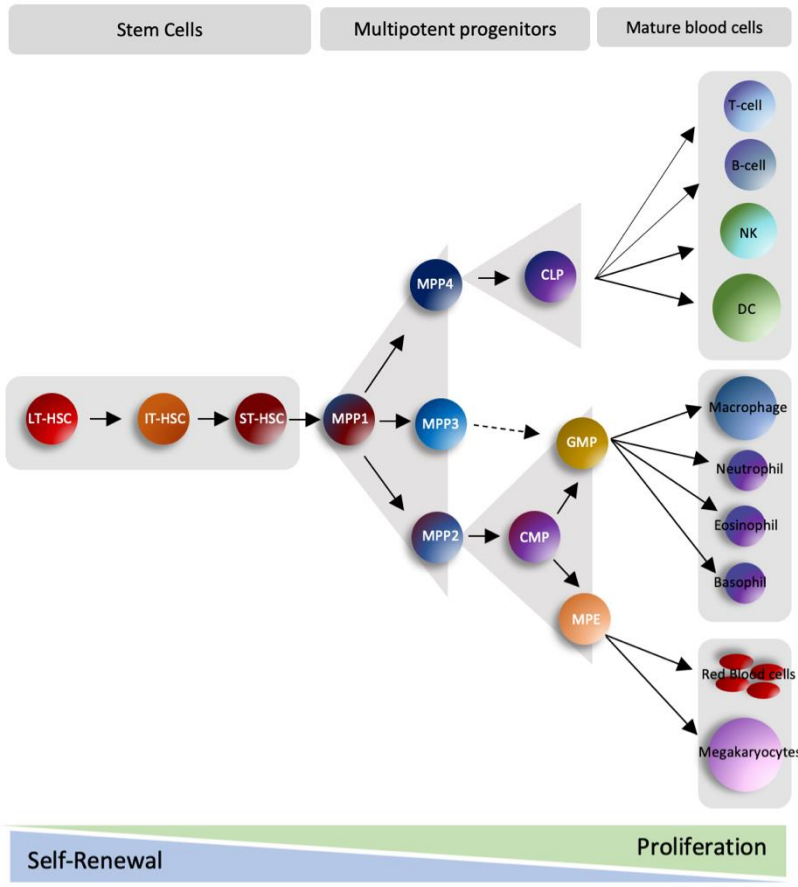

Figure 1.1 Representation of the classic hematopoietic hierarchy

Hematopoietic stem cells (HSCs) reside on top of the hematopoietic hierarchy. They retain the capacity to self-renew and differentiate into committed progenitors which generate fully matured blood cells. Along their differentiation, HSCs gradually lose their self-renewal capacity, whereas their progeny acquire proliferation capacity. Figure adapted from [Bryder et al, 2006] copyright permission, Elsevier.

1.2 Hematopoiesis during embryonic development

1.2.1 Early embryonic hematopoiesis

Adult HSCs reside in the bone marrow (BM) surrounded by different cell types that provide a supportive environment to maintain HSCs throughout adult life. These definitive adult repopulating HSCs take their origins during embryonic development. The first developmental studies to investigate the embryonic origin of blood cells were performed on chickens. The concomitant appearance of primitive blood cells and vascular cells in the same embryonic compartment raised the idea that hematopoietic cells originate embryonically from a common mesodermal precursor: the hemangioblast (reviewed by (Choi 1998).

In the second half of the 60s, Moore and Owen conducted elegant experiments in avian and mouse embryos to study the origin of blood cells. The experiments performed in mouse embryos demonstrated that the yolk sac (YS) contained hematopoietic precursors capable to colonise the spleen and the bone marrow of lethally irradiated hosts (Moore and Owen 1965, Moore and Owen 1967, Moore and Metcalf 1970). These studies set the first paradigm that hematopoiesis and the generation of HSCs initiate in the YS during the embryonic development. It was in 1975 when a French scientist, Dieterlen-Lièvre, made an important shift in the dogma. The generation of YS chimeras in an experimental avian embryo model and the ability to morphologically discriminate chicken from quail embryonic cells allowed Dieterlen-Lièvre to demonstrate for the first time that HSCs originate from the embryo body and not from an external embryonic compartment such as the YS (Dieterlen-Lievre 1975). The impact of her pioneering work prompted the scientific community to re-consider the spatiotemporal origin of embryonic haematopoiesis and ask whether the same developmental process might be conserved in other vertebrates and particularly in mammalian vertebrates (mouse and human).

Mammalian hematopoiesis takes place in different embryonic compartments of the conceptus following distinct spatial and temporal events (Dzierzak and Speck 2008). Similar to chicken embryos, in mice, blood cells originate in the YS from a

mesodermal-derived group of cells defined as “hemangioblast” (Murray 1932). At day (E)7 of mouse embryonic development, these cells migrate from the primitive streak to the YS where they differentiate into endothelial cells (ECs) and blood islands. The blood islands are clusters or primitive erythroblasts surrounded by endothelial cells, which establish the YS vasculature (Ferkowicz and Yoder 2005, Ueno and Weissman 2006). The embryonic morphological and molecular similarities between endothelial and primitive hematopoietic cells postulated the idea of the hemangioblast as a common bipotent ancestor. This bipotent cell shares the expression of common surface mesodermal receptors: *brachyury* and the *foetal liver kinase 1* (Flk1). Lack of Flk1 resulted in embryonic lethality and impaired production of mesodermal intermediates and blood islands (Yamaguchi, Dumont et al. 1993).

The first wave of hematopoiesis initiates in the YS between E7 and E8.5 of murine embryonic development (**Figure 1.2**) (Dzierzak and Speck 2008). During this first wave of *de novo* hematopoiesis, “primitive” erythrocytes and myeloid progenitors (macrophages and megakaryocytes) are produced prior the establishment of the circulation, which occurs around E8.25-8.5 (McGrath, Koniski et al. 2003). Primitive erythrocytes are nucleated and express an embryonically distinct (βH1) globin (Palis, Robertson et al. 1999), YS-derived macrophages are thought to mature directly from the blood islands (Manwani and Bieker 2008). The end of the first wave overlaps with the beginning of the second one. This new wave takes place in the YS from E8.25 and it is characterized by *de novo* production of hematopoietic cells with multipotent myeloid and/or lymphoid potentials (Palis, Robertson et al. 1999, Dzierzak and Speck 2008). This second wave is often called “definitive” as it gives rise to more functionally competent progenitors that closely relate to adult blood cells. The most abundant haematopoietic progenitor population is represented by the erythroid-myeloid progenitors (EMPs), which are generated from E8.25 to E10 and express the *tyrosine receptor kinase* (cKit or CD117), CD41 and CD16/32 (McGrath, Frame et al. 2015) (**Figure 1.2**). Moreover, a rare population of B-cells (B1a) and T cell lymphoid progenitors with low multilineage repopulation activity arise just after the onset of EMPs (Yoshimoto, Porayette et al. 2012).

1.2.2 The onset of mouse HSC development

The third wave of hematopoietic generation is also known as definitive and begins with the generation of the first adult-repopulating HSCs, which represent the basis of the hematopoietic system throughout adult life. In mice, the first adult-type HSC arises at E10.5 from an intraembryonic region called aorta gonad mesonephros (AGM) (Medvinsky and Dzierzak 1996) (**Figure 1.2**). Cell tracing experiments performed in mouse embryos showed that HSCs directly originate from a subset of vascular endothelial cells (ECs) lining the ventral wall of the dorsal aorta. (Zovein, Hofmann et al. 2008). These ECs undergo a trans-differentiation process described as endothelial-to-hematopoietic cell transition (EHT) (Jaffredo, Bollerot et al. 2005, Kissa and Herbomel 2010). The EHT is a well conserved process that has been widely investigated in different organisms (Kissa and Herbomel 2010). During the transition, few cells bulge from the endothelium into the lumen of the aorta to form the intra-aortic hematopoietic cells that are found in clusters (IAHCs).

Three-dimensional imaging analysis of whole mouse embryo demonstrated that hematopoietic clusters can be detected in the major embryonic arteries (Yokomizo and Dzierzak 2010). In the embryonic aorta, the total number of IAHCs peaks at E10.5 (~600) among which only few HSCs are generated (Kumaravelu, Hook et al. 2002), whilst the rest are HPCs. Each IAHC is made of 2 to 20 cells that are defined to be cKit+CD31+SSEA1. Immunostaining assays performed on those cells revealed the presence of 3 different cell populations within the IAHCs. Flk1+ identified cells that reside in the basal region of the dorsal aorta, CD45+ defines the outer cells and CD41+ marks the cells that transit from Flk1+ to CD45+ (Yokomizo and Dzierzak 2010). These findings suggested that the IAHC cell composition is heterogeneous.

Recent studies reported that IAHC formation begins from cells with polyclonal origin and high-proliferative activity as result of a Notch-dependent two-step process (Batsivari, Rybtsov et al. 2017, Ganuza, Hall et al. 2017, Zape, Lizama et al. 2017, Porcheri, Golan et al. 2020). Studies suggest that the IAHCs can be considered as the intimate supporting niche of the nascent HSCs (Porcheri, Golan et al. 2020). Emerging blood cells mature within the clusters to lose the endothelial properties and begin to express a hematopoietic genetic programme. This maturation generates intermediates

that are primed to became HSCs. Explant studies on IAHCs reported that endothelial (VE-Cadherin+) CD43-CD41+CD45- and CD43+CD41^{low}CD45+ subpopulations can differentiate into mature HSCs *ex-vivo* after re-aggregated and matured with stromal cells (Taoudi, Gonneau et al. 2008). These subsets of cells are described as pre-HSC type I and type II respectively and reside within the endothelial and subendothelial layers. The dissociation and re-aggregation approach contributed to identify another primed hematopoietic precursor, pro-HSC that arises at E9.5 of mouse embryonic development (Rybtsov, Batsivari et al. 2014). According to these studies, the EHT is described as a step wise process whereby mature HSCs are generated from HECs through a progressive maturation of defined intermediates: pro-HSC, pre-HSC type I, pre-HSC type II (Taoudi, Gonneau et al. 2008, Rybtsov, Sobiesiak et al. 2011, Rybtsov, Batsivari et al. 2014).

Advances in time-lapse vital imaging and the establishment of a novel transgenic mouse model allowed researchers to follow the EHT in real time (Boisset, van Cappellen et al. 2010). Boisset and colleagues took advantage of transgenic embryos (*Ly6a-GFP*) where the green-fluorescent protein (*GFP*) is under the control of the *Ly-6A* (known also as *Sca1*) transcriptional elements (Ma, Robin et al. 2002). As *Sca1* is a marker of HSCs, all the embryonic and adult HSCs express the GFP reporter in transgenic mice (de Bruijn, Ma et al. 2002). The time lapse imaging of the EHT in mouse embryonic aorta showed very few HSCs bulging out from the ventral aortic CD31+GFP+ endothelial cells. The newly generated HSCs co-express CD31+cKIT+GFP+ markers and no emerging GFP+ cKit+ cells were observed before E10.5. The use of this mouse model contributed to the isolation of different cell intermediates to study the EHT and provided new insights on the transcriptional and molecular changes that occur in the HECs when committed to become functional HSCs.

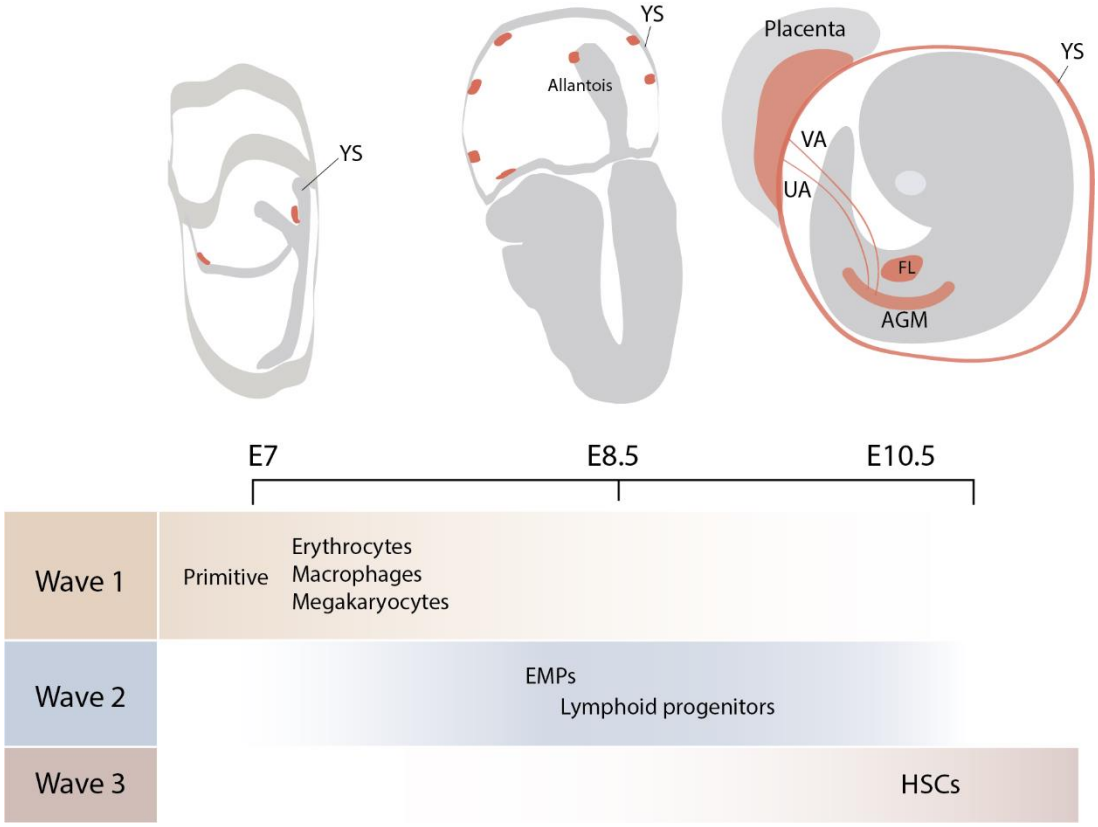

Figure 1.2 Hematopoiesis in the mouse embryo

The first blood cells are generated at E7 of mouse embryonic development from an extraembryonic compartment, the YS. This first wave of generation produces primitive erythrocytes, macrophages and megakaryocytes. At E8.5, the second wave generates erythroid-myeloid progenitors (EMPs) and hematopoietic progenitors with lymphoid potential. Hematopoietic stem cells (HSCs) are generated during the third wave at E10.5 in the embryonic compartment called AGM. HSCs are also generated in the vitelline (VA), umbilical (UA) arteries and placenta. Figure adapted from Kauts et al, 2018.

1.2.3 Transcription factors involved in hematopoiesis

The temporal and lineage-specific activation of hematopoietic programs is controlled by the cooperative effect of nuclear transcription factors. Transcription factors (TFs) are proteins that bind to DNA regulatory sequences to enable or repress the transcription of a group of genes. They recognise consensus DNA binding motifs that reside within the promoter region of downstream genes or distant genomic regions called enhancers. While some TFs are commonly expressed in all cell types to regulate the basal cellular activity, others are tissue-specific and are important in initiating the expression of pattern of genes that confer specific genetic programs. *Scl, Lyl1, Lmo2, Gata2, Runx1, Meis1, Pu.1, Erg, Fli-1 and Gfi1b* are conserved TFs that play pivotal roles in haematopoiesis (Wilson, Foster et al. 2010). Haploinsuffiencies or null mutations of these key hematopoietic TFs impair profoundly the function and the production of HSPCs, whereas genomic translocations are frequently associated with blood-related malignancies, particularly leukaemia and lymphomas (Shima and Kitabayashi 2011).

The role of each TF in haematopoiesis has been investigated using conditional and temporally inducible knock out (cKO) mouse models. This was necessary since the full knock out of TFs such as Scl, Runx1 and Gata2 have been shown to elicit hematopoietic defects and midgestation embryonic lethality (Tsai, Keller et al. 1994, Shivdasani, Mayer et al. 1995, Yokomizo, Hasegawa et al. 2008). These *in vivo* studies examined the contribution of the TFs at different stages of embryonic hematopoiesis. For instance, *Scl* functions at early stages of hematopoiesis. Embryos that lack of *Scl* resulted in early embryonic lethality due to the absence of YS primitive erythropoiesis and myelopoiesis (Robb, Lyons et al. 1995, Shivdasani, Mayer et al. 1995). Similarly, *Lmo2* is critical to the YS-derived erythropoiesis and does not contribute for definitive haematopoiesis (Warren, Colledge et al. 1994, Yamada, Warren et al. 1998). On the other hand, *Runx1* plays a critical role in definitive haematopoiesis (Cai, de Bruijn et al. 2000). *Runx1-/-* homozygous embryos are lethal at E12.5 accompanied by severe anaemia and haemorrhages (Okuda, van Deursen et al. 1996). The absence of *Runx1* in the endothelial cells impaired the generation of IAHCs in the embryonic arteries and no functional HSCs were produced in the AGM

(North, Gu et al. 1999, Cai, de Bruijn et al. 2000, Yokomizo, Ogawa et al. 2001, Chen, Yokomizo et al. 2009).

Nevertheless, it would be reductive to think that each different embryonic hematopoietic stage is regulated by a single TF. The acquisition of different hematopoietic genetic programs is the result of the combinatorial interaction between different TFs and co-factors. These interactions establish a variety of regulatory networks that define the cell identity in the hematopoietic system (Wilson, Calero-Nieto et al. 2011). The integration of chromatin immunoprecipitation (ChIP) assay with bioinformatic analyses demonstrated that 7 HSPC-associated "*heptad"* TFs (*Scl, Lyl1, Lmo2, Gata2, Runx1, Erg* and *Fli-1)* interact together to regulate HSPC specification (Wilson, Foster et al. 2010). Functional experiments performed in *Runx1+/-::Gata2+/-* heterozygous mouse embryos confirmed the *in vivo* synergy between *Runx1* and *Gata2,* as no double heterozygous were generated and the number CFU-Cs from FL of *Runx1+/-::Gata2+/-* embryos was reduced (Wilson, Foster et al. 2010).

1.2.4 Gata2 role in HSC generation

Functional studies have reported GATA TFs (*Gata 1-6*) as an important class of regulators in embryonic development (Bresnick, Lee et al. 2010). This family of zinc-finger TFs takes its name from the DNA consensus sequence that is able to bind (A/TGATAA/G). Although they share similar biochemical features, the different members exhibit distinct biological roles. *Gata 1-3* are mainly involved in hematopoiesis, whereas *Gata 4-6* are TFs associated with the embryonic development of endoderm and mesoderm derived organs such as heart and lung. *Gata1* is associated with erythroid, eosinophils and megakaryocytes development (Tsai, Martin et al. 1989), *Gata3* with T-lymphocytes and neurons (Lim, Lakshmanan et al. 2000) while *Gata2* is a master regulator of HSCs, multipotent hematopoietic progenitor and mast cell generation (Kobayashi-Osaki, Ohneda et al. 2005, Kauts, De Leo et al. 2018).

The requirement of *Gata2* for the embryonic hematopoiesis and the generation of the HSPCs was highlighted by *in vitro* and *in vivo* studies. *Gata2* homozygous deletion in the germline generates no viable mice (Tsai, Keller et al. 1994). Interestingly, no *Gata2-/-* embryos survived beyond E11.5 and 67% were found dead at E10.5

accompanied by severe anaemia. These findings supported the hypothesis that *Gata2* is critical for the onset of the embryonic HSCs and for the establishment of definitive hematopoiesis. Viable mutant *Gata2-/-* embryos collected at E9.5 showed no defect in YS endothelium, vitelline vasculature and foetal membranes (Tsai, Keller et al. 1994). Red blood cells generated from the primitive wave appeared normal although the total number in the YS was significantly reduced. The YS of *Gata2-/-* embryos appeared very pale and the embryos were affected from severe anaemia due to the impaired production of blood cells beyond primitive hematopoiesis. The generation of GATA-2 chimeras examined the role of Gata2 in hematopoiesis. *GATA2-/-* cells were unable to contribute to hematopoiesis in adult hematopoietic sites such as bone marrow, spleen and thymus (Tsai, Keller et al. 1994).

Further *in vivo* studies have tried to describe the temporal and spatial role of *Gata2* expression in embryonic hematopoiesis. Two different *Cre-LoxP* transgenic mouse models have been used to overcome the limitations of the non-viable germline *Gata2* KO embryos. The *Gata2-VEC* (vascular endothelial cadherin)-*Cre* conditional KO model (Chen, Yokomizo et al. 2009) has been used to study the effect of the lack of *Gata2* during the EHT (de Pater, Kaimakis et al. 2013) . In this mouse model, the *Cre* recombinase is under the control of the *Vec* promoter, whereas the *LoxP* sites flank *Gata2* genomic locus. The *VEC* promoter is activated in endothelial cells forming the major embryonic vasculature. Approximately 30% of endothelial cells deleted both *Gata2* alleles. *VEC-Cre:Gata2*$^{f/f}$ embryos are viable at E10.5-11 and survived until E14 despite suffering of foetal anaemia. *VEC-Cre:Gata2*$^{f/f}$ E10 and E11 whole mount immunostaining showed a decrease of the total number of the IAHC and the aortic cKit+ population. *In vitro* CFU-C assays of *VEC-Cre:Gata2*$^{f/f}$ AGM and FL derived HSPCs showed a profound reduction in the number of haematopoietic colonies. Similarly, transplantation of E11 HSCs isolated from *VEC-Cre:Gata2*$^{f/f}$ failed to repopulate lethally irradiated adult recipients. These experiments confirmed that *Gata2* is essential for the embryonic HSC generation.

The *VAV-Cre* transgenic mouse was adopted (Ogilvy, Metcalf et al. 1999, Stadtfeld and Graf 2005) to characterize the role of *Gata2* in HSCs after their generation (de Pater, Kaimakis et al. 2013) . In this model, the CRE recombinase is under the control of the *VAV* pan-hematopoietic cell promoter. As consequence, up to 70% of

hematopoietic cells, HPCs and the newly embryonically generated HSCs lack *Gata2*. Functional analyses highlighted the importance of *Gata2* for the HSC survival (de Pater, Kaimakis et al. 2013). Indeed, HSCs isolated from *VAV-Cre:Gata2$^{f/f}$* AGM and FL did not long-term reconstitute the hematopoietic system after transplantation in recipient mice. In addition, the number of CFU-C colonies derived from AGM *VAV-Cre:Gata2$^{f/f}$* HSPCs was decreased when compared to the wild type (de Pater, Kaimakis et al. 2013).

The generation of the *Gata2Venus* ES cell line and reporter mouse model have been crucial to isolate Gata2 expressing and non-expressing cells and examine their function and transcriptomic profile (Kaimakis, de Pater et al. 2016, Kauts, Rodriguez-Seoane et al. 2017). In this mouse model, the *Venus* fluorescent reporter labels the *Gata2* expressing cells without affecting the level and the function of *Gata2* TF. Immunostaining performed on *Gata2Venus* mouse AGM at E10.5-E11 showed that all the IAHCs are *Gata2* expressing (Kaimakis, de Pater et al. 2016). Of note, functional analyses performed on AGM-derived *Gata2* expressing cells demonstrated that all the HSCs and the majority of the HPCs are *Venus+* (Kaimakis, de Pater et al. 2016). Similarly, the majority of HSPCs derived *in vitro* from *Gata2Venus* mouse ES cells are Venus+ (Kauts, Rodriguez-Seoane et al. 2017).

Taken together, these experiments provided insights of Gata2 function during embryonic hematopoiesis. *Gata2* is a pivotal haematopoietic transcription factor that is essential for the EHT and HSC generation, and its expression is indispensable for HSCs survival and expansion in the foetal liver and bone marrow after their production. Moreover, the generation of *Gata2Venus* ES cells together with *Gata2Venus* mouse models have been advantageous tools to isolate and study HSCs and HPCs.

1.3 The long road to HSC *de novo* generation

The identification of hematopoietic lineage-specific TFs prompted the idea that would it be possible to *de novo* generate HSCs for therapeutic approaches. The current therapies to treat blood-related disorders rely on the allogenic transplantation of BM LT-HSCs. Sometimes, this approach is characterized by the graft-versus-host disease (GVHD), which is caused by the inaccurate matching of the donor human leukocyte antigen (HLA) with the host. The ideal alternative considers the patient autologous HSC transplantation. Nevertheless, this strategy has still important limitations such as the lack of robust protocols to enrich for HSCs and expand them *ex vivo* exponentially (Wilkinson, Ishida et al. 2019). Therefore, the derivation of human pluripotent stem cells (hPSCs) and the discovery of induced pluripotent stem cells (iPSCs) derived from somatic differentiated cells reprogrammed with pluripotency TFs (Takahashi and Yamanaka 2006) opened new alternative strategies to generate *in vitro* HSCs. These strategies consist of instructing hPSCs to differentiate toward HSC fate or reprogramming patient-derived differentiated cells with a panel of hematopoietic TFs to become HSCs (reviewed in (Vo and Daley 2015). Although different approaches have been adopted to achieve these goals, none of these methods successfully produced adult transplantable HSCs. Nonetheless, it is noteworthy to highlight the great achievements have been made to improve each of these techniques to reach a step closer to make HSCs.

1.3.1 Generation of HPCs from ESC differentiation

The possibility to generate HSCs from human pluripotent stem cells was demonstrated with the injection of iPSC into immunocompromised mice (Amabile, Welner et al. 2013). CD34+CD45+ HSPC population was isolated from iPSC-derived teratoma and transplanted subcutaneously into recipient irradiated immunocompromised mice (Amabile, Welner et al. 2013, Suzuki, Yamazaki et al. 2013). Despite the demonstration that these teratoma-derived HSPCs retained only low engraftment potential, they were able to reconstitute the hematopoietic system after serial transplantations. This finding provided the first proof of concept of the possibility that human functional HSCs can be theoretically generated from hPSCs under defined conditions. Nevertheless, the direct injection of hPSCs into recipients to derive HSCs

remains an uncontrolled and stochastic events that causes tumor formation into the hosts (Vo and Daley 2015). A deep understanding on how haematopoiesis develops embryonically is crucial to recreate *in vitro* the molecular paths to instruct hPSCs to produce functional LT-HSCs. Several groups made considerable and important progresses on generating short-lived hematopoietic progenitors from hPSCs by attempting to recapitulate primitive and definitive haematopoiesis *in vitro*. However, the path to generate transplantable LT-HSCs from murine and human ESCs is profoundly complex as they require to undergo intermediate stages before becoming functional HSCs. A big challenge is represented by the existence of overlapping and heterogeneous cell populations that are technically difficult to isolate using only cell surface markers.

Different protocols have been adopted to generate *in vitro* HSPCs. These protocols exploited conditioned media supplemented with cytokines in the presence or absence of foetal bovine serum (FBS) (Ditadi, Sturgeon et al. 2015). The cytokines adopted in these media have the role to activate or inhibit pathways involved in embryonic haematopoiesis. The most advanced hPSC differentiation protocol enables the production of human primitive or definitive hematopoietic progenitors (Kennedy, Awong et al. 2012). In the first 72 hours of *in vitro* differentiation, hPSCs are primed into mesoderm before generating the hemangioblast intermediate (KDR+). This step is regulated by the balancing of the nodal-activin and Wnt-bcatenin pathways (Kennedy, D'Souza et al. 2007). The differential activation of these two pathways instructs the hemangioblast towards primitive (KDR+CD235a+) or definitive (KDR+CD235a-) haematopoiesis. Primitive haematopoiesis is mainly promoted by the activation of the nodal-activin pathway, whereas definitive haematopoiesis by the activation of Wnt-bcatenin (Wang and Nakayama 2009). Nevertheless, the path that follow the specification from the hemangioblast into hemogenic endothelium (HE) is widely unknown. Mouse studies demonstrated that the hemogenic endothelial cells (HECs) derive mainly from arterial rather than the venous vasculature (de Bruijn, Speck et al. 2000). These *in vivo* evidences raised the idea that the *in vitro* arterial specification is a pre-requisite for HECs to enter into the EHT programme (Elcheva, Brok-Volchanskaya et al. 2014). However, the *in vivo* emergence of HSCs from HECs

is directed by a variety of intrinsic and extrinsic signals whose role needs to be fully explored yet.

1.3.2 Reprogramming PSC and differentiated cells using TFs

Relevant improvements have been made in reprogramming iPSCs or terminally differentiated cells into *HSC-like* cells. These approaches involve the forced expression of few or a group of haematopoietic TFs. In this regard, the first attempt was made by the conditional expression of *Hoxb4* in murine ES cells (Kyba, Perlingeiro et al. 2002). This transcription factor belongs to the big family of homeobox genes, a group of transcription factors that are involved in the embryonic morphogenesis. *Hoxb4* has been described in haematopoiesis to control the expansion and the engraftment capacities of hematopoietic progenitors (Sauvageau, Lansdorp et al. 1994). The conditional expression of *Hoxb4* in murine ESCs was sufficient to confer self-renewal capacity and long-term multilineage reconstitution after primary and secondary transplantations ((Helgason, Sauvageau et al. 1996, Kyba, Perlingeiro et al. 2002). However, recipient mice displayed a low chimerism as well as poor lymphoid engraftment. Of note, *Hoxb4* overexpression in hPSCs enhanced the number of CFU-Cs but no long-term reconstitution was reported (Zhang, Beard et al. 2008).

Two separate groups were able to generate *in vitro* myeloid hematopoietic progenitors from hESCs using a combination of TFs. Doulatov and colleagues, used *Hoxa9*, *Erg* and *Rora* to endow myeloid progenitors with *in vitro* self-renewal and multilineage potentials whereas other two transcription factors (*Sox4* and *Myb*) were sufficient to confer short-term engraftment. Conversely, Elcheva and colleagues were able to direct the production of pan-myeloid and erythro-megakaryocytic lineages with different groups of TFs: *Gata2*, *Etv2* and *Tal1*, *Gata2* respectively. However, in none of these studies were the reprogrammed myeloid progenitors able to long-term engraft recipient immunocompromised mice (Doulatov, Vo et al. 2013, Elcheva, Brok-Volchanskaya et al. 2014).

1.3.3 Direct reprogramming of differentiated cells

Some scientists embraced the possibility to directly reprogram somatic cells into *HSC-like* phenotype. The concept of direct reprograming describes the approach of switching the fate of differentiated cells directly into HSPCs without transit through a pluripotent stage. This possibility encouraged some groups to seek the minimal and sufficient combination of TFs that are able to convert mouse fibroblasts into an *HSC-like* cells. Taking advantage of an engineered mouse (*H2B-GFP*) reporter fibroblast cell line, Pereira and colleagues, identified a minimal combination of 4 TFs (*Gata2, Gfi1b, cFos* and *Etv6*) that able to activate the HE program in differentiated mouse embryonic fibroblasts (MEFs) (Pereira, Chang et al. 2013). Reprogrammed HECs differentiated into *HSC-like* phenotype after coculturing with stromal cells. Although no *in vivo* functional experiments were performed to confirm the generation of LT-HSCs, these cells reprogrammed *HSC-like* cells generated CFU-C colonies after been reaggregated with mouse placental cells (Pereira, Chang et al. 2013). A similar approach was adopted by Batta and colleagues. With the ectopic expression of 5TFs (*Erg, Gata2, Lmo2, Runx1c, Scl),* the authors converted embryonic and adult murine fibroblasts into HPCs with short term engraftment potential. Of note, the reprogramming efficiency was improved using p53-/- fibroblasts (Batta, Florkowska et al. 2014). The two aforementioned studies gave an important contribution into our understanding of which factors may contribute to reprogramming of somatic differentiated cells into hematopoietic fate and what limitations still remain.

Developmentally appropriate niches are an essential source of supportive microenvironment for HSC generation and thus, are an important consideration in attempting de novo production of HSCs. The limitation of MEFs as a supportive niche is in their lack of plasticity and parallel niche development. The niche plays a role in not only affecting hematopoietic development and differentiation through activating TF expression but also affects the HSC epigenetic landscape. The following studies benefited from these considerations and have achieved the best results so far reported in HSC reprogramming. Rather than differentiated cells, Riddell and colleagues reprogrammed haematopoietic lymphoid progenitors (Pro-B cells) with a pool of 6TFs that have been selected *in vivo* (*Hlf, Runx1t1, Pbx1, Lmo2, Zfp37, Prdm5*). Pro-B cells were transfected with doxy-inducible lentiviral particles carrying these 6TFs

and injected into recipient mice. The activation of the 6TF together with the supportive *in vivo* microenvironment contributed to the generation of induced (i)HSCs. Although the transcriptome profile of the iHSCs appeared to be fairly comparable with the native HSCs, *in vivo* functional analyses on iHSCs resulted poorly reproducible (Riddell, Gazit et al. 2014). Lis and colleagues took advantage of the ontological similarities between the ECs and HSCs to transduce adult murine ECs with the FGRS TFs (*FosB, Gfi1, Runx1* and *Spi1*) and propagate them on a vascular niche microenvironment (Lis, Karrasch et al. 2017). The angiocrine factors provided by the microenvironment were crucial for the conversion of ECs into stable and self-renewing HSCs (called rEC-HSCs). These rEC-HSCs retained long term engraftment potential and hematopoietic reconstitution of both myeloid and lymphoid lineages. The same FGRS TFs were able to reprogram human umbilical vein-ECs (HUVEC) into hMPPs. These reprogrammed induced MMPs had *in vivo* engraftment capacity in recipient immunodeficient mice but lacked donor-derived lymphoid lineage contribution (Sandler, Lis et al. 2014). The most recent study combined the morphogen-directed differentiation of hPSCs to generate the HE. Afterwards, the *in vitro* derived HECs were successfully converted in iHSCs with 7 *in vivo* selected TFs (*Erg, HoxA5, HoxA9, HoxA10, Lcor, Runx1* and *Spi1*). However, the conversion is not consistently reproducible and the iHSCs lack of robust engraftment. Moreover, the molecular and functional properties need to be carefully evaluated (Sugimura, Jha et al. 2017).

All together, these studies demonstrated that *HSC-like* cells are produced by a combination of intrinsic and extrinsic factors, i.e. the expression of key TFs and signals sent by the surrounding microenvironment. The generation of LT-HSCs *in vitro* can be obtained only with a deep understanding of the embryonic genetic profiles and the signalling pathways that drive the HECs to become HSCs. Nonetheless, these complex regulatory networks remain largely unknown.

1.4 Gpr56 is a novel regulator of HSC generation

In a study carried out by our lab, Solaimani et colleagues analysed the differentially expressed genes (DEGs) between highly enriched ECs, HECs and HSCs to identify novel molecules that regulate the emergence of HSCs *in vivo* (Solaimani Kartalaei,

Yamada-Inagawa et al. 2015). Using the *Ly6A-GFP* reporter mouse model with CD31 and cKit markers, the authors profiled the transcriptomic signature of aortic ECs, HECs and HSC during EHT. The comparative analysis of the transcriptome of each population allowed to find 139 DEGs in ECs versus HECs and 340 DEGs in HECs versus HSCs. We found that most of the hematopoietic genes become active within the HEC population, whereas the endothelial signature is gradually lost as ECs progress towards HECs. Of note, a discrete number of angiogenetic genes were expressed in the HECs as compared to the ECs, demonstrating the crosstalk between the HECs and the supportive vascular niche. The study revealed Gpr56 as novel potential regulator of HSC emergence. *Gpr56* is the highest differentially expressed gene in the transition from HECs into HSCs. Interestingly, chromatic immuno-precipitation analysis reported *Gpr56* being a target of the heptad transcription factors as they bind the Gpr56 -37 upstream predicted enhancer region. Functional analyses performed in zebrafish demonstrated that Gpr56 is required for the EHT. *gpr56* knockdown in zebrafish severely reduced the frequency of HSCs (cmyb+) and hematopoietic progenitors (CD41+). Conversely, the injection of *Gpr56* transcripts (murine and zebrafish) in morpholino larvae, rescued the production of HSPC population and revealed ectopic hematopoiesis (Solaimani Kartalaei, Yamada-Inagawa et al. 2015). These results highlighted the crucial role of Gpr56 during the EHT.

The next section will provide insights on the structural and molecular features of this important receptor with a specific focus on its role in tissue development and malignancies.

1.4.1 Gpr56 structure and molecular features

Gpr56 (ADGRG1) is a well conserved orphan receptor that belongs to the largest G-protein coupled receptor (GPCR) superfamily. GPCRs encoded by the human genome are grouped into five families: glutamate, rhodopsin, adhesion, frizzled and secretin. Gpr56 is part of the adhesion GPCR (aGPCR) family which represents the second largest with 33 members (Fredriksson, Lagerstrom et al. 2003, Schioth and Fredriksson 2005).

The aGPCR family can be further divided into nine subfamilies: ADGRL (lathrophilins), ADGRA, ADGRC (CELSRs), ADGRD, ADGRG, ADGRV, ADGRE, ADGRF and ADGRB, most of which share a share a common protein architecture. The molecular structure presents a twofold protein structure that consist of a long extracellular domain (ECD) of ~320-5878 residues, a highly conserved 7-pass transmembrane (7TM) domain followed by an intracellular domain (ICD) which is responsible for initiating the signalling cascade upon activation. aGPCR family possesses a unique auto-proteolytical cleavage at the GPCR proteolysis site (GPS) within a conserved GPCR autoproteolysis inducing domain (GAIN) (Lin, Chang et al. 2004). The GAIN domain is the only shared domain among almost all aGPCRs (32 out 33, is absent ADGRA1) and it consists of domain A (6 alpha-helices) and domain B (twisted beta-sandwich with 13 beta-strands and 2 alpha-helices (Arac, Boucard et al. 2012). As part of aGPCR family, Gpr56 is characterized by a 7TM, a juxtamembrane GAIN domain and a ECD that mediates the adhesion-related interactions with extracellular signals (Langenhan, Aust et al. 2013). Although the biological role of the ECD remains poorly understood, the 7TM is responsible to initiate the signalling cascade whereas the GAIN domain undergoes to post-translational modifications along protein maturation. Indeed, the receptor maturation culminates with an autoproteolytic cleavage within the GAIN domain which generates two different fragments non-covalently associated on the plasma membrane: N-terminal fragment (NTF) and C-terminal fragment (CTF) that contains a cryptic tethered peptide called *Stachel* domain (**Figure 1.3**). The *Stachel* domain has been subject of several studies as it plays a critical role in the receptor activation mechanism.

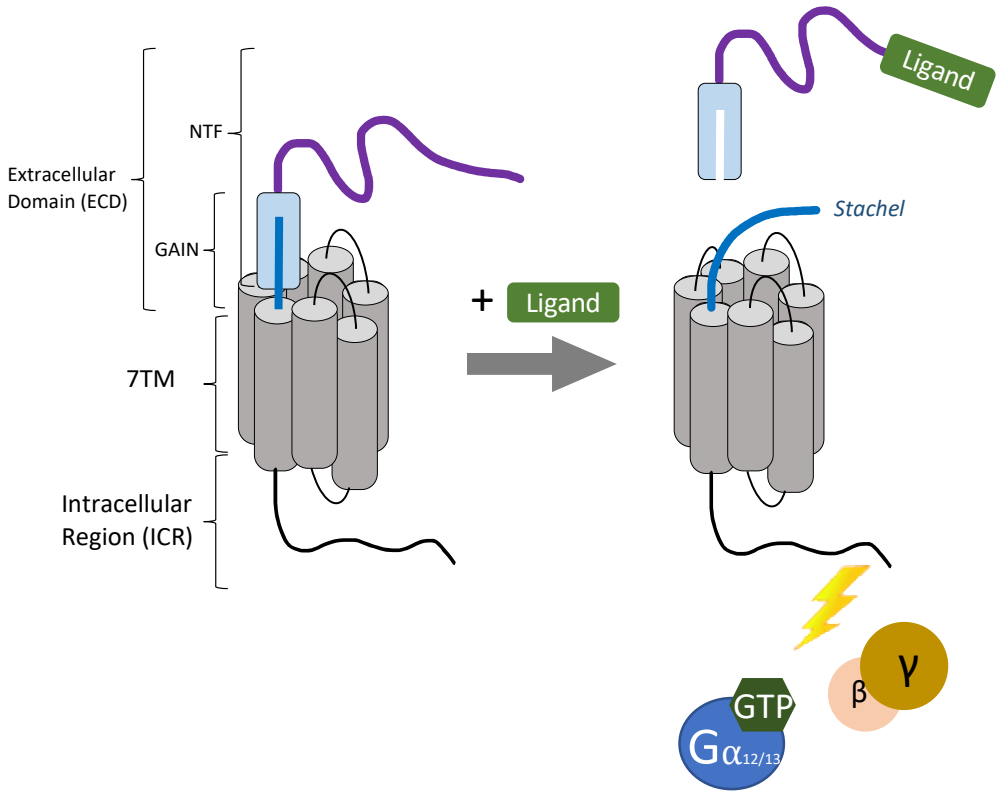

Figure 1.3 Gpr56 protein structure and mechanism of activation

Gpr56 belongs to the adhesion GPCR family. It consists of an extracellular domain (ECD), which contains the GAIN domain and the N-terminal fragment (NTF), a conserved 7 transmembrane domain (7TM) and an intracellular region. The exposure of the *Stachel* domain due to mechanical forces or upon the binding of the NTF to an extracellular ligand, triggers the downstream signalling cascade.

These studies prompted the proposal of two activation mechanisms: cleavage independent (Kishore, Purcell et al. 2016) and cleavage dependent (Stoveken, Hajduczok et al. 2015) (**Figure 1.3**). Two non-mutually exclusive cleavage-dependent models have been suggested for Gpr56 activation. According to the first model ("shedding"), the *Stachel* domain is exposed by the ligand-dependent dissociation of the NTF from the CTF domain (Liebscher, Schon et al. 2014, Stoveken, Hajduczok et al. 2015), whereas the alternative model suggests that the presence of the NTF portion *per se* inhibits the receptor activity. As a consequence, the deletion of the NTF constitutively activates the downstream signalling through the 7TM domain (Paavola, Stephenson et al. 2011). From the cytosolic portion of the 7TM domain the internal signalling cascade starts with the phosphorylation of the heterotrimeric Gα12/13 and Gβγ proteins. Thereafter, these proteins interact with a downstream effector of the

Rho GTPase protein family: RhoA. RhoA becomes active by exchanging guanosine diphosphate (GDP) to guanosine triphosphate (GTP) thanks to the guanidine nucleotide exchange factor (GEF). The resulting activated RhoA-GTP regulates important biological processes such as actin cytoskeleton reorganization, myosin contractility, cell migration and proliferation (Ihara, Muraguchi et al. 1998, Jaffe and Hall 2005, Hall 2012).

Such a variety of biological responses and the wide expression of Gpr56 in different cell types presented the idea that different ligands might activate the receptor. To date, the molecules known to activate Gpr56 are two natural ligands, collagen III (Col3a) and transglutaminase2 (TG2), one small agonist molecule, 3-α-acetoxydihyl-drodeoxygedunin (3-α-DOG) and a 19-amino-acid synthetic peptide that mimics the *Stachel* domain (P19) (Zhu, Luo et al. 2019). These ligands activate Gpr56 in different ways. Zhu et colleagues performed experiments examining the ligand-dependent mechanism of Gpr56 activation (Zhu, Luo et al. 2019). By taking advantage of a cleavage-deficient receptor ($GPR56^{H381S}$), they demonstrated that both collagen III and TG2 ligands activate the receptor via a *Stachel*-dependent mechanism. According to this model, the binding of these ligands to the extracellular portion of the receptor causes conformational changes which lead to the NTF shedding. The exposure of the *Stachel* domain triggers the 7TM activation. Differently from collagen III, TG2-mediated activation requires the simultaneous binding of the ligand with the NTF receptor domain and a constituent protein of the extracellular matrix: laminin. On the other hand, the non-natural agonist molecules (3-α-DOG and P19) engage the receptor orthosteric site to interact with the *Stachel* domain directly. P19 acts as natural tethered agonist as it is capable to reach the orthosteric domain regardless receptor cleavage, whereas 3-α-DOG is unable to activate the Gpr56 uncleavable form. This might be explained by considering the Gpr56 spatial conformation. The NTF three-dimensional conformation of the uncleavable receptor might hamper the interaction between 3-α-DOG and the *Stachel* domain to prevent the signalling cascade (Zhu, Luo et al. 2019).

Altogether, these insights enforce the crucial role of the *Stachel* domain. The exposure or the directly binding of the *Stachel* domain is sufficient to modulate the receptor

activity. Several groups have used this feature to develop large-scale *in vitro* cell-based assays to study a wide range of aGPCRs with similar molecular structure. These assays rely on the dynamic expression of downstream effectors such as TCF, SRE, SRF, NFAT. The expression levels of the transcriptional regulators correlate with the receptor activity (Shashidhar, Lorente et al. 2005, Kishore, Purcell et al. 2016). *In vitro* drug discovery platforms might take advantage of these well-established assays to identify new cell specific agonist and antagonist compounds.

1.4.2 Biological functions of Gpr56

Despite Gpr56 is largely involved in physiological processes, the pathological conditions such as cancer, cardiovascular and neuronal diseases contributed profoundly to understand its protein structure and signalling pathway. As membrane receptor, Gpr56 is a suitable pharmacological target for therapeutic approaches and drug discovery screenings.

The Gpr56 receptor has been widely studied in cerebral cortical development (Langenhan, Piao et al. 2016) . It is expressed on neural progenitor cells (NPCs) that undergo a “radial migration” which leads to the formation of the mature neurons. Patients with mutations in GPR56 suffer from epilepsy, mental retardation and language impairment: a neurological disorder known as bilateral frontoparietal polymicroglia (BFPP) (Ke, Ma et al. 2008) . These mutations cause a poor expression of the receptor at the cell membrane as Gpr56 is retained in the ER/Golgi (Santos-Silva, Passas et al. 2015). Other studies examined the role of Gpr56 in zebrafish and murine oligodendrocyte development (Ackerman, Garcia et al. 2015, Giera, Deng et al. 2015). In these studies, the authors demonstrated that Gpr56 is abundantly expressed during the early stages of oligodendrocyte development and gradually decrease in mature myelinating oligodendrocytes. In the absence of Gpr56, oligodendrocytes were specified normally but hypomyelinated and reduced in number due to a decrease in the oligodendrocyte progenitor cell (OPC) proliferation. In addition, Gpr56 regulates OPC proliferation via Gα12/13 and RhoA signalling pathway (Luo, Jeong et al. 2011, Ackerman, Garcia et al. 2015, Giera, Deng et al. 2015). Gpr56 is also involved skeletal muscle cell development as it is upregulated during the early fusion of human myoblasts (Cerletti, Molloy et al. 2006). Its

expression is found in myocytes, in the nascent myotubes and it supports myoblast differentiation via the activation of SRE and NFAT signalling. Although Gpr56-deficient myoblasts decreased their fusion capacity *in vitro*, no relevant defects have been reported in the phenotype of muscles of Gpr56 knock-out mice (Wu, Doyle et al. 2013, White, Wrann et al. 2014).

The expression of Gpr56 was found in different type of cancer. Xu and colleagues performed a gene expression analysis on metastatic variants of melanoma cells. They found that Gpr56 is remarkably downregulated on highly metastatic variants, whereas the TG2-mediated GPR56 activation contributes to suppress melanoma metastasis and tumor growth (Xu, Begum et al. 2006). Other studies supported the evidence that the dysregulated expression of Gpr56 is implicated in several cancers such us pancreatic, colon, ovarian, hematopoietic and glioblastoma/astrocytoma (Shashidhar, Lorente et al. 2005, Ke, Sundaram et al. 2007, Liu, Huang et al. 2017). Amongst them, it is important to highlight the relevance of GPR56 in leukemia.

1.4.3 The relevance of Gpr56 in leukaemia

Compelling studies demonstrated that the prolonged and high level expression of Gpr56 in blood cells correlates with hematological malignancies and, specifically, with acute myeloid leukaemia (AML) (Daga, Rosenberger et al. 2019). Patients affected by AML suffer an abnormal proliferation and differentiation of a myeloid stem cells (blasts). The onset of such uncontrolled cell proliferation (leukemogenesis) is mainly driven by a combination of two different events: chromosomal translocations and genomic mutations. Such mutations alter the physiologic function of epigenetic regulators or effector proteins involved in proliferative pathways (De Kouchkovsky and Abdul-Hay 2016). Although the chemotherapy allows the complete remission for the 60% of the AML patients, the remaining relapse. The high rate of relapsing is mainly attributed to few leukemic stem cells (LSCs) that persist after the standard therapy. These aggressive LSCs are heterogenous and share the majority of the biological features with healthy HSCs: self-renewal, quiescence and the ability to resist to drug treatments (Kreso and Dick 2014, Fong, Gilan et al. 2015). Therefore, it is necessary to identify therapeutic targets to eradicate those aggressive LSCs and find

prognostic factors to discriminate responsive patients from those that relapse after standard therapies.

Ng and colleagues contributed to develop a rapid and powerful prognostic tool to screen high-risk AML patients before starting chemotherapy (Ng, Mitchell et al. 2016) . In this study, gene expression analysis was performed on LSCs isolated from 78 AML patients. From this analysis, the authors generated a 17-gene score (LSC17) panel that defines biomarkers related to the "stemness" properties of LSCs. Interestingly, they found GPR56 as part of these highly selected biomarkers that characterize the LSCs signature (Ng, Mitchell et al. 2016). Different studies performed in patient derived AML samples, found that Gpr56 expression identifies aggressive subset of LSCs (Pabst, Bergeron et al. 2016). To identify novel determinants in primary human AML, LSCs from a cohort of 179 patients were analysed combining RNA-seq with functional *in vivo* assays. Gpr56 was found to be a marker of leukemic subpopulations with high engrafting capacity in *NOD-Scid-gamma* immunodeficient mice. LSC activity fall within Gpr56+CD34+ and Gpr56+CD34- subpopulations but not in the Gpr56- fraction. Furthermore, high GPR56 expression was found in the enriched LSC in CD34+CD38- sub compartment when compared to CD34+CD38+ or CD34-. Of note, the high level of Gpr56 protein correlates with an upregulation of drug efflux transporters ABCG1, ABCC1 and ABCA2 indicating a possible association of Gpr56 expression and drug resistance (Pabst, Bergeron et al. 2016, Daga, Rosenberger et al. 2019).

The association of high GPR56 expression and drug resistance LSCs emerged also in another study. In this work, Saito and colleagues found that GPR56 is highly expressed in EVI1^{high}AML, a class of chemotherapy-resistant AML with poor prognosis (Barjesteh van Waalwijk van Doorn-Khosrovani, Erpelinck et al. 2003, Saito, Kaneda et al. 2013). The high expression of GPR56 in EVI1^{high}AML cells led to an improved cell adhesion and apoptotic resistance whereas its downregulation reduced their cellular adhesion, viability and increased their susceptibility to chemotherapeutic agents (Saito, Kaneda et al. 2013). These evidences prompted the idea to consider Gpr56 as potential therapeutic target to eradicate those chemo resistant LSCs present in EVI1^{high} and in most of the AML subcategories.

1.4.4 Other GPCRs involved in hematopoiesis

To date, only a few GPCRs are known to play a role in hematopoiesis *in vivo* and *in vitro*. Apelin receptor (*APLNR*) is a GPCR expressed on ECs in the mouse embryonic AGM region and *in vitro* hPSC-derived ECs that differentiate into the hematopoietic lineage. Although its role *in vivo* has not been determined, *APLNR* activation enhances blood cell formation *in vitro* (Yu, Hirst et al. 2012). A pulse of Apelin ligand added in the early stage of hESC differentiation enhanced the EB size, the number of hemangioblast colony-forming cells (BI-CFCs) and induced the growth of ESC-derived endothelial cells (Yu, Hirst et al. 2012). Another recent study performed in mouse ESCs demonstrates that Apelin receptor defines a transient population of ESC-derived mesodermal cells committed to hematopoietic fate. *In vitro* hematopoiesis is impaired in Apelin-null mouse ESC, leading a significant reduction of HPCs (Jackson, Fidanza et al. 2020). Interestingly, the activation of Apelin pathway in AGM explants decreases the number of LT-HSCs and promotes myeloid differentiation (Jackson, Fidanza et al. 2020). Other GPRCs are known to regulate HSC generation through the modulation of the EHT. Thrombin Receptor (F2r) is a GPCR belonging to the proteinase-activated receptors (PAR) family and it is activated by its ligand thrombin (F2). Although F2r expression is required for vascular development, Yue and colleagues demonstrated that it might act as molecular switch to keep the balance between vascular and haematopoietic fate decisions. Using mESC and zebrafish model systems, they showed that F2r negatively regulates EHT and HSC generation via RhoA/ROCK pathway. Indeed, the inhibition of the F2r-RhoA/ROCK pathway promotes the EHT transition towards the generation of haematopoietic cells whereas its overexpression showed the opposite effect (Yue, Li et al. 2012).

Another GPCR involved in the EHT is Gpr183. In zebrafish, this receptor is the most upregulated GPCR expressed in those ECs that undergo EHT (Zhang, He et al. 2015). Functional analyses demonstrated that, upon activation, Gpr183 modulates HSPC generation through the repression of the Notch signalling pathway. Conversely, Gpr183 inhibition resulted in a persistent activation of *Notch1* that culminates with the abrogation of EHT and the HSPC generation (Zhang, He et al. 2015). Another study investigated the relationship between GPCRs and transcription factors (TFs). Gao and colleagues used bioinformatic analyses to identify GATA-2 induced GPCRs

that promote HSPC generation. They found that the expression of Gpr65 suppresses haematopoiesis by repressing a genomic +9.5 *Gata2-cis* element that enhances *Gata2* expression and EHT *in vivo* (Gao, Wu et al. 2016).

Taken together GPCRs are involved in EHT and HSC generation, normal function and malignancy. Most importantly to our study is the Gpr56 receptor. Its expression and function are poorly characterized and hence, how Gpr56 acts in the production of HSC in vivo, in vitro and in leukemic stem cells is the focus of my thesis.

1.5 Hypothesis

Gpr56 is required for HSPC function and production in mammals.

1.6 Aims

To investigate the functional role of murine and human HSPCs when Gpr56 expression is altered.

1. To test the function of HSPCs that lack Gpr56
    a. *In vivo,* using *VEC:Cre* and *VAV:Cre* Gpr56 cKO mouse models (Chapter 3)
    b. *In vitro,* using Gpr56 knock out (KO) ESC line (Chapter 4)

2. To investigate the functional output of human iPSC-derived HSPCs that overexpress GPR56 during hematopoietic differentiation (Chapter 5)
    a. Establishment of an inducible iPSC line that overexpresses GPR56 at different time points of hematopoiesis

2 MATERIALS AND METHODS

2.1 Mice and embryo production

Gpr56^{fl} (Giera, Deng et al. 2015), *VavCre* (Stadtfeld and Graf 2005) and *VECCre* (Chen, Yokomizo et al. 2009) mouse colonies were established. Embryos were generated by crossing *Gpr56*^{fl} (C57BL/6) mice with *VavCre:loxGpr56* or *VECCre:loxGpr56* (C57BL/6HsdJOla) animals (all 2-6 months old). The day of vaginal plug discovery was E0 and embryo staging was by somite pair counts. Ly5.1 mice (B6.SJL-*Ptprc*^{a}*Pepc*^{b}/BoyCrl, 2-4 months old) were recipients for transplantations. All mice were housed and bred in University of Edinburgh animal facilities in compliance with Home Office regulations and all procedures performed under a Home Office UK Project License.

2.2 Flow cytometry

Embryo cells. Yolk sacs (YS) were digested (37°C, 45') in 0.125% type 1 collagenase (C0130, Sigma-Aldrich) and washed and resuspended in PBS+10%FBS. FL cells were obtained by passing the tissue (5x) through a 30G needle. YS cells were stained with CD41- eFluor450, CD31-BV605, CD16/32-PE, c-Kit-APC and CD45-AF450 (**Table 3.1**) and FL LSK-SLAM ($CD3^{-}B220^{-}Gr1^{-}Ter119^{-}NK1.1^{-}CD48^{-}$ and $Sca1^{+}cKit^{+}CD150^{+}$) were sorted. PBS/FBS washed cells were run on a LSR Fortessa (BD Bioscience) and data analysed with FlowJo v10 (BD) software. Dr. Samanta Antonella Mariani and Chris Vink helped with the embryo dissections. Dr. Samanta Antonella Mariani performed the *in vivo* FACS analyses. QMRI Flow Facility helped in setting up the flow cytometric gates and sorted the cells of interest.

ES cells. Day 6 and 10 differentiated mouse EBs were PBS-washed and dissociated (37°C, 5-10 minutes) in 500µl TrypLE Express (Gibco). Cells were incubated (4°C, 30 minutes) with antibodies against CD41, CD45, CD16/32, and cKit (**Table 3.1**). Washed cells (10% FBS/PBS) were run on Aria III/Fusion (BD) and results analysed with FlowJo software. Dead cell exclusion was by Hoechst 33342 (Invitrogen) and

gates set based on unstained WT and fluorescent-minus-one (FMO) controls. Sorted cells were collected in 50% FBS/PBS buffer for functional analyses (CFU-C assay).

2.3 Hematopoietic assays

CFU-C. LSK-SLAM sorted FL cells ($CD3^-B220^-Gr1^-Ter119^-NK1.1^-CD48^-$ and $Sca1^+cKit^+CD150^+$) were cultured (100 LSK-SLAM per plate) in Methylcellulose (M3434, Stem Cell Technologies, CN; 37°C, 5%CO_2) and colonies counted after 10 days.

LTR-HSC. FL LSK-SLAM cells were injected intravenously into irradiated Ly5.1 recipients (2x4.5 Gy γ-irradiation) at 1 FL/recipient or 3, 10 or 30 LSK-SLAM cells/recipient. For secondary transplantations, LSK bone marrow cells of primary recipients were injected into Ly5.1 irradiated mice. After 4, 16 and 23 weeks, peripheral blood was analysed by CD45.1- and CD45.2- flow cytometry. Multilineage analysis on bone marrow, spleen, thymus and lymph nodes was performed 23 weeks post-transplantation. Recipient mice were considered reconstituted at ≥2.5% donor-derived cells. Chris Vink performed the transplantations.

2.4 Molecular analyses

Genotyping. DNA from CFU-C colonies, ear notches or sorted cells was extracted in PCR Buffer with Non-Ionic Detergent (PBND: 50mM KCl, 10mM TrisHCl, pH 8.3, 2.5mM $MgCl_2$, 0.1mg/ml gelatin, 0.45% (v/v) Igepal/NP40, 0.45% (v/v) Tween20) + Proteinase K (10mg/ml, 1h, 55°C) and heat-inactivated (95°C, 10'). 1µl of solution was used for *Gpr56* PCR. Touchdown PCR program was used to genotype embryos using Kapa HiFi Hotstart DNATaq Polymerase, according to the manufacturer protocol. PCR amplification protocol:

Step1:	3’	94 °C	
Step2:	30’’	94°C	
Step3:	30’’	64°C-0.5°C/cycle	
Step4:	1’	72°C	
Step5:	18x to step 2		
Step6:	30’’	94°C	
Step7:	30’’	54°C	
Step8:	1’	72°C	
Step 9:	15x to step 6		
Step10:	5’	72°C	
Step 11:	end		

Gene Ruler 1kb Plus (Thermo Scientific cat# 11511635) was used as DNA ladder in the agarose gel. Dr. Carmen Rodriguez Seoane performed the embryo genotypes.

RT-qPCR analysis. RNA was isolated using the RNeasy Micro kit (Qiagen). cDNA was synthesized with oligo(dT) (Invitrogen) and SuperScriptIII (Life Technologies). qRT PCR was performed with FastSybrGreen master mix (Life Technologies). See **Table 3.2** for primers.

Cloning. The *mCherry-p2a-hGPR56, mCherry-p2a-SP-his-hGPR56* and *mCherry-p2a-SP-hGPRCA* cassettes were generated using Gibson Assembly mix (NEB, cat #E5510S) and cloned into the pcDNA3.1+ expression plasmid (Addgene #V790-20). The Gibson assembly ligates two or more adjacent fragments seamlessly in a one-step isothermal reaction (50˚C). This is possible by generating fragments that overlaps ~15 to 40 base pairs at their 5’ and 3’ ends. These fragments are mixed together with the Gibson Mastermix, which contains an exonuclease, DNA polymerase and a DNA ligase. The exonuclease chews the 5’ ends of each fragment, so the fragments anneal as they share overlapping sequences. The DNA polymerase fills the gaps and the DNA ligase seals the nicks (Gibson, Young et al. 2009). 10-beta NEB (New England Biolabs #C3019H) competent bacteria were transformed according to the manufacturer protocol. Bacteria were PCR-screened using a set of primes that span from *mCherry* to *hGpr56* genes (Table 3.2). The PCR was performed following the *Taq* Polymerase (cat#10342053) manufacturer protocol. *GPR56* full length coding sequence (2082bp) was PCR amplified from BC-GPR56 plasmid (BC-GPR56 was a gift from Lei Xu, Addgene plasmid #44197). The donor *AAVS1-TetOn* backbone was kindly provided by Forrester Lab. All the regulatory elements of the *Tet-ON* system

are included within the *AAVS1* HAs. The backbone contains the neomycin resistance gene to select those cell clones that positively integrate the donor vector. In addition, the backbone holds a single SalI restriction enzyme (RE) sites to insert the *hGPR56* cassettes (**Figure 5.4 A**). The *mCherry* and *hGRP56* full length sequences were amplified from Addgene plasmids #58476 and #52297 respectively. The amplicons designed for Gibson Assembly were PCR-amplified using the Phusion High-Fidelity Taq Polymerase (cat#M0530S) following the manufacturer protocol. Primers used for Gibson Assembly are listed in **Table 3.2**. *AAVS1-TetOn* backbone was kindly provided by Forrester laboratory. NEB10-beta competent E.*coli* were transformed with the ligated plasmids according to the manufacturer protocol. Plasmid digestions were performed using New England Biolabs restriction enzymes. Gene Ruler 1kb Plus (Thermo Scientific cat# 11511635) was used as DNA ladder on agarose gel in all the PCR and enzymatic products.

Western blotting. 10^6 ESC were washed 2x with PBS, re-suspended in ice cold RIPA buffer + protease and phosphatase inhibitors (ThermoFisher) and incubated (30', ice). Samples were sonicated and centrifuged (maximum speed, 15'). Total protein in supernatant was quantified using BSA kit (BioRad). Equal amounts of protein for each sample were boiled (95°C, 5') in SDS sample buffer (BioRad), were separated in SDS- polyacrylamide gel (NuSTep) and transferred (30'; 20V) to a nitrocellulose membrane (Amersham). The membrane was blocked (5% semi-skimmed milk in TBS-Tween20) and blotted overnight (4°C, 1.5% semi-skimmed milk in TBS-Tween) for Gpr56 detection. Incubation for β–Actin detection was at RT (2hr). Membranes were washed (3x, 5') in TBS-Tween and blotted with HRP-conjugated secondary antibodies (RT, 1hr). HRP signal was detected by Odyssey FC (Li-Cor) using Image Studio Lite (Li- Cor) software. See **Table 3.1** for antibodies. Dr. Samanta Antonella Mariani helped in performing western blot assay.

CRISPR/Cas9 genome editing. *G2V.56*$^{-/-}$, *G2V.56*$^{-/-}$*/97*$^{-/-}$ were generated following the protocol published by (Ran, Hsu et al. 2013). In brief, gRNAs were designed using e-CRISP tool (http://www.e-crisp.org/E-CRISP/index.html) and top score gRNAs (**Table 3.2**) were selected and cloned into *pSpCas9(BB)-2A-GFP* (Addgene plasmid ID: 48138) using BbsI restriction enzyme (R00539, New England Biolab). The resulting CRISPR/Cas9 plasmids were transfected into *G2V* ESC (provided by Dr.

Mari-Liis Lukke) using DreamFect (OzBiosciences, Cat#DF40500) according to the manufacturer protocol. Transfected GFP positive cells were single-cell sorted into 96 multiwell plates in a feeder layer of mouse embryonic fibroblasts (MEFs) and expanded for 5 to 7 days. Single-cell derived colonies were transferred into bigger MEF-covered plates (48 and 24-multiwell plates) for further expansion. RNA was extracted (RNeasy Micro kit, Qiagen cat# 74004) to assess the mRNA level of *Gpr56* and *Gpr97* (primers, **Table 3.2**). DNA was extracted and used for the Surveyor Assay (IDT, cat#706020) following the manufacturer protocol. The Surveyor Assay was used to detect mutations and polymorphisms in a specific genomic sequence. Genomic heteroduplexes made of wild type and gRNA-targeted sequences are recognised and cleaved by the surveyor nuclease at the site of any single nucleotide polymorphism or indels mutations.

2.5 Mouse ES cell maintenance and differentiation

IB10 ESCs (*WT, G2V, G2V.56*$^{-/-}$, *G2V.56*$^{-/-}$*/97*$^{-/-}$, genetic background C57BL/6 129/Ola were cultured (37°C, 5% CO_2) on irradiated mouse embryonic fibroblasts (MEFs) in ES medium, daily refreshed (DMEM, Lonza), 15% FCS (HyClone), 2mM GlutaMAX, 1mM Na-pyruvate, 1%P/S, 50mM ß-mercaptoethanol (all Gibco), 0.1mM non-essential amino acids (Lonza), 1,000U/mL LIF (Sigma). Karyotype on IB10 ESCs was performed routinely by Dr. Carmen Rodriguez Seoane. IB10 karyotype did not show any chromosomic alteration. However, karyotypes on the newly generated *G2V.56*^{ko} and *G2V.56*^{ko}*97*^{ko} ESC lines need to be performed to exclude genomic anomalies. MEFs (200.000cells per well of 24multiwell-plate) keep ESCs undifferentiated, in defined single cell-derived colonies. 1 day prior splitting ESCs, MEFs were plated in gelatine (0.01%) coated plates. When ESCs reach ~50% confluency, 500ul/well of Trypsin/EDTA was added into single well and cells were incubated at 37C for 5 minutes. Cells were spin down (1000rpm, 5 minutes, room temperature) and resuspended in complete medium. Over time, the splitting procedure allows to remove differentiating cells. To induce EB formation, confluent ESCs were trypsinized and MEFs depleted by 30' incubation in EB medium (Iscove's modified Dulbecco's medium (IMDM), 15%FCS (HyClone), 1%P/S (Gibco)). EB formation was induced (40 rpm; $25x10^3$ cells/mL) in EB medium, 2mM GlutaMAX (Gibco),

50mg/mL ascorbic acid (Sigma), $4x10^{-4}$M monothioglycerol (Sigma), 300mg/mL transferrin (Roche) and supplemented with 5% proteome-free hybridoma medium (Gibco) on day 3. From day 6 onward, 100ng/mL stem cell factor, 1ng/mL interleukin-3, 5ng/mL interleukin-11 (all from Peprotech) were added. 2,000 to 10,000 V+ and V- cells were FACS sorted to perform gene expression analyses. Dr. Carmen Rodriguez Seoane helped in maintaining and differentiating mESCs.

2.6 Human SFCi55 maintenance and differentiation

To study the functional role of hGPR56 in human hematopoiesis, I generated an inducible iPSC line (SFCi55) that will express constitutively active GPR56 by adding doxycycline in the culture media. The workflow is shown in **Figure 5.9** SFCi55 are targeted with the *AAVS1-Tet-On-mCherry-p2a-hGPR56CA* donor vector, which constitutively activates the GPR56 downstream signalling cascade upon expression (Paavola, Stephenson et al. 2011) (**Figure 5.9 A**). SFCi55 that integrated the donor vector will be selected by neomycin (**Figure 5.9 B**) and PCR screened to confirm the correct genomic location of the *AAVS1-Tet-On-mCherry-p2a-hGPR56CA* (**Figure 5.9 C**). The selected clones will be validated to test the *mCherry* and *hGPR56* expression induced by the doxycycline (**Figure 5.9 D**).

The SFCi55 iPSC line was kindly provided by Forrester laboratory (Yang, Ma et al. 2017). Cells were maintained and expanded into 6 multiwell plates coated with *CELLstart* xeno-free substrate (Thermofisher Scientific cat#A1014201) in serum-free medium (StemPro hESC SFM, Thermofisher Scientific, cat#A1000701), *ß*-mercaptoethanol (0.1mM, Gibco), BSA 25% and bFGF (20ng/ml). SFCi55 cells grow as well-defined round-shaped colonies. Medium was daily refreshed, and cells were constantly monitored under the microscope to examine their morphology. Spontaneous differentiating colonies appear with irregular borders. Although some degree of differentiated cells (<10% of the plate) is expected, higher frequency leads to poor HPC production. Differentiating cells can be marked and aspirated from the well to purify the colonies. Confluent SFCi55 cells (~60%) are passaged with mechanical dissociation, using the STEMPRO EZPassage disposable passaging tool (Thermofisher Scientific, cat#23181010), according to the manufacturer protocol. SFCi55 that reach 80% of confluency were transferred into low-profile 6-multiwell

plate to be differentiated into haematopoietic progenitors. Embryoid bodies formation (from day 0 to day 4) occurred in EB media containing 50ug/ml BMP4, 50ug/ml VEGF and 20ug/ml SCF (all from Peprotech). From day 5 to day 11 the differentiation media was supplemented with VEGF (15ng/ml), Dkk (150ng/ml), IL-6 (10ng/ul), IGF-1 (25ng/ml), IL-11 (5ng/ml), SCF (50ng/ml), EPO (2U/ml final), TPO (30ng/ml), IL-3 (30ng/ml) and Flt-3L (10ng/ml) as indicated in *(Kennedy, Awong et al. 2012)*. At day 11 of differentiation EBs were harvested and dissociated using TryplE (Gibco, cat#12563011), resuspended in FACS buffer (10% FBS/PBS) and stained with hCD38-PE and hCD34-eFluor450 (see **Table 3.1**). The *i55GPR56CA* iPSC line was established targeting the *AAVS1* locus. Left & Right Zinc Fingers nucleases were kindly provided by Forrester laboratory. 1x10^6 SFCi55 were transfected with Left (1ug) & Right (1ug) Zinc Fingers plasmids together with *AAVS1-TetOn-hGPR56CA* plasmid (3ug) using Nucleofector Technology (Lonza), according to the manufacturer protocol. Transfected (positive) clones were selected adding 400ug/ml Neomycin into the maintenance medium and kept in culture for 10 days. Single clones were picked, expanded in a 6-multiwell plate and screened using 2 set of primers (see **Table 3.2**). The *i55GPR56CA* line was validated adding doxycycline (1 mg/ml, according to the Tet-ON 3G inducible expression Systems User Manual manufacturer protocol, Clonotech) to the medium and GPR56 transcript levels were quantified using RT-qPCR assay (see **Table 3.2**). Karyotype on the newly generated *i55GPR56CA* iPSC line needs to be performed to exclude genomic anomalies.

2.7 Zebrafish embryos

The *in vivo* experiments were performed by Dr. Emma de Pater at the Erasmus Medical Center, Dept of Hematology, Rotterdam NL. Zebrafish (*Danio rerio*) embryos were raised at 28.5^{o}C (Solaimani Kartalaei, Yamada-Inagawa et al. 2015). Heterozygous - *6.0itga2b:EGFP* zebrafish (CD41-GFP) (Lin, Traver et al. 2005); - *0.8flt1:RFP* (Flt1:RFP) (Bussmann, Bos et al. 2010) were maintained by crosses with WT zebrafish and embryos imaged with Leica SP5 confocal microscope. All mRNA *in vitro* expression constructs were generated by amplification of appropriate cDNA with specific primers (see **Table 3.2**) and resulting PCR products were cloned into *p-*

GEM-T vector, sequence verified and mRNA was generated using Ambion sp6 or T7 mRNA generation kit.

2.8 Morpholino and mRNA injections

The experiments were performed by Dr. Emma de Pater at the Erasmus Medical Center, Dept of Hematology, Rotterdam NL. Antisense morpholino against the splice site of the second intron (**Table 3.2**; Gene Tools) was dissolved in MQ at a concentration of 1 mM (1 nl MO was injected in a 1/5 concentration in 0.1M KCl and phenol red). For mRNA rescue experiments, 1nl of 50 ng/µl mRNA and 200µM was injected.

2.9 Statistical Analysis

All graphs were generated using GraphPad Prism. A one-way ANOVA corrected by Bonferroni's test was used to compare more than 2 groups, whereas the Student t test was used when the groups to compare were only two. Significance was defined as *p≤0.05, **p≤0.01, ***p≤0.001.

Table 2.1 Antibodies

Antigen	Fluorophore	Clone	Company	Isotype
CD3	PE	17A2	BioLegend	Rat IgG2b, κ
CD3	PerCP-Cy5.5	145-2C11	eBioscience	Armenian hamster/IgG
B220	PE	RA3-6B2	BD Biosciences	Rat IgG2a, κ
Ly6C/Ly6G (Gr1)	PE	RB6-8C5	BD Biosciences	Rat IgG2b, κ
Ly6C/Ly6G (Gr1)	APC-Cy7	RB6-8C5	BD Biosciences	Rat IgG2b, κ
Ter119	PE	TER-119	BD Biosciences	Rat WI
Ter119	BV421	TER-119	BD Biosciences	Rat WI
CD11b	PE	M1/70	eBioscience	Rat IgG2b, κ
CD11b	BV605	M1/70	BioLegend	Rat IgG2b, κ
CD48	AF700	HM48-1	BioLegend	Armenian hamster/IgG
NK1.1	AF700	PK136	BioLegend	Mouse IgG2a, κ
Sca1	PE-Cy7	D7	eBioscience	Rat IgG2a, κ
CD150	BV605	TC15-12F12.2	BioLegend	Rat IgG2a, L
CD117 (c-Kit)	BV421	2B8	BD Biosciences	Rat WI
CD117 (c-Kit)	APC	2B8	BD Biosciences	Rat WI
CD31	BV605	390	BioLegend	Rat IgG2a, κ
CD41	eFluor450	MWReg30	eBioscience	Rat IgG1a, κ
CD45	AF700	30-F11	BioLegend	Rat IgG2b, κ
CD16/32	PE	93	eBioscience	Rat IgG2a, L
CD4	AF700	GK1.5	eBioscience	Rat IgG2b, κ
CD8	PE-Cy5	53-6.7	BioLegend	Rat IgG2a, κ
CD19	BV650	6D5	BioLegend	Rat
CD45.1	APC	A20	BD Biosciences	Mouse A.SW IgG2a, κ
CD45.2	PE	104	BD Biosciences	Mouse SJL IgG2a, κ
hCD38	PE	HIT2	BD Pharmingen	Mouse IgG1, κ
hCD34	eFluor450	4h11	eBioscience	Mouse IgG1, κ
Anti-His-Tag		MA1-21315	Thermofisher	Mouse IgG2b
Goat anti-mouse	Alexa Fluor-488	ab150113	Abcam	Goat

Table 2.2 Primer List

Genotyping	**Forward 5' – 3'**	**Reverse 5'- 3'**
VEC-Cre	CCCAGGCTGACC AAGCTGAG	GCCTGGCGATCC CTGAACATG
Vav-Cre	GGCGACAGTTAC	GCCTGGCGATCC
	AGTCACAGAAGAGG	CTGAACATG
Gpr56 fl/fl	TGGTAGCTAACCTAC TCCAGGAGC	CACGAGACTAGTGA GACGTGCTAC
$Gpr56^{WT}$	TGGTAGCTAACCTACTCCAGGAGC	GGTGACTTTGGTGTTCTGCACGAC
Cre recombination		
Gpr56	GTGAGGTCCAGGCA TACTCG	AGGAGCTCTGTGCATTGGAG
RT-qPCR		
ß-actin	CACCACACCTTCTTA CAATGAG	GTCTCAAACATGAT CTGGGTC
Mouse Gpr56	TCTGCTCTGGCTTGTCTTC	AGGTTCATGTGGACTTTGATG
Mouse Gpr97	CTGGGATATGGCTAA AGGAGAC	AAGGCGAAGAAGG TCAAGTG
Human GPR56	GAAACCTCGGGACTACACCA	CAGGGAGAAGTGCAGGAAGA
gRNAs		
Gpr56 top	CACCGtctgttgggtctggtt ccgc	
Gpr56 bottom	AAACgcggaaccagacccaacagaC	
Gpr97 -ex2-top	CACCGgaatgtctgccgtc ggcttc	
Gpr97 -ex2-bottom	AAACgaagccgacggcagacattcC	
Gpr97-ex10-top	CACCgcggttctcctggtcgcgaa	
Gpr97-ex10-bottom	AAACttcgcgaccaggagaaccgc	
Zebrafish mRNA generation		
gpr56 coding zf	ATGAACCAGAATCCA GCAAAG	TTAACACTTCTCGTT AGTTTGTA
Mouse mRNA generation		
gpr56 cDNA	TAGGAGTATAATGGC TGTCCA	CTTAGATGCGGCTG GAGGA
gpr97 cDNA	CTGATGGCGACAGCCAGGA	CTGCAGCCACCCATCATCA
gpr114 cDNA	AATACTGGCGAGGAC ATGGA	GAGCTGGGTCAGT GTGTCAT
MO sequences		
gpr56 Spl E2 I2-3	TGTAATGCTCGTTTA CTTACCTTGA	
Cloning		
hGPR56	ATGAGGGGCCACAGGGAAGACTTTCGCTT	TTAGATGCGGCTGGACGAGGTGCTGC
mCherry	ccaccATGGTGAGCAAGGGCGAGG	TGActgtacaGCTCGTCCATGCCGCCG
SP+his	ACTCCCCAGTCGCTGCTGCAGACGACACTGTT	ATGGTGATGGTGATGGTGATGATGGCCGTGG
i55GPR56CA screening		
SalI - cassette	CAATGTCGACcccaccATGGTGAGCAA	CTAGGTCGACTTAGATGCGGCTGGAC
AAVS1-directional screening	CCTCGTCCAGCCGCATCTAA	ctgcctgctgacgctcttga
AAVS1-integration-PCR1	ATGGTGAGCAAGGGCGAG	TTAGATGCGGCTGGACGAG
AAVS1-integration-PCR2	tcagaagaactcgtcaagaaggcg	GCCTGTGCTGACCCATGC
Gibson Assembly		
mCherry_backbone_hGpr56	TCCAGCACAGTGGCccaccATGGTGAGC	GCAGCGACTGGGGAGTAGGTCCAGGGTTCTC
hGpr56_mCherry_backbone	GAGAACCCTGGACCTACTCCCCAGTCGCTGC	CGCGGGCCCTCTAGTTAGATGCGGCTGGA
SP_hGPr56_Cterm	TCCAAGGTGCCCACGGCACCTACTTTGCAGTG	CACTGCAAAGTAGGTGCCGTGGGCACCTTCGA
SP_his_Nterm	CACGGCCATCATCACCATCACCATCACCATAGGGGCCACAGGGAAGACTT	CCCCTATGGTGATGGTGATGGTGATGATGGCCGTGGGCACCTTGGACCAG
***mCherry_p2a_hGPR56* cassette**		
Primers	**Sequence**	**size of amplicon**
1	TCCAGCACAGTGGCccaccATGGTGAGC	809 bp
2	GCAGCGACTGGGGAGTAGGTCCAGGGTTCTC	
3	GAGAACCCTGGACCTACTCCCCAGTCGCTGC	2108 bp
4	CGCGGGCCCTCTAGTTAGATGCGGCTGGA	
mCherry_p2a_his_hGPR56 cassette		
Primers	**Sequence**	**size of amplicon**
5	TCCAGCACAGTGGCccaccATGGTGAGC	880 bp
6	CCCCTATGGTGATGGTGATGGTGATGATGGCCGTGGGCACCTTGGACCA	
7	CACGGCCATCATCACCATCACCATCACCATAGGGGCCACAGGGAAGACT	2051 bp
8	CGCGGGCCCTCTAGTTAGATGCGGCTGGA	
mCherry_p2a_hGPRCA cassette		
Primers	**Sequence**	**size of amplicon**
9	TCCAGCACAGTGGCccaccATGGTGAGC	884 bp
10	CACTGCAAAGTAGGTGCCGTGGGCACCTTGGA	
11	TCCAAGGTGCCCACGGCACCTACTTTGCAGTG	967 bp
12	CGCGGGCCCTCTAGTTAGATGCGGCTGGA	

3 UNEXPECTED REDUNDANCIES OF GPR56 AND GPR97 DURING HEMATOPOIETIC CELL DEVELOPMENT AND DIFFERENTIATION

The work presented in this chapter was accepted for publication as:

A. Maglitto, S.A. Mariani, E. de Pater, C. Rodriguez Seoane, C.S. Vink, X. Piao, M-L Lukke and E. Dzierzak. *Unexpected redundancy of Gpr56 and Gpr97 during hematopoietic cell development and differentiation.* Blood Advances

3.1 Introduction

Hematopoietic stem cells (HSCs) are the rare and self-renewing cells that sustain lifelong blood cell production and are used clinically for reconstitution of the blood system in therapeutic transplantations. We identified Gpr56 as the most differentially expressed receptor gene during EHT in the mouse embryonic day (E) 10.5 and its expression localized to emerging hematopoietic cells (Solaimani Kartalaei, Yamada-Inagawa et al. 2015). Gpr56 is an orphan receptor belonging to the adhesion G-protein coupled receptor family, the major class of GPCRs that mediates cell-cell and cell-matrix interactions (Langenhan, Aust et al. 2013) and is well-conserved across vertebrate species. The protein contains a long external N-terminal domain, 7-transmembrane domain and C-terminal cytoplasmic domain. Adhesion GPCRs are characterized by a GPCR-Autoproteolysis-INducing (GAIN) domain located between the N-terminus and transmembrane domain (Zhu, Luo et al. 2019). Upon ligand-binding, an auto-proteolytic cleavage divides the protein in two non-covalently linked fragments and the cytoplasmic domain is thought to signal through RhoA and ROCK to trigger downstream cellular functions (Luo, Jeong et al. 2014, Ackerman, Garcia et al. 2015, Olaniru, Pingitore et al. 2018).

Gpr56 is important in several biological development processes. For example, Gpr56 deletion in the mouse causes a severe reduction in CNS myelination due to defective oligodendrocyte precursor cell maturation (Ackerman, Garcia et al. 2015, Ackerman, Luo et al. 2018). In some cases, its dysfunction is linked to human genetic disorders. Mutations in human GPR56 cause a recessive brain malformation called bilateral frontoparietal polymicroglia (BFPP), defective cerebral cortex and CNS hypomyelination (Piao, Hill et al. 2004, Cauley, Hamed et al. 2019). Interestingly, aberrant expression of GPR56 in leukemic stem cells (LSC) is associated with high-risk/poor-treatment outcome in AML patients (Barjesteh van Waalwijk van Doorn-Khosrovani, Erpelinck et al. 2003, Groschel, Sanders et al. 2014, Daria, Kirsten et al. 2016, Pabst, Bergeron et al. 2016). Although Gpr56 is well-characterized in CNS development, its role in normal embryonic and adult hematopoiesis is uncertain and controversial.

Key results in Gpr56 knockdown zebrafish embryos revealed a dramatic reduction in aortic HSPC (hematopoietic stem/progenitor cell) generation during EHT (Solaimani Kartalaei, Yamada-Inagawa et al. 2015). The HSPC deficiency in zebrafish Gpr56 morphant embryos could be rescued by both zebrafish and mouse *Gpr56* mRNA injection. Moreover, Gpr56 overexpression resulted in enhanced and ectopic hematopoiesis. Thus, Gpr56 is necessary and sufficient for zebrafish aortic HSPC development (Solaimani Kartalaei, Yamada-Inagawa et al. 2015). In contrast, although Gpr56 is highly expressed within mouse HSPCs (Rao, Marks-Bluth et al. 2015), one study in a germline Gpr56 (exon 2-3) deletion mouse model showed surprisingly small changes in HPC numbers and in HSC-repopulating activity (Rao, Marks-Bluth et al. 2015) whereas another study (Saito, Kaneda et al. 2013) showed reduced self-renewal activity of HSC upon secondary *in vivo* transplantation. As some Gpr56 protein was detected in this mouse model (possibly because of failure to delete the S4 splice variant (Rao, Marks-Bluth et al. 2015)), a role for Gpr56 in normal mammalian hematopoietic development remains uncertain.

In this study, we examine the functional role of Gpr56 *in vivo* and *in vitro* during mouse hematopoietic development. The lab generated the transgenic mice and consolidated the mouse ESC maintenance and differentiation protocols at the time when I started y

PhD. We show that *in vivo* transplanted Gpr56 conditional knockout mouse fetal liver HSCs and *Gpr56* null mouse embryonic stem cell (ESC)- derived HPCs are myeloid-lineage biased, that mouse *Gpr97* mRNA can rescue HSPC generation in *gpr56* morphant zebrafish embryos, and that deletion of Gpr56 in mouse fetal liver (FL) HSCs and ESC-derived HPCs results in upregulated *Gpr97* expression. Deletion of both Gpr56 and Gpr97 in mouse ESC results in almost complete loss of HPC production, thus revealing previously unrecognized and important redundant roles for these two G-protein coupled receptors in mouse hematopoietic development and differentiation.

3.2 Results

3.2.1 Phenotypic yolk sac HPCs are reduced in Gpr56 conditionally deleted embryos

A conditional knockout (cKO) approach with VEC (Vascular endothelial cadherin) *Cre:loxGpr56* was taken to specifically delete all isoforms of *Gpr56* during early development of the hematopoietic system. Yolk sacs (YS) were isolated from *VECCre:loxGpr56 cKO* and control wild type (WT) littermates (**Figure 3.1 A**) at embryonic day (E) 9.5 (24-29 somite pairs). Sorted CD31+ YS endothelial cells were verified for Gpr56 deletion (**Figure 3.1 B**), and RT-qPCR analysis showed a marked decrease in relative *Gpr56* mRNA in the cKO YS cells as compared to WT controls (**Figure 3.1 C**). Dr. Samanta Antonella Mariani, Chris Vink and Dr. Carmen Rodriguez Seoane helped dissecting the mouse embryos. Dr. Carmen Rodriguez Seoane performed the embryo's genotypes.

Examination of phenotypic hematopoietic cells by flow cytometric analysis (**Figure 3.2 A**) showed that the percentage of cKit+ YS cells was significantly decreased in the cKO embryos compared to WT (**Figure 3.2 B**). Also, the percentage of erythro-myeloid progenitors (EMPs; CD41+cKit+CD16/32+), and other progenitors (CD31+cKit+ and CD45+cKit+) was slightly decreased in the cKO YS compared to WT. The number of CFU-C/YS was significantly lower in the cKO compared to WT controls (**Figure 3.2 C**), indicating some early Gpr56-related hematopoietic developmental defects. Dr. Samanta Antonella Mariani performed the FACS analyses.

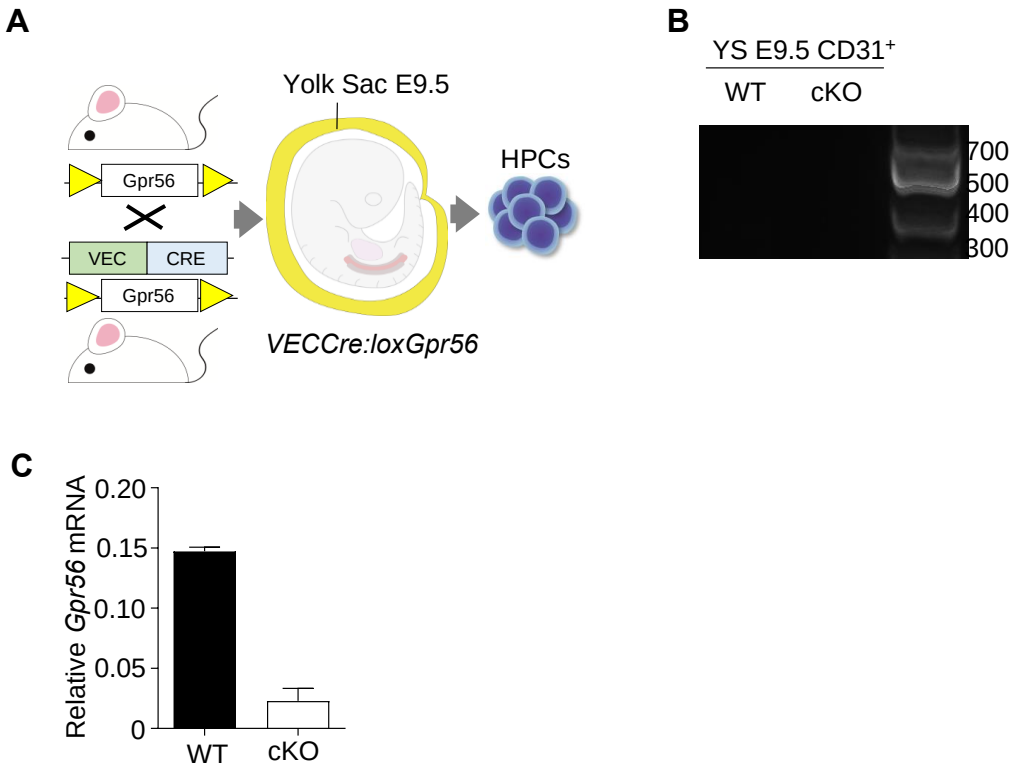

Figure 3.1 Gpr56 is down-regulated in *VECCre:loxGpr56* YS-derived HPS.

(A) Experimental setup for E9.5 yolk sac (YS) hematopoietic progenitor cell (HPC) analyses. **(B)** Genomic PCR analysis verifying Gpr56 deletion in CD31+ E9.5 YS cells (single embryos) from *VECCre:loxGpr56* cKO as compared to control WT CD31+ yolk sac cells. (**C)** Relative expression of *Gpr56* in wild type (WT) and *VECCre:loxGpr56* conditional knockout (cKO) E9.5 YS cells normalized to *β-actin* by qRT-PCR analysis (n=2). Dr. Samanta Antonella Mariani, Chris Vink and Dr. Carmen Rodriguez Seoane helped dissecting the mouse embryos. Dr. Carmen Rodriguez Seoane performed the embryo's genotypes.

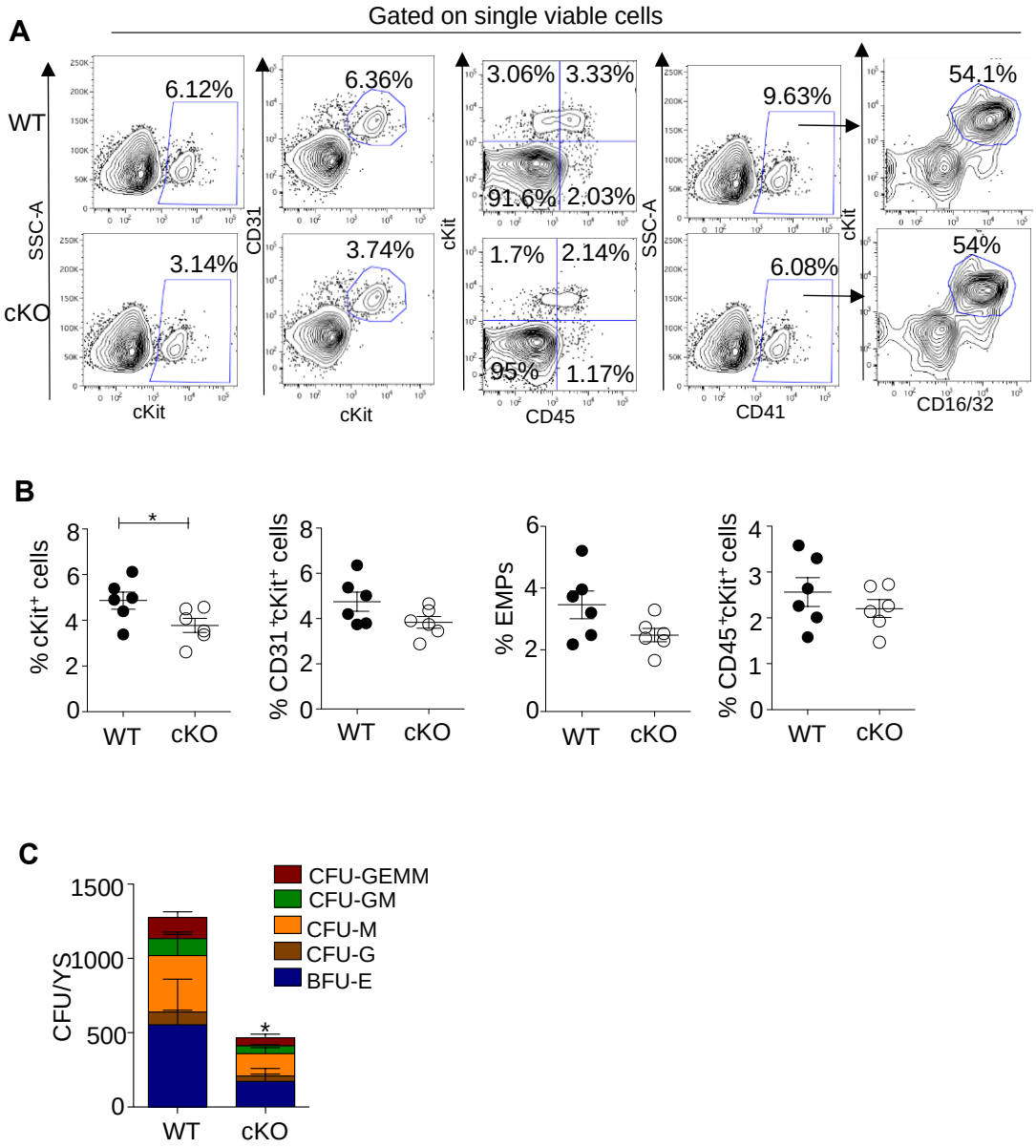

Figure 3.2 Gpr56 deficiency affects early hematopoietic development in *VEC-Cre* mouse embryos.

(A) Flow cytometric gating parameters for SSC-A, cKit, CD45, CD41 and CD16/32 cells from Gpr56 in wild type (WT) and *VECCre:loxGpr56* cKO E9.5 YS cells. **(B)** Percentages of cKit$^+$, CD41$^+$cKit$^+$CD16/32$^+$ (EMP=erythro-myeloid progenitor), CD31$^+$cKit$^+$ and CD45$^+$ckit$^+$ cells in WT and cKO E9.5 yolk sacs (n=6). Mean±SEM are shown. (**C)** Number of colony forming units (CFU) per WT and cKO E9.5 YS (n=3, 3 wild types and 3 cKO embryos from 2 different litters in 2 different days). Distinct colony types are indicated. CFU-GEMM=granulocyte, erythroid, macrophage, megakaryocyte; - GM=granulocyte, macrophage; -M=macrophage; G=granulocyte; BFU-E=burst forming unit-erythroid. Mean±SEM are shown. Dr. Samanta Antonella Mariani performed the FACS analyses.

3.2.2 HPC and HSC function is largely unaffected in E13.5 *Gpr56* cKO fetal liver

To examine whether Gpr56 loss affects definitive hematopoietic progenitor cells (HPCs) and/or HSCs, E13.5 *VAVCre:loxGpr56* cKO embryos were generated and LSK- SLAM fetal liver (FL) cells isolated (**Figure 3.3 A and B**). RT-qPCR analysis verified reduced levels of *Gpr56* transcripts in the cKO cells as compared to WT controls (**Figure 3.3 C**). No differences in the number of LSK-SLAM per E13.5 FL (**Figure 3.3 D**) were found and HPC in vitro analyses showed no significant changes in CFU-C/100 LSK-SLAM cKO as compared to WT cells (**Figure 3.3 E**). When CFU colonies obtained from the cKO cells were tested by DNA PCR for the *Gpr56* gene, all (100%) of 14 colonies examined revealed that both alleles of Gpr56 were recombined (**Figure 3.3 F**). Thus, Gpr56 appears to be dispensable for FL HPC growth and function. Dr. Samanta Antonella Mariani, Chris Vink and Dr. Carmen Rodriguez Seoane helped dissecting and preparing the mouse embryos. Dr. Carmen Rodriguez Seoane performed the embryo's genotypes.

E13.5 FL LSK-SLAM cells were examined for HSC *in vivo* repopulating activity (**Figure 3.4 A**). Adult irradiated recipients (Ly5.1) injected with one FL LSK-SLAM cell equivalent (approximately 100 HSCs) of *VAVCre:loxGpr56* cKO and WT cells (Ly5.2) showed no difference in the percentage of mice engrafted or peripheral blood (PB) donor cell chimerism at 4 and 16 weeks post-injection (**Figure 3.4 B and C**). Dr. Samanta Antonella Mariani, Chris Vink and Dr. Carmen Rodriguez Seoane helped dissecting and preparing the mouse embryos. Dr. Carmen Rodriguez Seoane performed the embryo's genotypes. Chris Vink performed the transplantations. Dr. Samanta Antonella Mariani performed the FACS analyses.

Donor cell chimerism in the bone marrow **(Figure 3.5 A)**, spleen (**Figure 3.5 B)**, thymus (**Figure 3.6 A)**, and lymph nodes (**Figure 3.6 B)** of cKO recipients at 18 weeks post-transplantation was also equivalent to WT cell transplanted controls **(Figure 3.6 C)**. Dr. Samanta Antonella Mariani and Chris Vink helped harvesting the mouse tissues. Dr. Antonella Mariani performed the FACS analyses.

Thus, Gpr56 appears to be dispensable for engraftment by large numbers of FL HSCs.

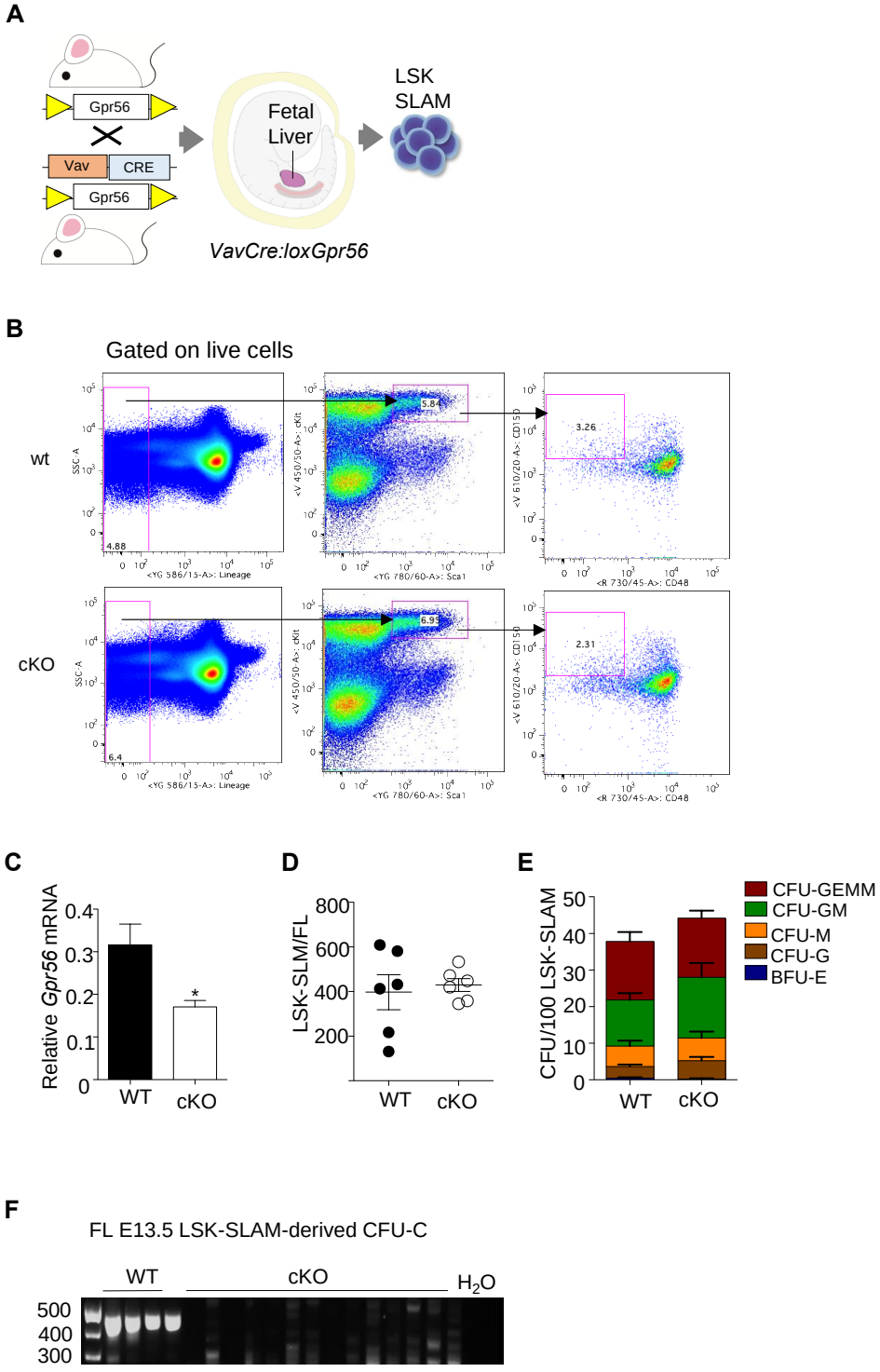

Figure 3.3 Functional analyses of *VAV-Cre* FL *Gpr56* cKO LSK-SLAM population

(A) Experimental setup for E13.5 fetal liver (FL) HPC analyses. **(B)** Flow cytometry gating strategy to sort FL LSK-SLAM cells. **(C)** Relative expression of *Gpr56* in WT and *VAVCre:loxGpr56* cKO LSK-SLAM sorted E13.5 FL cells normalized to *β-actin* by qRT-PCR analysis (n=5). Mean±SEM are shown. *p≤0.05. **(D)** Number of LSK-SLAM cells per

WT and cKO E13.5 FL (n=6). Mean±SEM are shown. **(E)** Number of CFU per WT and cKO E13.5 FL LSK=SLAM cells (n=4). Distinct colony types are indicated. Mean±SEM are shown. (F) Genomic PCR analysis verifying *Gpr56* deletion in individual colonies (containing >50 cells) generated from WT control (4 CFU-C) and conditional knockout (cKO) *VAVCre:loxGpr56* (14 CFU-C) E13.5 fetal liver cells. Dr. Samanta Antonella Mariani, Chris Vink and Dr. Carmen Rodriguez Seoane helped dissecting and preparing the mouse embryos. Dr. Carmen Rodriguez Seoane performed the embryo's genotypes.

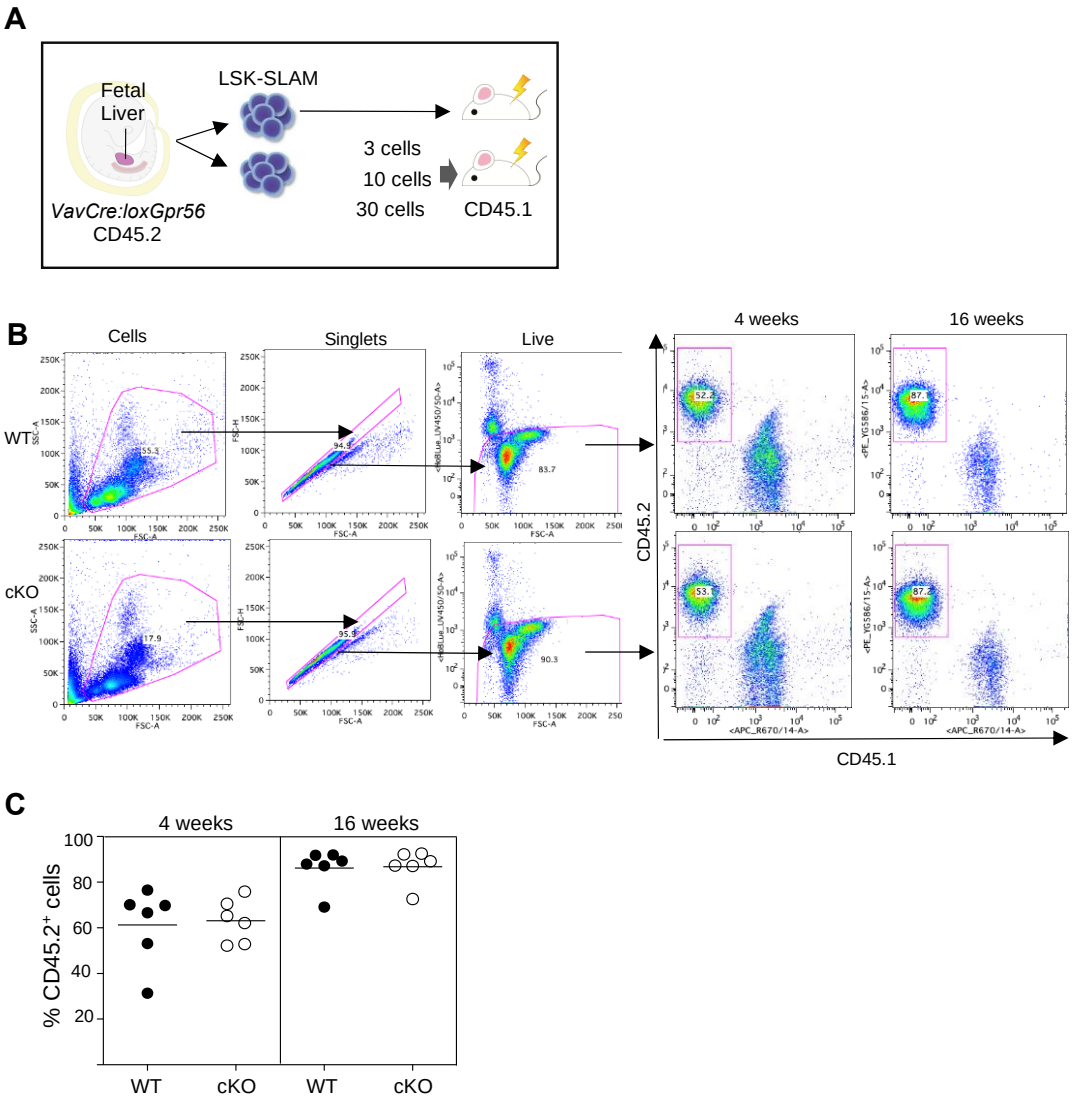

Figure 3.4 Assessment of repopulation activity of transplanted FL-LSK SLAM population in recipient PB.

(A) Experimental setup for *in vivo* transplantation of E13.5 fetal liver (FL) bulk cells and limiting dilutions of sorted LSK-SLAM cells **(B)** Representative gating strategy to assess the frequency of the donor-derived blood cells in recipient PB. Live blood cells (Hoechst-) were analysed for CD45.2 (donor) and CD45.1 (recipient) cell surface markers. **(C)** Peripheral blood (PB) analysis at week 4 and 16 post-transplant. Dr. Samanta Antonella Mariani, Chris Vink and Dr. Carmen Rodriguez Seoane helped dissecting and preparing the mouse embryos. Dr. Carmen Rodriguez Seoane performed the embryo's genotypes. Chris Vink performed cell transplantations. Dr. Samanta Antonella Mariani performed the FACS analyses.

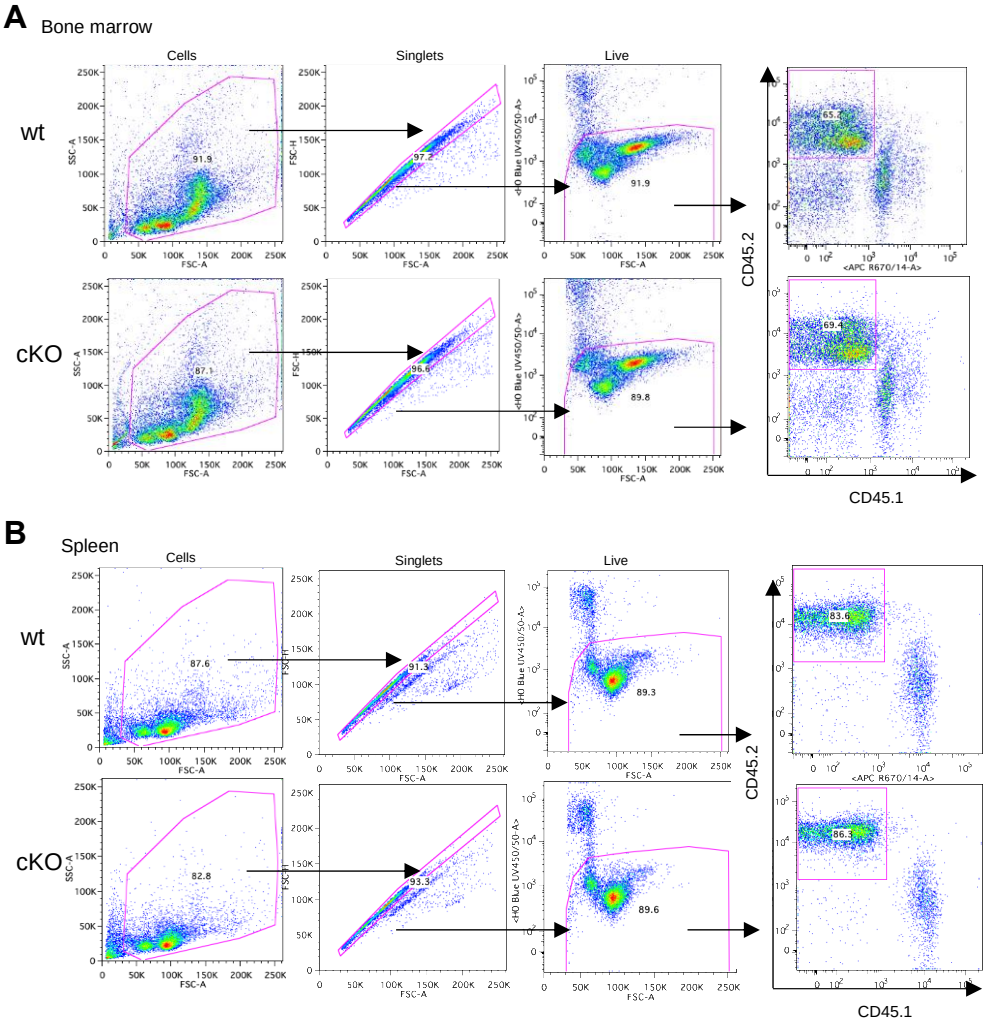

Figure 3.5 Repopulation activity of transplanted FL-LSK SLAM population in other organs.

Representative flow cytometry gating strategy to assess the frequency of the donor-derived blood cells in the bone marrow **(A)** and the spleen **(B)** of recipient mice. Live blood cells (Hoechst-) were resolved for CD45.2 (donor) and CD45.1 (recipient) cell surface markers. Dr. Samanta Antonella Mariani and Chris Vink helped harvesting the mouse tissues. Dr. Antonella Mariani performed the FACS analyses.

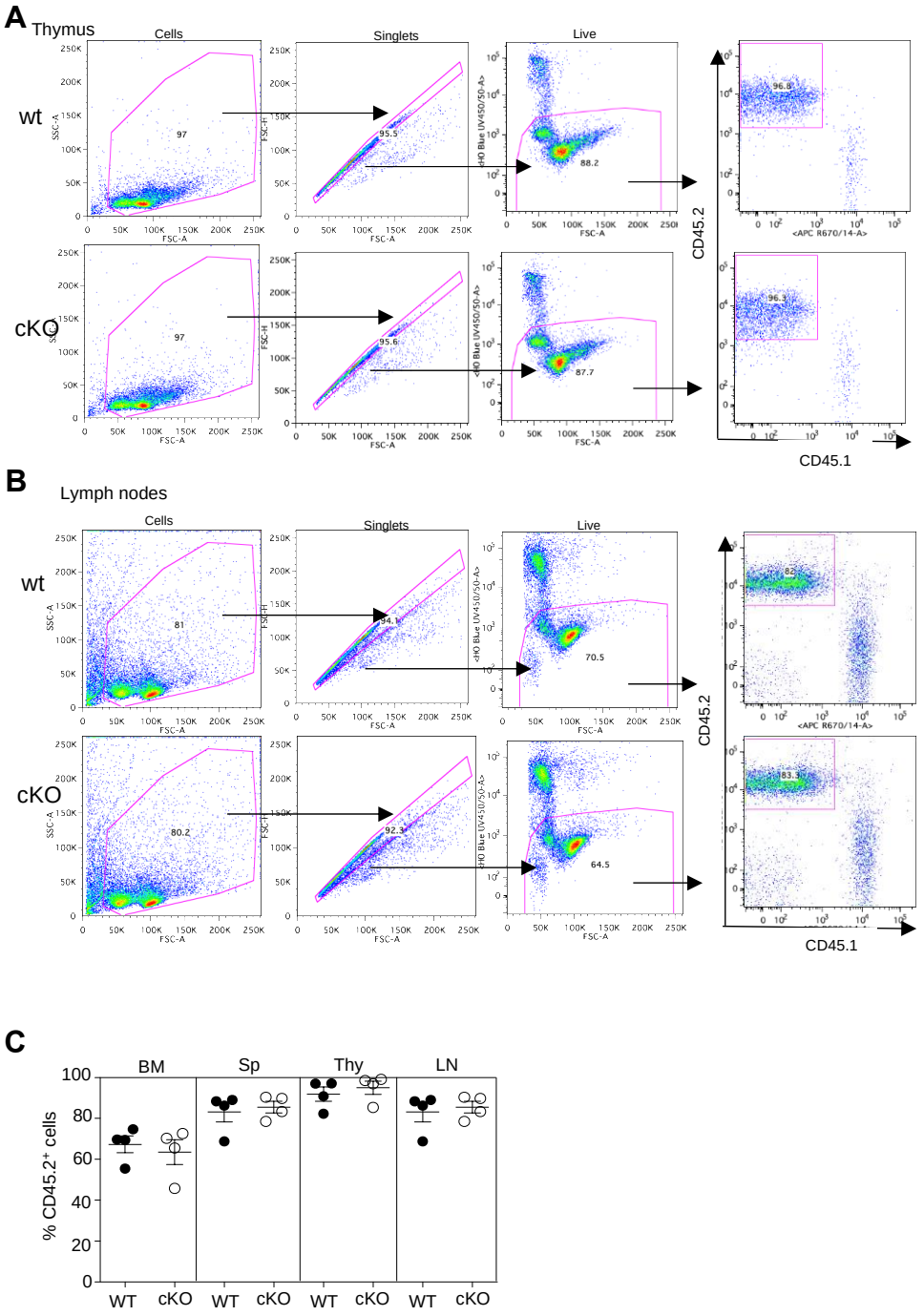

Figure 3.6 Repopulation activity of transplanted FL-LSK SLAM population in other organs.

Representative flow cytometry gating strategy to assess the frequency of the donor-derived blood cells in the thymus **(A)** and the lymph nodes **(B)** of recipient mice. Live blood cells (Hoechst-) were resolved for CD45.2 (donor) and CD45.1 (recipient) cell surface markers. **(C)** Hematopoietic tissues at week 18 post-transplant. Analysis is by Ly5.1/Ly5.2 flow cytometry. Mean±SEM are shown. n=6 per group. BM=bone marrow; Sp=spleen; Thy=thymus;

LN=lymph nodes. Dr. Samanta Antonella Mariani and Chris Vink helped harvesting the mouse tissues. Dr. Antonella Mariani the FACS analyses.

3.2.3 Clonal *in vivo* transplantation reveals a role for Gpr56 in self-renewal and maintaining balanced and lymphoid-biased fetal liver HSCs

To understand if Gpr56 affects HSC quality and/or function in a clonal *in vivo* transplantation scenario, 3, 10 and 30 LSK-SLAM FL cells (Ly5.2) from E13.5 *VAVCre:loxGpr56* embryos and WT littermates were injected into irradiated adult recipient mice (Ly5.1). Engraftment level of ≥5% donor-derived cells was used as the criterion for reconstitution. Injection of 3 LSK-SLAM cells from cKO and WT FLs failed to reconstitute. Injection of 10 or 30 LSK-SLAM FL WT cells (black squares) led to long-term (23 week) reconstitution in 75% (12 of 16) of recipients, whereas only 50% (8 of 16) of recipients receiving 10 or 30 cKO cells (white squares) showed reconstitution **(Figure 3.7 and 3.8).** Dr. Samanta Antonella Mariani and Chris Vink helped performing FACS analyses.

At both 16 and 23 weeks post-injection of 30 cells, significant decreases were found in the average percentage donor chimerism in the PB of cKO recipients as compared to WT (**Figure 3.8**). Similar to the PB, the percentage donor cell chimerism was decreased in the bone marrow (BM) (Figure 3.9 A), spleen (Sp) (Figure 3.9 B), lymph nodes (LN) (Figure 3.10 A) and thymus (Thy) (Figure 3.10 B) of these recipients (**Figure 3.10 C**), thus confirming HSC dysfunction. *Gpr56* downregulated expression was verified in CD45.2+ LSK cells isolated from the PB of these cKO transplanted animals (**Figure 3.11 A**). Dr. Samanta Antonella Mariani, Chris Vink helped performing FACS analyses.

To further examine qualitative effects of Gpr56 deletion on FL HSC reconstitution, the donor-derived lymphoid-myeloid ratio was examined in the PB of the cKO and WT E13.5 LSK-SLAM FL reconstituted recipients at 23 weeks post-injection (**Figure 3.11 B**). Lineage output was determined by B plus T lymphoid cell percentages to granulocyte plus macrophage percentages ($B+T^{value}/G+M^{value}$), with ratios of >10, 10-3 and 3-0 considered lymphoid-biased, balanced or myeloid-biased respectively

(Sieburg, Cho et al. 2006). Flow cytometry with markers for myeloid (granulocytes and macrophages, G-M) and lymphoid (B and T cell, B-T) lineages showed lymphoid-biased and balanced lineage output in the PB of the 12 recipients injected with WT HSCs, whereas PB of the 10 recipients of cKO HSC clones yielded myeloid-bias and balanced lineage output, and only 2 with lymphoid-bias (**Figure 3.11 C**). Examination of BM cell lineage representation showed a similar myeloid-bias by the cKO cell recipients: WT recipients showed all three outputs whereas cKO recipients showed only lymphoid- and myeloid-biased outputs (**Figure 3.11 D and E).** Secondary transplantations were performed with BM Ly5.2 cells from several of the primary recipients (**Figure 3.11 F)** to examine HSC self-renewal. None of the 12 recipients of cKO cells were repopulated, whereas 4 out of 12 recipients of WT cells showed PB chimerism from 2.5-15.3%. Dr. Samanta Antonella Mariani performed the FACS analyses. Chris Vink performed the transplantations.

Together, these data suggest that Gpr56 maintains the *in vivo* quality of HSCs, preserving HSC self-renewal and lineage (balanced, lymphoid-biased) output.

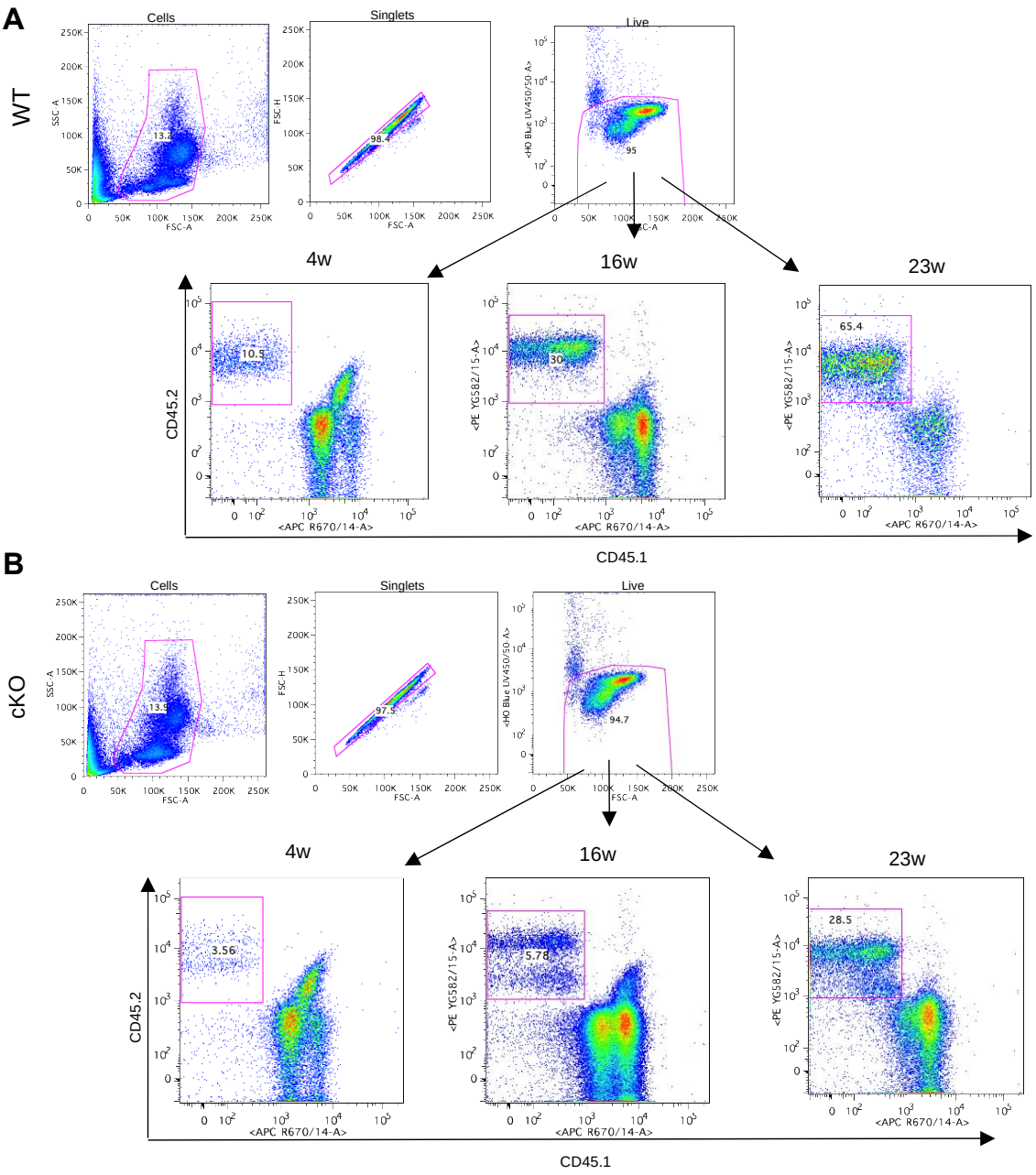

Figure 3.7 Flow cytometry strategy to assess the engraftment potential of clonal transplanted FL LSK-SLAM donor cells.

Representative gating strategy to assess the engraftment of FL-derived WT **(A)** and *VAV-Cre* **(B)** LSK-SLAM population in the PB of recipient mice. Live blood cells (Hoechst-) were analysed for CD45.2 (donor) and CD45.1 (recipient) cell surface markers. Dr. Samanta Antonella Mariani, Chris Vink helped performing FACS analyses.

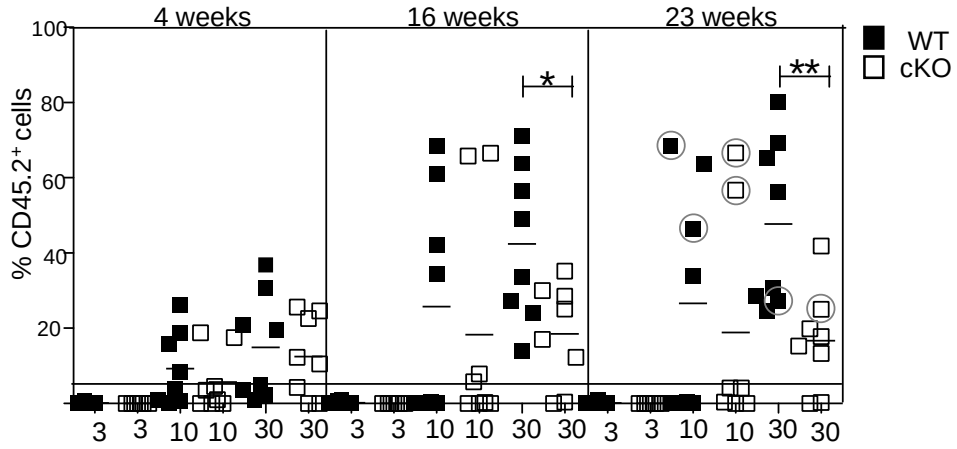

Figure 3.8 Engraftment potential of Gpr56 cKO *VAV-Cre* clonal FL-LSK-SLAM donor-cells.

Percentage of donor cell engraftment of individual adult irradiated recipient mice as measured by Ly5.1/Ly5.2 flow cytometry of peripheral blood at 4, 16 and 23 weeks post- injection of 1, 3 and 10 LSK-SLAM E13.5 FL cells. Wild type controls (WT=black) and *VAVCre:loxGpr56* knockout (cKO=white). n=8 per group. Horizontal line at 5% indicates cutoff for reconstitution. Horizontal lines indicate average percentage engraftment. Circled individual symbols indicate mice used for secondary transplantations. *p0.05; **p0.01. Dr. Samanta Antonella Mariani performed the FACS analyses. Chris Vink performed the cell transplantations.

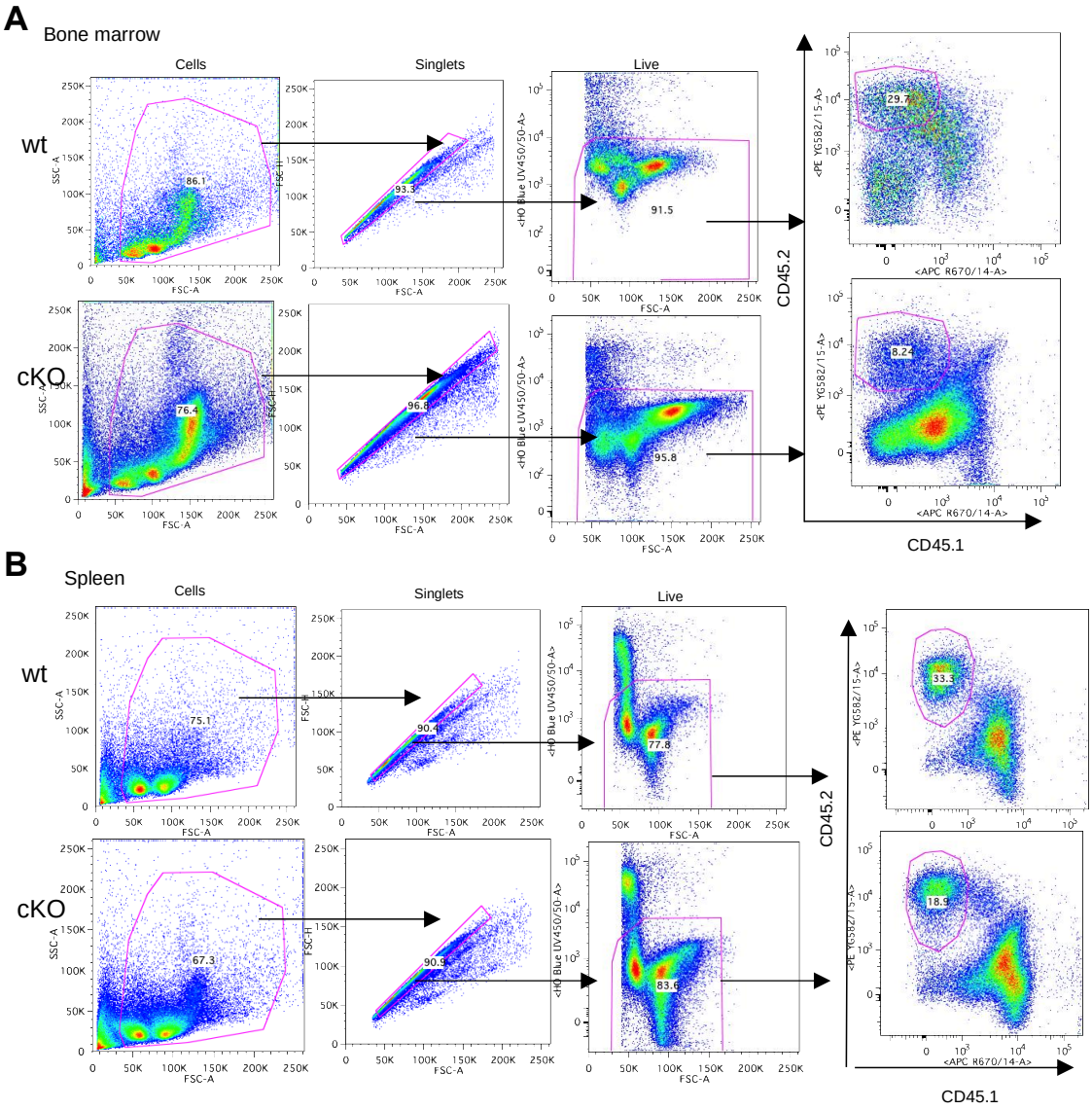

Figure 3.9 Repopulation activity of clonal transplanted FL-LSK SLAM population in different organs.

Representative flow cytometry gating strategy to assess the frequency of the donor-derived blood cells in the bone marrow **(A)** and the spleen **(B)** of recipient mice. Live blood cells (Hoechst-) were resolved for CD45.2 (donor) and CD45.1 (recipient) cell surface markers. Dr. Samanta Antonella Mariani and Chris Vink helped harvesting the tissues and performing the FACS analyses.

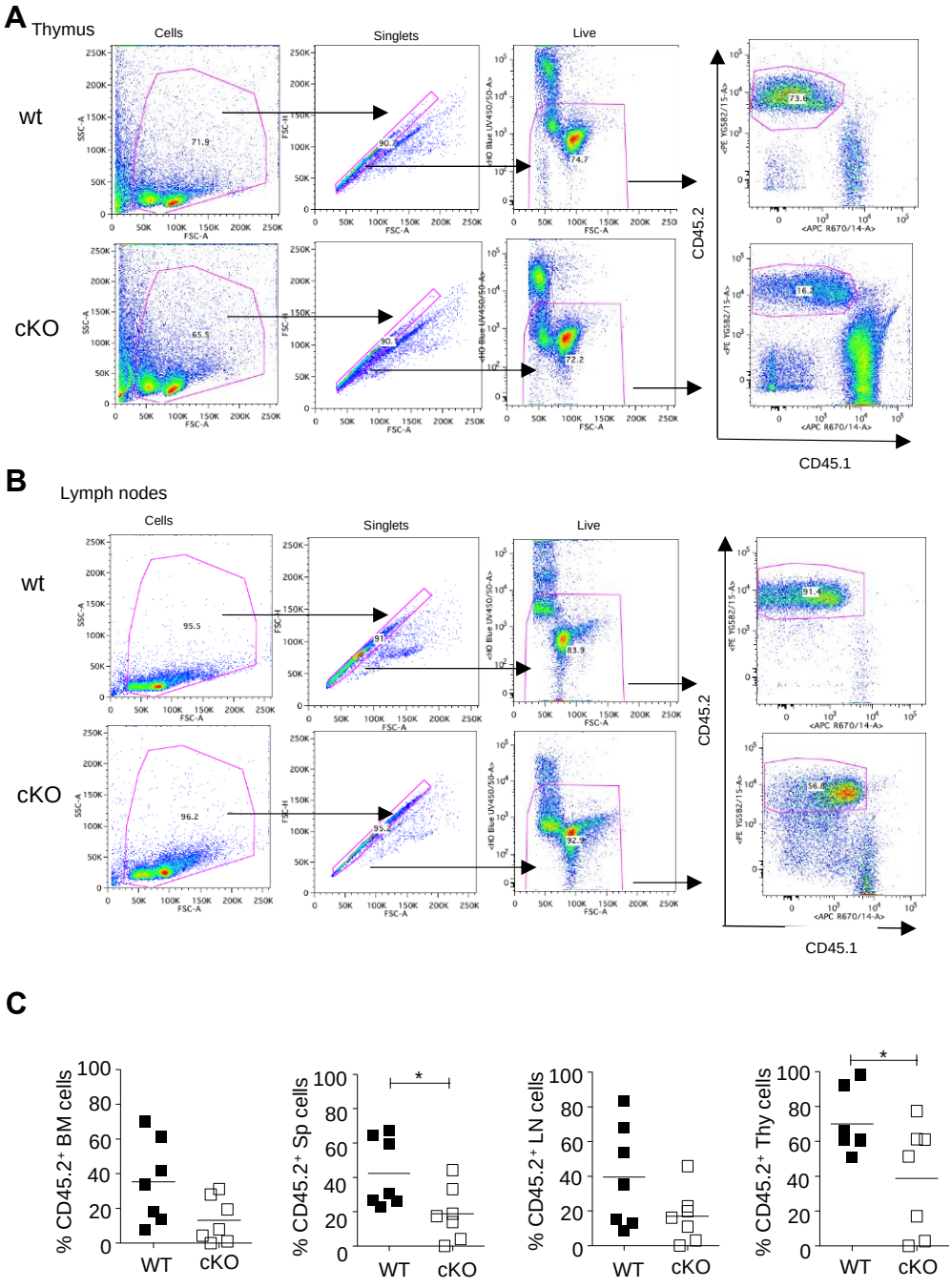

Figure 3.10 Repopulation activity of clonal transplanted FL-LSK SLAM population in different organs.

Representative gating strategy to assess the engraftment of FL-derived WT (A) and *VAV-Cre* (B) LSK-SLAM population in the PB of recipient mice. Live blood cells (Hoechst-) were analysed for CD45.2 (donor) and CD45.1 (recipient) cell surface markers. Dr. Samanta Antonella Mariani and Chris Vink helped harvesting the tissues and performing the FACS analyses.

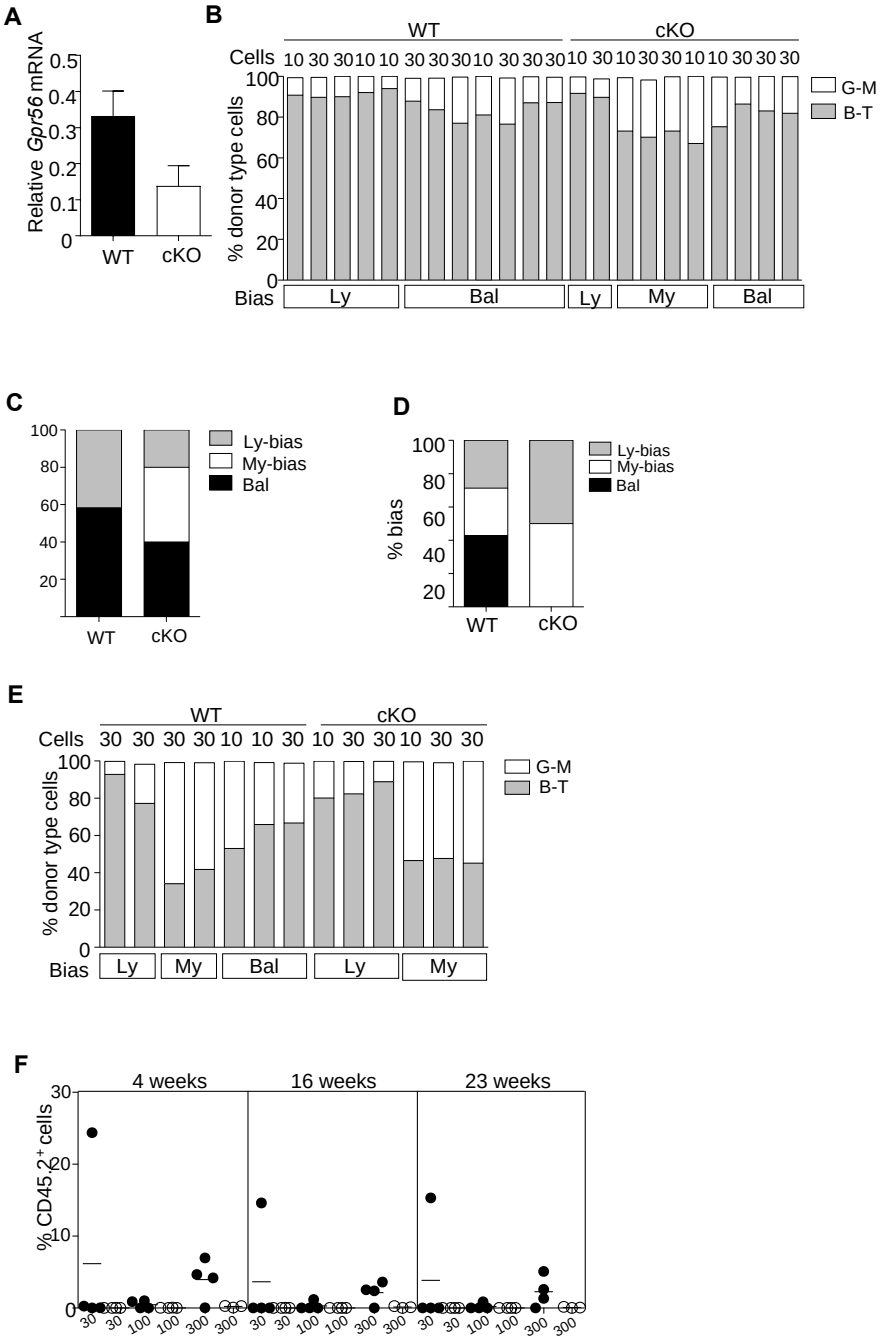

Figure 3.11 Blood lineage analyses of Gpr56 cKO FL-HSCs

(A) RT-qPCR relative expression of Gpr56 normalized to *b-actin* in LSK BM cells from primary recipients injected with WT and *VAVCre:loxGpr56* cKO sorted E13.5 FL cells (n=5).

Mean±SEM are shown. **(B)** Percentage of lymphoid and myeloid cell contribution in PB of 22 individual adult irradiated recipient mice as measured by flow cytometry of peripheral blood at 23 weeks post-injection of 10 and 30 LSK-SLAM WT control and *VAVCre:loxGpr56* cKO E13.5 FL cells. Ly=lymphoid bias; B=balanced; My=myeloid bias. >87% B-T=Ly; 75- 87% B-T=B; <75% B-T=My. **(C)** Percentage of lymphoid, balanced and myeloid biased recipients in the cohort of 12 WT and 10 cKO FL LSK-SLAM cell transplant adult irradiated mice in Figure 4.4 B. **(** (**D)** Percentage of BM lymphoid, balanced and myeloid biased recipients in the cohort of 7 WT and 6 cKO FL LSK-SLAM cell transplanted adult irradiated mice. **(E)** Percentage of lymphoid and myeloid cell contribution in bone marrow (BM) of 13 individual adult irradiated recipient mice as measured by flow cytometry of peripheral blood at 23 weeks post-injection of 10 and 30 LSK-SLAM WT control (n=7) and *VAVCre:loxGpr56* cKO E13.5 FL cells (n=7). Ly=lymphoid bias; B=balanced; My=myeloid bias. >87% B-T=Ly; 75-87% B-T=B; <75% B-T=My.**(F)** Donor cell-derived chimerism of PB of secondary recipient mice at 4, 16 and 23 weeks post-transplantation of bone marrow LSK cells from primary recipients of WT and *VAVCre:loxGpr56* cKO sorted E13.5 FL cells. Percentage of CD45.2+ donor cells in PB is shown. Horizontal lines indicate average engraftment percentage. WT=black; cKO=white. n=4 per group. Dr. Samanta Antonella Mariani performed the FACS analyses. Chris Vink performed the transplantations.

4 GPR56 IS EXPRESSED IN ESC-DERIVED HEMATOPOIETIC PROGENITOR CELLS

The work presented in this chapter was accepted for publication as:

A. Maglitto, S.A. Mariani, E. de Pater, C. Rodriguez Seoane, C.S. Vink, X. Piao, M-L Lukke and E. Dzierzak. *Unexpected redundancy of Gpr56 and Gpr97 during hematopoietic cell development and differentiation.* Blood Advances.

To further examine the role of Gpr56 during hematopoietic development and lineage differentiation, we took advantage of our unique *Gata2Venus* (*G2V*) mouse reporter ESC line (Kaimakis, de Pater et al. 2016) which, upon *in vitro* differentiation, facilitates the isolation of large numbers HSPCs for molecular and functional analyses (Kaimakis, de Pater et al. 2016, Kauts, Rodriguez-Seoane et al. 2017). We previously found that only the Venus-expressing (V^+) cell fraction of *G2V* ESC hematopoietic differentiation cultures contains hematopoietic potential. *G2V* ESCs were differentiated towards the hematopoietic lineage, harvested at several time points and tested for *Gpr56* mRNA and protein expression (**Figure 4.1 A**). RT-qPCR analysis on cells from unsorted day (d) 0, 6, 10 and 12 differentiation cultures showed significant increases in *Gpr56* transcript levels (**Figure 4.1 B**). When V^+ and V^- cell fractions of *G2V* ESC differentiation cultures were sorted (**Figure 4.1 C and D**), *Gpr56* expression significantly increased in the V^+ cells, reaching a maximum threshold at d10 and 12 (**Figure 4.1 E**). The low level of *Gpr56* expression found in non-hematopoietic V^- cells was expected (Ackerman, Garcia et al. 2015). Western blotting of whole cell extracts from unsorted differentiated *G2V* ESC showed Gpr56 protein expression at d12 compared to d0 (**Figure 4.1 F, left**). Moreover, Gpr56 protein expression at d12 of *G2V* ESC hematopoietic differentiation was much higher in the V^+ fraction as compared to the V^- fraction (**Figure 4.1 F, right**). Dr. Mari-Liis Lukke performed the western blotting analyses. Members of the QMRI FACS Facility helped on setting the

FACS strategy. Thus, the *G2V* ESC line is a suitable platform to examine the role of Gpr56 during *in vitro* hematopoietic differentiation.

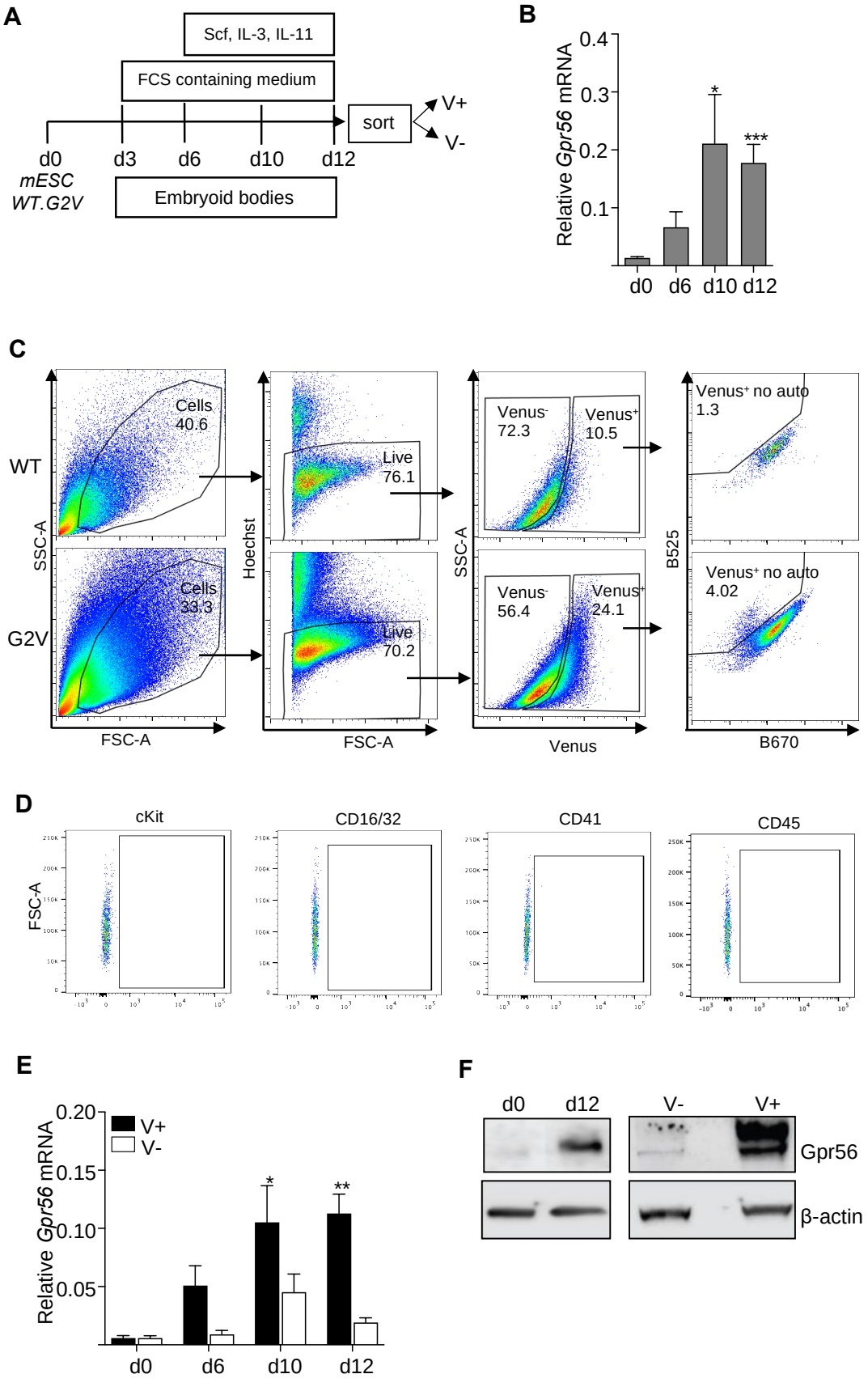
A
Scf, IL-3, IL-11
FCS containing medium
sort
V+
V-
d0
d3
d6
d10
d12
mESC
WT.G2V
Embryoid bodies
B
Relative Gpr56 mRNA
0.4
0.3
0.2
0.1
*
***
d0
d6
d10
d12
C
WT
G2V
Cells
40.6
Cells
33.3
SSC-A
FSC-A
Hoechst
Live
76.1
Live
70.2
Venus-
72.3
Venus+
10.5
Venus-
56.4
Venus+
24.1
Venus
Venus+ no auto
1.3
Venus+ no auto
4.02
B525
B670
D
cKit
CD16/32
CD41
CD45
FSC-A
E
Relative Gpr56 mRNA
0.20
0.15
0.10
0.05
V+
V-
*
**
d0
d6
d10
d12
F
d0
d12
V-
V+
Gpr56
β-actin

Figure 4.1 Gpr56 is expressed during ESC hematopoietic differentiation.

(A) ESC differentiation culture methodology. Mouse *Gata2Venus (mG2V)* ESC (wild type (WT) and 56^{KO} were differentiated in hematopoietic factor-containing medium for 12 days and unsorted/sorted $Venus^{+}$ (V^{+}) and $Venus^{-}$ (V^{-}) cells were examined for *Gpr56* mRNA (RT-qPCR) and Gpr56 protein (Western blot; WB) expression. (**B)** Time course RT-qPCR analysis of relative *Gpr56* expression (normalized to *β–actin*) in unsorted *G2V* ESC hematopoietic differentiation cultures. **(C)** Example of the gating strategy used to enrich V+ and V- fractions. Forward scatter (FSC), side scatter (SSC), Venus, and Venus minus autofluorescence plots are shown. Forward scatter (FSC), side scatter (SSC), Venus, and Venus minus autofluorescence plots are shown in upper panels. After gating on live cells, the Venus+ cells are plotted against a dump neighbor channel (B525-Venus vs B670) to exclude auto-fluorescent cells. Only the cells positive in the B525 channel and not in the B670 channel are considered Venus+. WT cells are used as control to set the gates. Fluorescent minus one (FMO) controls for cKit, CD16/32, CD41, CD45 antibodies in lower panels. **(D)** Fluorescent minus-one (FMOs) controls for cKit, CD16/32, CD41 and CD45 antibodies **(E)** Time course qRT-PCR analysis of relative *Gpr56* expression (normalized to *β-actin*) in Venus-sorted *G2V* ESC hematopoietic differentiation cultures. (**F)** Western blot analysis of Gpr56 protein expression in day 0 and day12 unsorted *G2V* ESC hematopoietic differentiation cultures (left panel) and day 12 Venus sorted *G2V* ESC hematopoietic differentiation cultures (right panel), with β–actin as protein normalization control. The two bands correspond to different Gpr56 forms: native (upper, 75kDa) and cleaved activated (lower, 62kDa) receptor. Gpr56 has a self-proteolytic domain that cleaves the N-terminal ligand binding domain in the presence of ligand, thus decreasing the size of the active receptor. The bulk population does not show the double band as the majority of the cells express Gpr56 in the native state (not active). When we enrich for the $Venus^{+}$ HPC population, we observe the second lower band, presumably indicating cleaved receptor, n=2. Dr. Mari-Liis Lukke performed the western blotting analyses. Members of the QMRI FACS Facility helped on setting the FACS strategy.

4.1.1 *Gpr56* knockout affects hematopoietic output during ESC differentiation

To test if Gpr56 affects ESC hematopoietic differentiation, *Gpr56* knockout *G2V* ESC lines (56^{KO}) were generated by *CRISPR/Cas9* gene editing. *Gpr56* is located on mouse chromosome 8, has 14 exons and a coding sequence of 2064 base pairs (**Figure 4.2)**. Guide RNA (gRNA) to exon 2 (common to all transcript variants) were cloned into *pSP-Cas9-2A-GFP* and transfected into *G2V* ESCs (**Figure 4.3 A**). At 48 hours post transfection, ~10% of *G2V* ESCs were GFP^+ (**Figure 4.3 B & C**). Single viable GFP^+ cells were expanded on MEFs and clones established. Two undifferentiated GFP^+ ESC clones, #5 and #21, were examined by Western blot (**Figure 4.3 D**) and showed a complete lack of Gpr56 protein as compared to wild type (WT; #1 and #2) undifferentiated *G2V* ESC clones. RT-qPCR analysis revealed a total absence of *Gpr56* transcripts in clone #5 (Figure 4.3 E) and #21 (Figure 4.3 F) following d6, 10 and 12 of *in vitro* differentiation as compared to WT differentiated ESC, thus confirming the successful knockout of *Gpr56*. However, karyotype on $G2V.56^{ko}$ ESC lines (#5 and #21) remains to be assessed to exclude genomic anomalies. Dr. Mari-Liis Lukke performed the wester blotting analyses.

Flow cytometry for HPC frequencies (McGrath, Frame et al. 2015) and CFU-C analyses were performed on cells from d6 (primitive HPCs) (**Figure 4.4 A, B, C)** and d10 (EMPs) (**Figure 4.5 A, B, C, D**) differentiated 56^{KO} and WT ESC cultures. After gating out autofluorescent cells, the percentage of V^+ cells in the d6 and d10 56^{KO} (#5 and #21) cultures was found to be significantly increased (2.8±0.95 fold) as compared to the *WT* cultures (**Figures 4.4 B and 4.5 B**). At d6 a significant decrease in the frequency of $cKit^+$ (#5) and $cKit^+CD41^+$ cells in the V^+ fraction (#5 and #21) of 56^{KO} cultures was found compared to WT (**Figure 4.4 B)**, whereas d10 56^{KO} ESC differentiation cultures showed a significant increase in $cKit^+$ (#5 and #21; 1.3±0.2) and phenotypic EMP percentages (#21; 3±1.3) **(Figure 4.5 B)**.

When d6 56^{KO} V^+ cells were tested for HPC function, we found a 4-fold reduction in the number of CFU-C/10^4 V^+ cells for both 56^{KO} clones as compared to WT, indicating an almost complete absence of hematopoietic progenitor potential (**Figure 4.4 C**). In contrast, V^+ cells from d10 56^{KO} (#5 and #21) differentiation cultures revealed a trend

(p=0.33 and p=0.68) towards increased numbers of CFU-C/10^4 cells as compared to *WT* V^+ cells (**Figure 4.5 C**). A trend in the total number of CFU-C colonies was observed for both clones (**Figure 4.5 D**). Hence, the reduction in primitive early HPCs and the contrasting increase in the EMPs at d10 of 56^{KO} ESC differentiation agrees with *in vivo Gpr56* cKO results and suggests that Gpr56 plays different roles at distinct development times and/or distinct emerging cells.

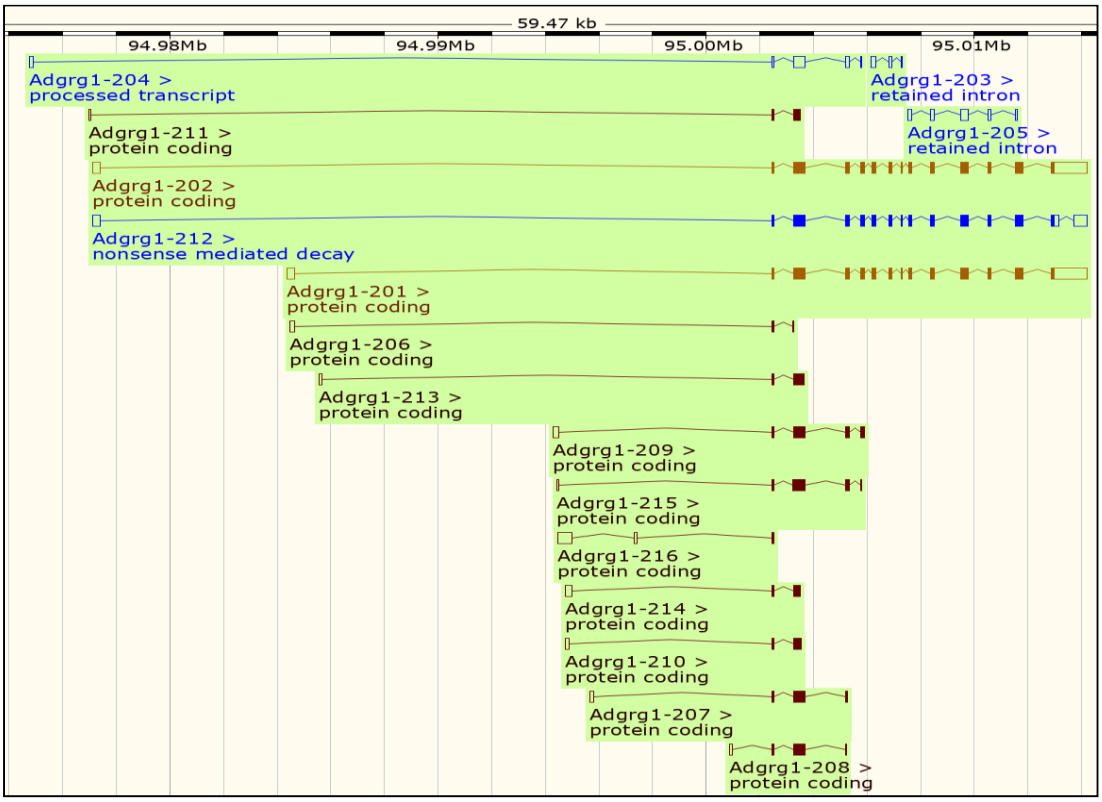

Figure 4.2 *Gpr56* gene and isoforms as taken from Ensembl genome browser.

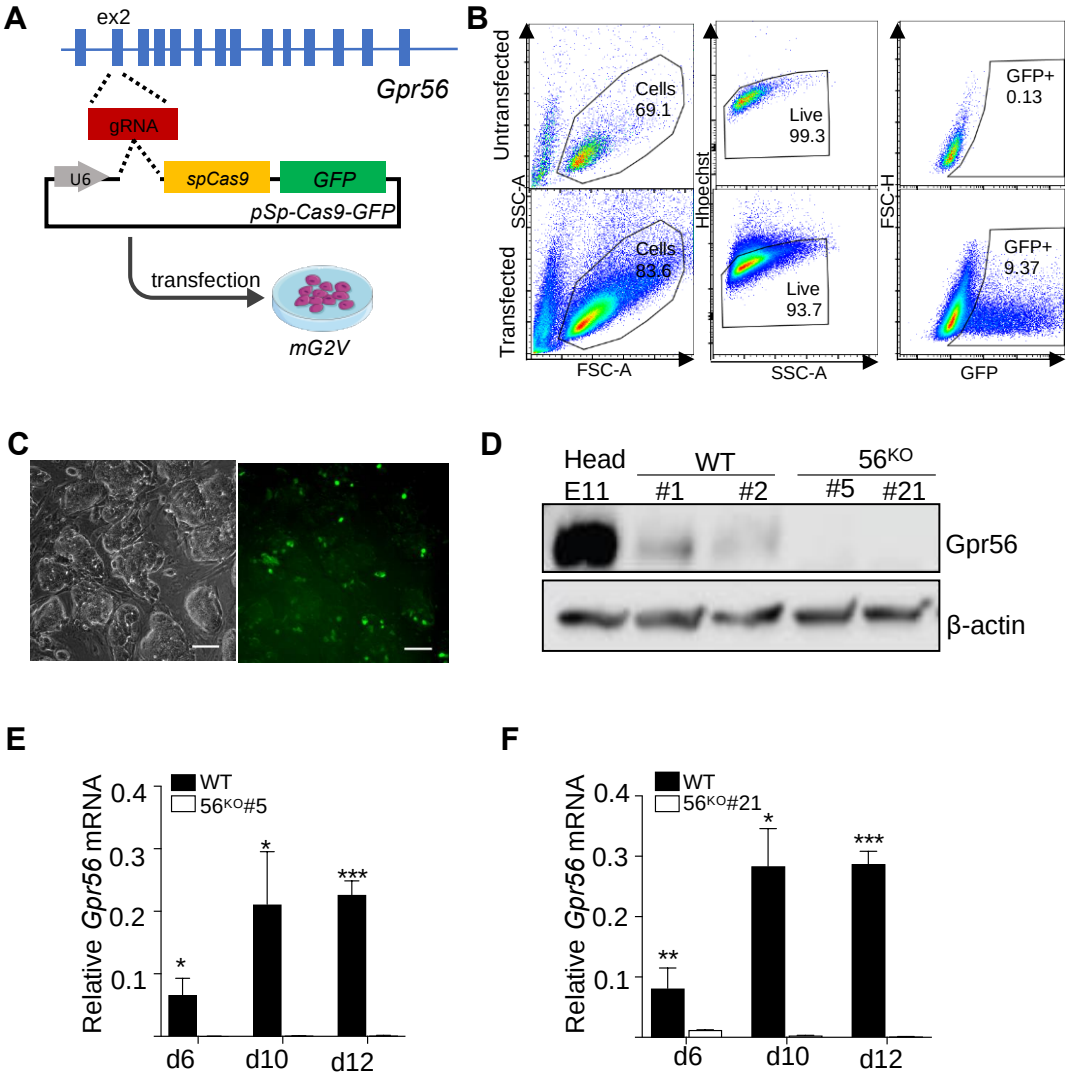

Figure 4.3 Generation of *Gpr56*-deleted G2V ESCs

(**A)** *CRISPR/Cas9* strategy showing *gRNA* for *Gpr56* exon 2 and insertion in *pSp-Cas9-2A-GFP* vector used for transfection of *G2V* ESCs. (**B)** Flow cytometric analysis of transfected and untransfected control ESCs for forward (FSC) and side scatter (SSC), viability and GFP expression. (**C)** Fluorescence microscopic images of untransfected and transfected ESCs at 48 hours post- transfection (bright field on the left, GFP on the right). **(D)** Western blot analysis of Gpr56 protein expression in day 6 *G2V.WT* (clones 1 and 2) and *56^{KO}* (clones 5 and 21) ESCs, with β–actin as protein normalization control. **(E)** Time course RT-qPCR analysis of relative *Gpr56* expression (normalized to *β–actin*) in unsorted *G2V.WT* and *G2V. 56^{KO}* clone #5 and clone #21 **(F)** ESC hematopoietic differentiation cultures. d=day of culture harvest; n=3, Mean±SEM. *p≤0.05: **p≤0.01; ***p≤0.001. Dr. Mari-Liis Lukke performed the wester blotting analyses.

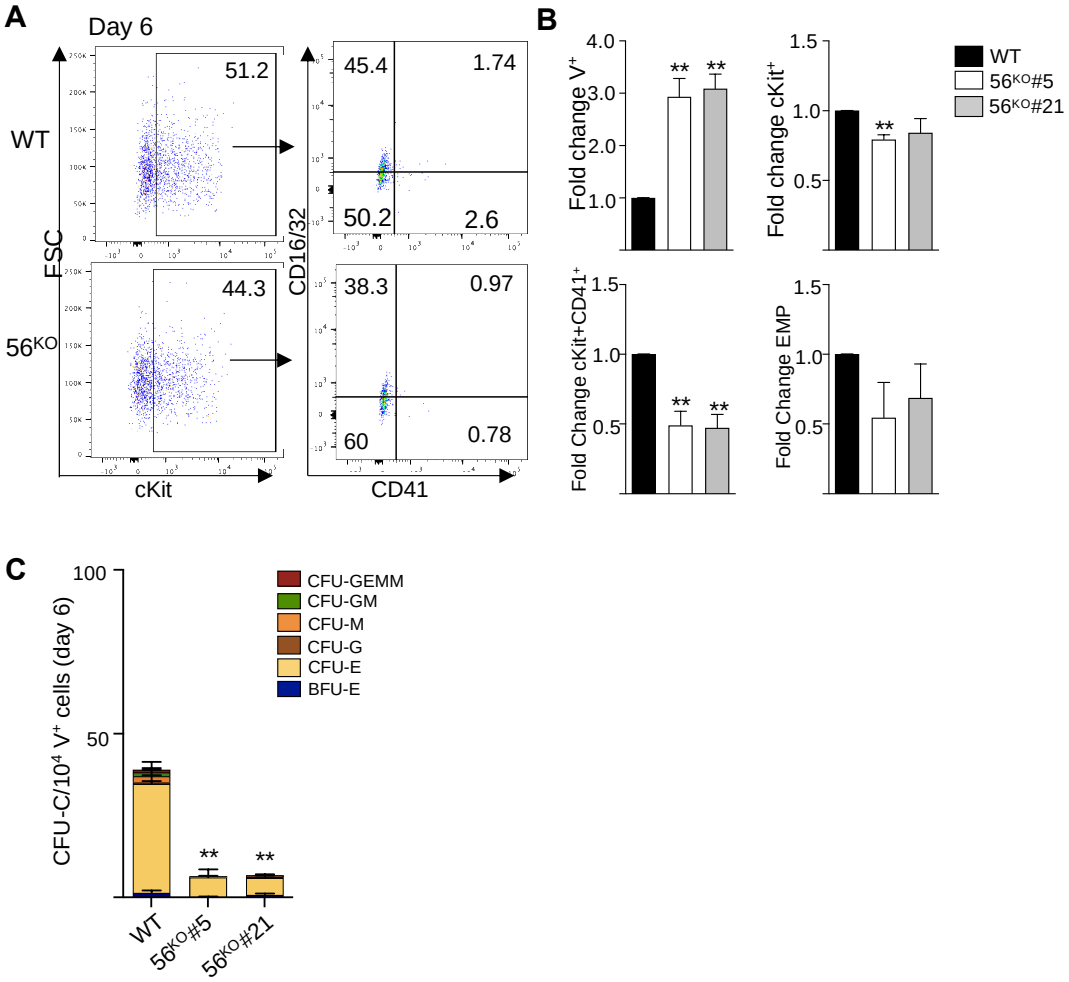

Figure 4.4 Output of Gpr56-KO derived hematopoietic and progenitor cells in the primitive wave (day 6) of *in vitro* hematopoiesis.

Representative flow cytometric plots of (**A)** day 6 *G2V.WT* and *G2V.56^{KO}* differentiation cultures showing percentages of CD16/32 and CD41 cells in cKit^{+} gated in Venus+. V+cKit^{+}CD41^{+}CD16/32^{+} = EMP (erythro-myeloid progenitors), n=3. **(B)** Fold change in the percentages (Mean±SEM) of Venus^{+}, cKit^{+}, cKit^{+}CD41^{+} and EMPs (n=3). **(C)** CFU-C per 10,000 V+ plated cells are shown. Distinct colony types are indicated by colour. n=3; Mean±SEM; CFU-GEMM=granulocyte, erythroid, megakaryocyte, macrophage; -GM=granulocyte, macrophage; -G=granulocyte; M=macrophage; E=erythroid; BFU-E=burst forming unit- erythroid (n=3), Mean±SEM. **p≤0.01;

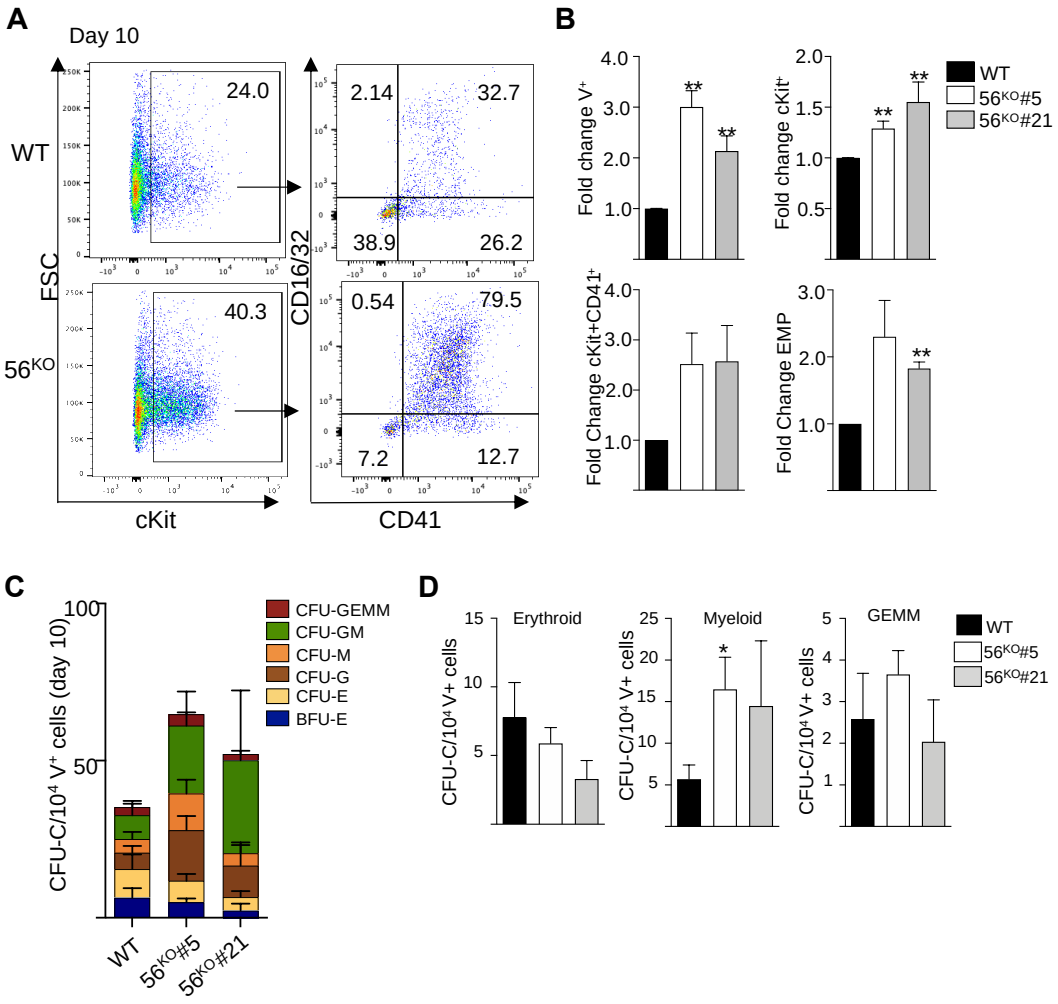

Figure 4.5 Day 10 ESC-derived hematopoietic cell production and progenitor output in the absence of Gpr56.

Representative flow cytometric plots of (**A)** day 10 *G2V.WT* and *G2V.56^{KO}* differentiation cultures showing percentages of CD16/32 and CD41 cells in cKit^{+}, gated in Venus+. V+cKit^{+}CD41^{+}CD16/32^{+} = EMP (erythro-myeloid progenitors). **(B)** Fold change in the percentages (Mean±SEM) of Venus^{+}, cKit^{+}, cKit^{+}CD41^{+} and EMPs. **(C)** CFU-C per 10,000 V+ plated cells is shown. Distinct colony types are indicated by colour. n=3; Mean±SEM; CFU-GEMM=granulocyte, erythroid, megakaryocyte, macrophage; -GM=granulocyte, macrophage; -G=granulocyte; M=macrophage; E=erythroid; BFU-E=burst forming unit-erythroid. **(D)** Frequency of erythroid, myeloid and GEMM CFU types of 56KO#5 and 56KO#21 as compared to the WT cell line, n=3. Mean±SEM. *p≤0.05.

4.1.2 Gpr97 expression is upregulated *in vitro* and *in vivo* in the absence of Gpr56

The discrepancy between the involvement of Gpr56 in HSPC development in zebrafish and mouse embryos may be a result of GPCR redundancy. In mouse, *Gpr56* is genetically linked with *Gpr97* and *Gpr114* within a 122Kbp region (*Gpr114* is 77Kb upstream and *Gpr97* is 48Kb downstream). In zebrafish, *gpr56* and *gpr97* are both on chromosome 7, but distantly located at different ends of the chromosome (**Figure 4.6 A**). Mouse *Gpr97* and *Gpr114* are highly homologous to *Gpr56*. As they are so closely linked and are co-expressed in enriched AGM HSCs 10, they may compensate for Gpr56 loss.

To functionally test redundancy between Gpr56 and Gpr97, we examined whether mouse *Gpr97* and *Gpr114* mRNA, as we have shown for mouse Gpr56 (Solaimani Kartalaei, Yamada-Inagawa et al. 2015), could rescue hematopoietic development in gpr56 morphant zebrafish. Transgenic zebrafish embryos (*CD41GFP* and *Flt1RFP* which report HSPC generation) (**Figure 4.6 B)** were injected with the *gpr56* morpholino (MO) alone or in combination with zebrafish *gpr56*, mouse *Gpr56*, mouse *Gpr97* or mouse *Gpr114* mRNA (**Figure 4.6 C**). Double expressing CD41dimFlt1+ (GFP+RFP+) HSPCs in the caudal hematopoietic cell tissue (CHT) at 48 hpf were counted. Significant increases in the average number of HSPCs were found in *gpr56* morpholino injected with zebrafish *gpr56,* mouse *Gpr56* and mouse *Gpr97* mRNAs versus *gpr56* morpholino controls, and HSPC numbers were equivalent to those found in WT controls. In contrast, mouse *Gpr114* mRNA did not restore production of HSPC (**Figure 4.6 C**). These experiments were performed by Dr.Emma de Pater. Thus, in mouse hematopoietic development, Gpr97 but not Gpr114 may function redundantly in the absence of Gpr56.

To test for possible redundancy of Gpr56 and Gpr97 during mouse embryonic development, we first examined whether WT *G2V* ESCs express Gpr97 at d0, 6, 10 and 12 of hematopoietic differentiation. Gpr97 was not readily detected at d0 and d6, but high expression was found within the V+ fraction, increasing temporally to peak at d10 and d12 (**Figure 4.7 A**). Next, *G2V.56*^{KO} and control ESCs were differentiated for 6 and 10 days and V+ cells were examined for relative *Gpr97* mRNA. As compared

to WT cells, *56^{KO}* cells showed significantly increased *Gpr97* expression at d10 but not d6 (**Figure 4.7 B**), highlighting differences in possible Gpr97 redundancy in the absence of Gpr56 during early and late ESC hematopoietic differentiation.

To understand if *Gpr97* is highly expressed *in vivo* in Gpr56-cKO mouse embryos, Gpr97 expression levels in *VECCre:loxGpr56* and *VAVCre:loxGpr56* cKO embryos (**Figure 4.6 C**) were examined. RT-qPCR analyses on E9.5 YS CD31+ cells showed similar levels of Gpr97 in WT and Gpr56 cKO embryos. In contrast, E13.5 FL LSK-SLAM cells showed a significant upregulated expression of Gpr97 in Gpr56 cKO (~1.5 fold) versus WT cells (**Figure 4.6 C**). Interestingly, relative Gpr97 expression in the donor-derived LSK sorted bone marrow cells from the recipients of 30 cKO E13.5 LSK-SLAM FL cells was not upregulated in the cKO compared to the WT cells (**Figure 4.6 C**). Thus, Gpr97 may function redundantly in late embryonic hematopoietic development both *in vitro* and *in vivo*, but not at early stages or in the adult.

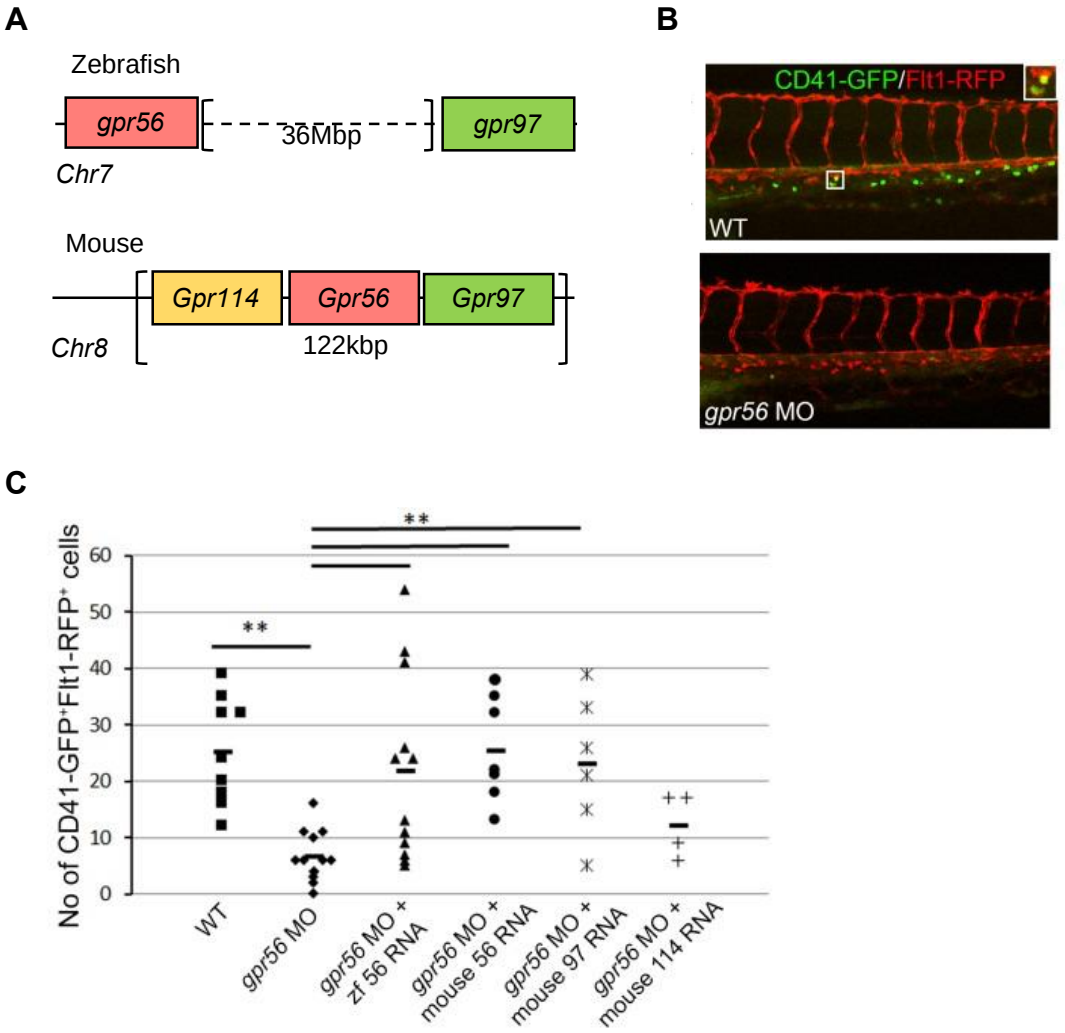

Figure 4.6 *In vivo* experiments to assess Gpr97 redundant function in zebrafish

(A) Schematic of the *Gpr56* locus in zebrafish and mouse. Two highly homologous genes, *Gpr114* and *Gpr97* are located 5' and 3' respectively within the mouse *Gpr56* locus. (**B)** Representative images of CD41GFP^{dim}Flt1RFP^{+} cells (yellow fluorescence) in the caudal hematopoietic tissue (CHT) of *gpr56* morpholino (MO) injected and control (WT) double transgenic zebrafish embryos at 48 hpf. CD41=green; Flt1= red; double positive definitive HSPC=yellow. **(C)** Rescue of HSPC production as determined by the number of CD41GFP^{dim}Flt1RFP^{+} cells in the CHT of WT and *gpr56* morphant zebrafish at 48 hpf when zebrafish *gpr56*, mouse *Gpr56*, mouse *Gpr97* and mouse *Gpr114* mRNA was injected. Number of experiments=2; Number of injected and analysed embryos=9, 12, 12, 7, 6, 4 respectively; bars=mean; **p<0.01. These experiments were performed by Dr.Emma de Pater.

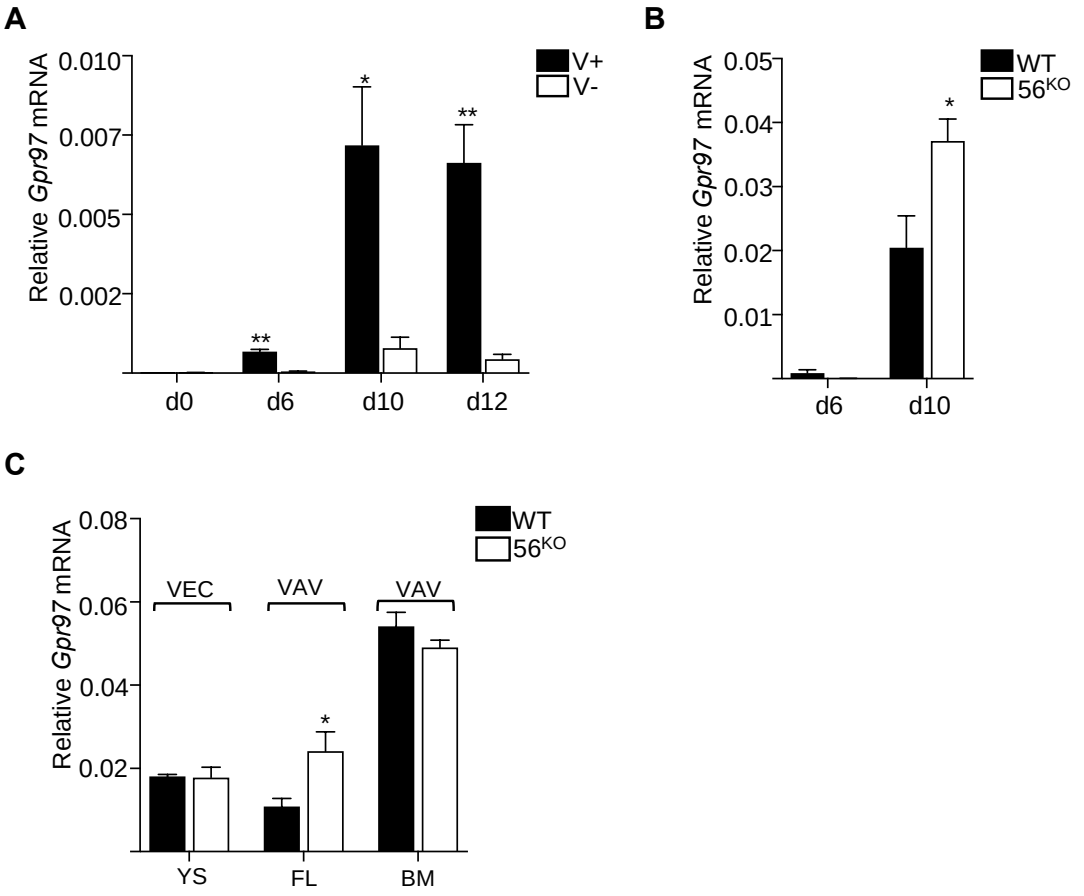

Figure 4.7 *Gpr97* upregulation in mouse ESCs and embryonic tissues

(A) Time course RT-qPCR analysis of *Gpr97* expression relative to β-actin in V+ and V- sorted cell fractions of *G2V* WT ESCs from hematopoietic differentiation cultures n=3. Mean±SEM. **(B)** RT-qPCR analysis of relative *Gpr97* expression (normalized to β-actin) in sorted V+cKit+ fractions of *G2V* WT and 56^{KO} day 6 and day 10 differentiated ESCs. n=3; *p≤0.05. **(C)** RT-qPCR analysis of relative *Gpr97* expression in E9.5 *VECCre:loxGpr56* cKO yolk sac (YS) cells (n=2), E13.5 *VavCre:loxGpr56* cKO fetal liver (FL) cells (n=5) and LSK bone marrow cells (n=5) from primary recipients of *VAVCre:loxGpr56* cKO cells. *p≤0.05.

4.1.3 Simultaneous deletion of both Gpr56 and Gpr97 severely reduces ESC-derived hematopoiesis

To explore the functional contribution of Gpr97 during *in vitro* differentiation upon loss of Gpr56, we generated a mouse *G2V.56^{KO}97^{KO}* ESC line (*56^{KO}97^{KO}*). Guide RNAs (gRNA) designed to target exon 2 and exon 10 were used with CRISPR/Cas9 methodology to knockout out all 5 potential isoforms and/or decay RNA transcripts of *Gpr97* (**Figure 4.8 A**). The *56^{KO}* cell line was transfected with the gRNA plasmid (**Figure 4.8 B**) and 48 hours later cells expressing GFP (6.5%) were single cell deposited into multiwells (**Figure 4.8 C**). Of eleven clones expanded and RT-qPCR screened, 4 clones (B3, C10, H9, H10) showed few/no transcripts. The surveyor assay verified that clone B3 had a mismatch in Gpr97 (**Figure 4.8 D**) and sequencing confirmed the presence of indels in the targeted exons (for more details, see **Appendix A**) The absence of *Gpr97* transcripts in undifferentiated and differentiated (d6 and d10) cells was confirmed by RT-qPCR (**Figure 4.9 B**). Hereafter, the B3 clone (*56^{KO}97^{KO}*) was used for phenotypic and functional studies. Karyotypes on the *G2V.56^{ko}97^{ko}* ESC line remains to be performed to exclude genomic anomalies. Hematopoietic output of d10 differentiated *56^{KO}97^{KO}*, *56^{KO}* and WT ESC was performed by flow cytometry (**Figure 4.9 C**). The same high percentage of viable cells (>90%) was found for all three ESC lines (**Figure 4.10 A**). Whereas the increased percentage of the V+ population in the *56^{KO}* cells was significant and in line with our previous data, *56^{KO}97^{KO}* differentiated cells showed no significant difference in the percentage of V+ cells as compared to WT cells. However, significant decreases in CD45+ hematopoietic cells and CD41+cKit+CD16/32+ (EMP) cells were observed in the *56^{KO}97^{KO}* differentiated cells as compared to WT (**Figure 4.10 A)**. This suggests that Gpr56 together with Gpr97 is involved in hematopoietic cell generation and/or differentiation of ESCs. CFU-C assays were performed to quantitate HPC production in cultures of d10 differentiated *56^{KO}97^{KO}*, *56^{KO}* and *WT* ESCs. V+ cells were sorted, seeded into methylcellulose and colonies scored. In contrast to *56^{KO}* V+ cells in which total CFU-C frequency was similar or slightly increased to WT V+ cells, *56^{KO}97^{KO}* V+ cells showed a significant large reduction in the frequency of CFU-C (**Figure 4.10 B**). Moreover, there was a significant reduction in the frequency of erythroid, myeloid and multipotent CFU types (**Figure 4.10 C**) as compared to the WT cell line. Thus, we

conclude that definitive HPC production is dependent upon expression of both Gpr56 and Gpr97.

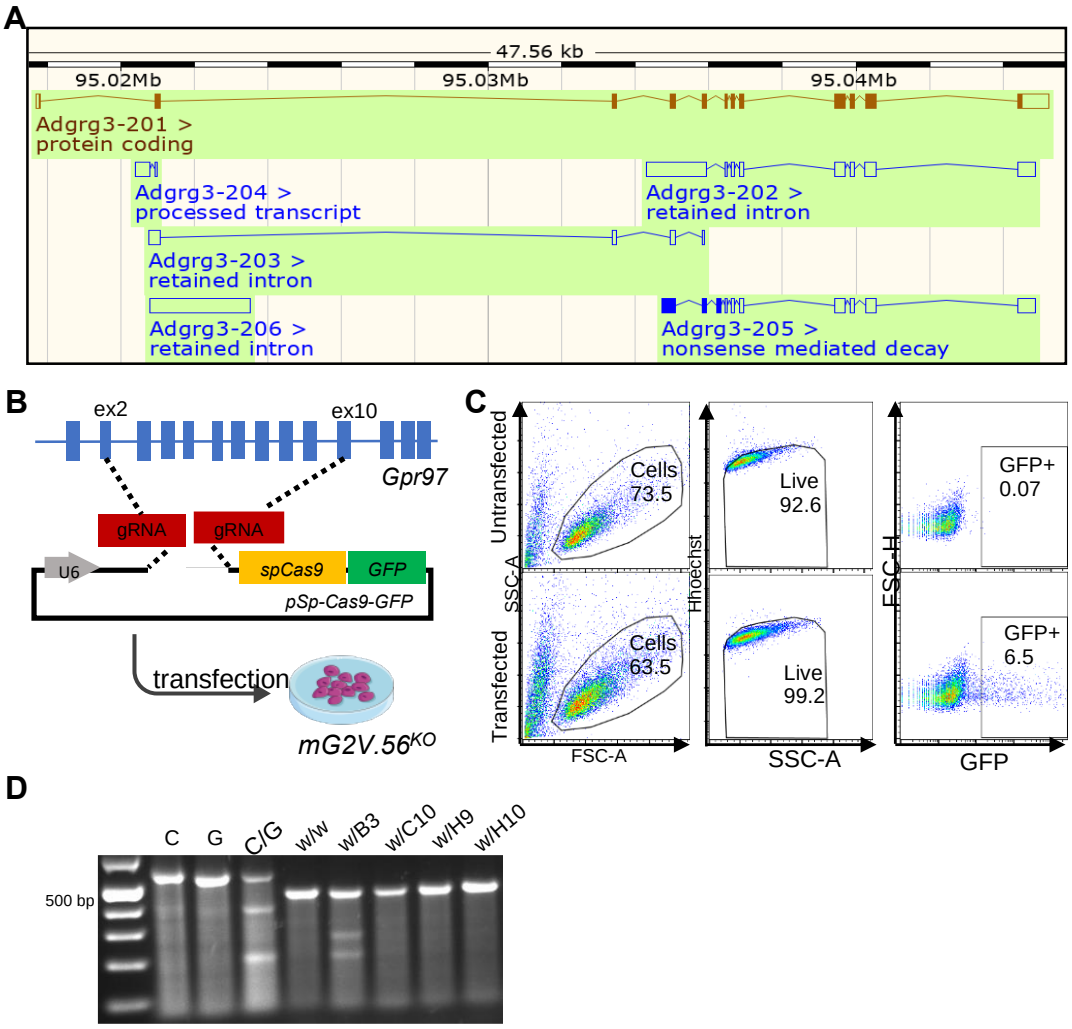

Figure 4.8 Generation of *Gpr56:Gpr97* double deleted *G2V* ESCs.

(A) *Gpr97* gene and splice isoforms as taken from Ensembl database. (**B)** *CRISPR/Cas9* strategy showing *gRNAs* for *Gpr97* exons 2 and 10 and insertion in *pSp-Cas9-2A-GFP* vector used for transfection of *G2V.56*^{KO} ESCs. (**C)** Flow cytometric analysis of transfected and untransfected control ESCs for forward and side scatter, viability and GFP expression. (**D)** Surveyor assay on DNA from 4 CRISPR/Cas9 ESC clones that were negative for *Gpr97* mRNA. Clone B3 shows a mismatch in *Gpr97* genomic sequence. C and G are negative and C/G is positive controls.

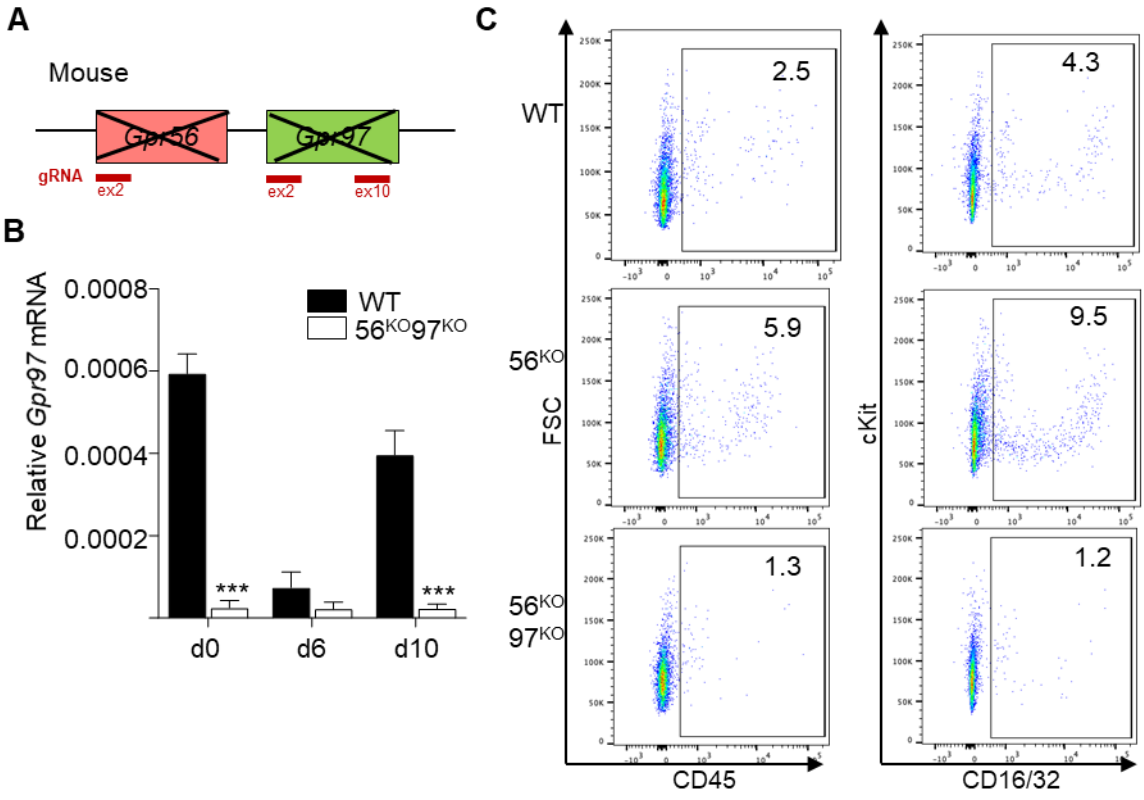

Figure 4.9 *In vitro* functional analyses of *G2V.56^{ko}97^{ko}* ESCs

(A) Schematic of *Gpr56* and *Gpr97* deletion in mouse *Gpr56* locus. **(B)** RT-qPCR analysis of time course hematopoietic differentiation cultures of *G2V* WT and *G2V. 56^{KO}97^{KO}* ESCs. Relative *Gpr97* expression (normalized to *β-actin*) (n=3), Mean±SEM, ***p<0.01. **(C)** Representative flow cytometry plots for CD45^{+} hematopoietic cells and EMPs (V+CD41^{+}cKit^{+}CD16/32^{+}) from day 10 differentiated *G2V* WT, *G2V.56^{KO}* and *G2V.56^{KO}97^{KO}* ESC cultures. Percentages shown in each quadrant (n=3).

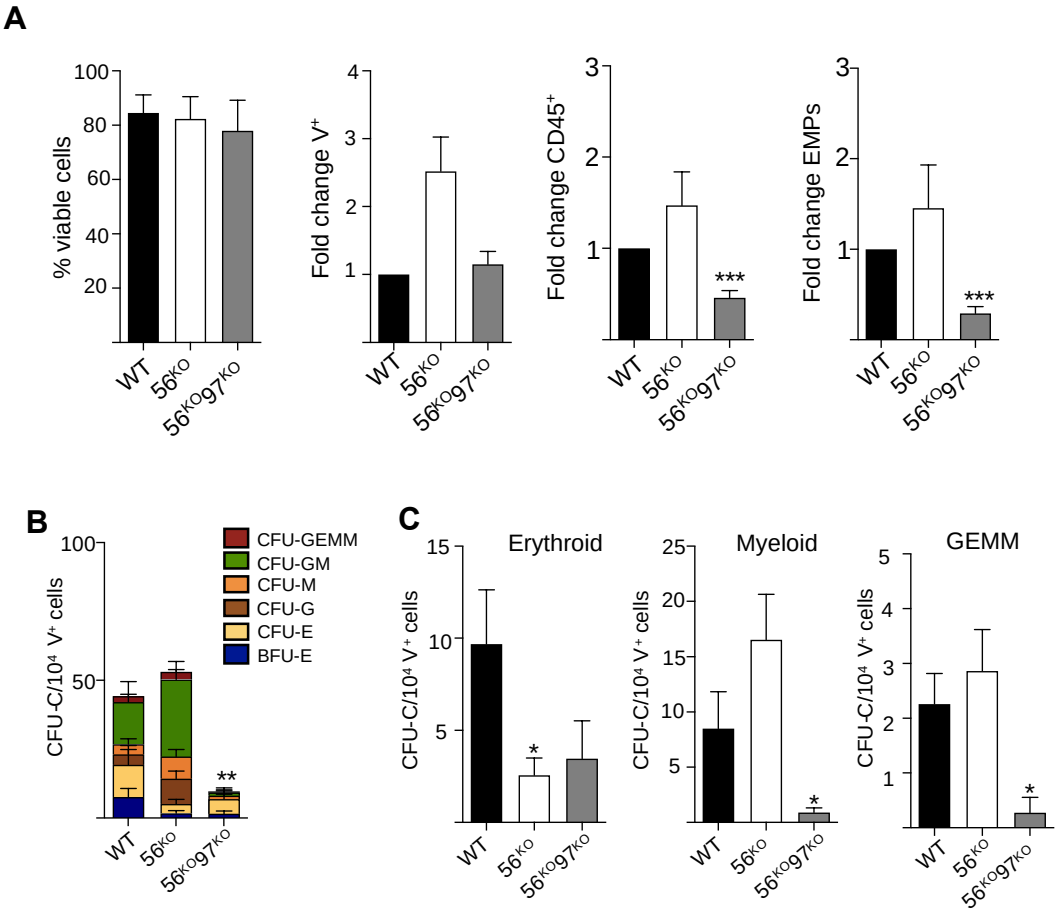

Figure 4.10 Decreased production of HPCs in the absence of *Gpr56* and *Gpr97*

(A) Percentage of viable cells and fold-change in percentages of Venus(V)$^{+}$, CD45^{+}, and EMPs from day10 differentiated *G2V* WT, *G2V.56^{KO}* and *G2V.56^{KO}97^{KO}* ESC cultures. n=3. Mean±SEM. (**B)** Frequency of colony forming unit-culture cells (CFU-C) in day 10 differentiated *G2V* WT, *G2V.56^{KO}* and *G2V.56^{KO}97^{KO}* ESC cultures. CFU-C per 10^4 Venus^{+} cells is shown with colony types indicated by color. CFU-GEMM=granulocyte, erythroid, megakaryocyte, macrophage; GM=granulocyte, macrophage; G=granulocyte; M=macrophage; E=erythroid; BFU- E=burst forming unit-erythroid. n=3. Mean±SEM. (**C)** Output of CFU-C per 10^4 Venus^{+} in E according to lineage. Erythroid=CFU-E + BFU-E; Myeloid=CFU-GM + G + M; Multilineage=CFU-GEMM. *p≤0.05; **p≤0.01; ***p≤0.001.

4.2 Discussion

We have shown that two G-protein coupled receptors within the Gpr56 locus, the closely-related Gpr56 and Gpr97, function in the production and qualitative output of HSPCs during mouse embryonic development. While the knockout of Gpr56 alone in mouse ESC partially affects HPC production and biases output to the myeloid lineage, the double knockout of Gpr56 and Gpr97 severely reduces definitive HPC production and differentiation. Moreover, Gpr56 deleted fetal liver HSCs show myeloid lineage-bias and decreased self-renewal in vivo. Together, these data support a role for Gpr56 in enforcing multi-lineage potential and conferring self-renewal on HSCs as they are generated in the embryo, reveal a time-dependent redundant function for Gpr97, and suggest that Gpr97 upregulation promotes the myeloid-bias of HPCs and HSCs.

4.2.1 Gpr56 deletion provides new insights into the regulation of mammalian hematopoiesis

Despite the predominant high expression of Gpr56 in quiescent adult bone marrow HSCs (Rao, Marks-Bluth et al. 2015), the function of this adhesion G-protein coupled receptor in HSCs has been a focus of controversy. Whereas a study in human leukemic cell lines and a germline *Gpr56-/-* mouse model claimed that EVI1 regulated GPR56 maintains the HSC pool in bone marrow niches (Saito, Kaneda et al. 2013), others have reported that this same germline knockout mouse model was not impaired in bone marrow HSPC maintenance or function during homeostasis or induced myeloablative stress(Rao, Marks-Bluth et al. 2015). It was suggested that the discrepancy was due to the generation of a hypomorphic allele *in vivo* with low level expression of the S4 splice variant, or to the background strain of the mice. Our finding of upregulated expression of Gpr56 in the emerging cells of the mouse embryo intra-aortic hematopoietic clusters and the impairment of aortic HSPC generation in Gpr56 morphant zebrafish embryos (Solaimani Kartalaei, Yamada-Inagawa et al. 2015) encouraged us to re-examine the role of Gpr56 and ask if or how it may be functioning at early developmental times in the mouse.

In our studies, Gpr56 was conditionally deleted (exon 2 floxed allele) in the HPCs and HSCs in the embryo with *VECCre* and *VAVCre*. E9.5 phenotypic yolk sac hematopoietic progenitors were quantitatively reduced, but E13.5 fetal liver LSK-

SLAM HSC numbers were unaffected. In contrast, clonal in vivo transplantations of FL derived LSK-SLAM cells did reveal qualitative changes in HSCs. The absence of Gpr56 profoundly impairs both lineage bias and self-renewal of HSCs, thus implicating several distinct roles for Gpr56 at embryonic, fetal and adult stages.

To explore this further, *Gpr56-/-* ESC hematopoietic differentiation cultures were examined. Similar to yolk sac, early day 6 differentiation cultures were decreased in phenotypic and functional HPCs. Day 10 differentiation cultures were slightly increased in phenotypic and functional HPCs, and like E13.5 fetal liver HSCs they showed a myeloid bias that was significant compared to control. Hence, Gpr56 likely affects early embryonic hematopoietic generation quantitatively, and at later developmental times and/or in distinct microenvironments it has a role in HSC quality.

4.2.2 Gpr97 influences hematopoietic development in the absence of Gpr56

In the context of the necessity and sufficiency of Gpr56 for HSPC generation in zebrafish embryos, the rather minor roles for Gpr56 in mouse hematopoietic development remained puzzling. If Gpr56 was essential for mouse HSPC generation, embryonic lethality would be expected. Instead, homozygous Gpr56 mutant adults could be produced, and the few hematopoietic defects found in the bone marrow were variable between labs (Saito, Kaneda et al. 2013, Rao, Marks-Bluth et al. 2015). Our rescue of Gpr56 morphant zebrafish embryo HSPC generation with mouse *Gpr56* and *Gpr97*, but not *Gpr114* mRNA raised the possibility of receptor redundancy in hematopoietic cell development and function. The location of *Gpr114* and *Gpr97* on the same locus as Gpr56 results in co-expression of these highly homologous receptors and the loss of genomic synteny of this region in zebrafish allowed us to identify a role for Gpr56. Similarly, the human *GPR56* locus also contains highly homologous *GPR114* and *GPR97* genes in the same 5’ to 3’ configuration. The evolutionary conservation between mouse and human genes/proteins, together with the strong similarities in the embryonic development of adult mouse and human hematopoietic systems suggest a separation and overlap in the functions of Gpr56 and Gpr97 that could explain the minor effects seen in the Gpr56 knockout mouse models.

Redundancy of these two G-protein coupled receptors during mouse hematopoietic development is supported by our results showing Gpr97 expression in cells of E9.5 yolk sac, E13.5 FL and adult bone marrow and also in cells of d6 and d10 ESC differentiation cultures. Importantly, in the absence of Gpr56, upregulated expression of *Gpr97* was found in E13.5 FL LSK SLAM cells and d10 differentiated ESC derived V+cKit+ hematopoietic cells. No changes were found in *Gpr97* expression in *Gpr56-/-* E9.5 yolk sac and adult bone marrow. Thus, the loss of Gpr56 function in the embryonic definitive stages of HSPC generation is replaced by a compensatory expression of Gpr97.

4.2.3 Positive role of Gpr97 or negative role of Gpr56 for myeloid bias?

We observed bias toward myeloid differentiation in cells from *in vitro* differentiated *Gpr56-/-* ESC cultures and *in vivo* in the peripheral blood and bone marrow of recipients of Gpr56 conditional knockout E13.5 fetal liver HSCs. Previously, clonal lineage-biased output of HSCs has been reported to be an age-related characteristic (Cho, Sieburg et al. 2008, Benz, Copley et al. 2012, Geiger, de Haan et al. 2013, Verovskaya, Broekhuis et al. 2013). As measured by long-term *in vivo* clonal transplantation, bone marrow HSCs from young mice yield lymphoid-biased and balanced lymphoid-myeloid cell output in the recipients. Bone marrow from aged mice show a higher frequency of myeloid-biased HSC output in recipients and a decreased self-renewal ability in serial transplantations. The myeloid-bias of Gpr56 cKO FL HSCs in primary recipients together with the reduced self-renewal of HSCs as found in our secondary transplantations strongly support a qualitative role(s) for Gpr56 in HSCs and suggest that Gpr56 is responsible for maintaining the multipotency and robustness of HSCs throughout development.

Indeed, these critical qualitative properties appear for the first time in midgestation mouse embryos when the first adult repopulating HSCs are generated in the aorta (Dzierzak and Speck 2008, Dzierzak and Bigas 2018). Highly upregulated Gpr56 expression was found to be localized in the emerging intra- aortic hematopoietic cluster cells at E10.5/11.5 after they transition from endothelial cells (Solaimani Kartalaei, Yamada-Inagawa et al. 2015). Importantly, transcriptomic studies of cells

undergoing EHT reveal expression of *Gpr97* but at lower FPKM levels relative to Gpr56 (Solaimani Kartalaei, Yamada-Inagawa et al. 2015).

The relationship of distinct Gpr56 and Gpr97 expression with the distinct function in HSCs is difficult to ascertain. Because of the overlap in expression it remains unclear whether Gpr56 functions to retain multipotency or functions in a repressive capacity to limit myeloid bias, or whether Gpr97 (especially its upregulated expression in the absence of Gpr56) activates myeloid-bias. Human GPR56 was reported to negatively regulate the immediate effector functions of human NK cells, such as inflammatory cytokine production and target cell killing (Chang, Hsiao et al. 2016). Another more recent study reports that human polymorphonuclear cells (precursors and mature granulocytes) highly express GPR97, whereas monocytes and lymphocytes do not (Hsiao, Chu et al. 2018). These results may highlight that the balance between these closed-related G-protein coupled receptors in specific subsets of hematopoietic cells is likely to be an important factor impacting on specific cellular functions. As we have demonstrated here that ESC-derived hematopoiesis is severely reduced in the absence of both Gpr56 and Gpr97, the specific functions of these two closely-related receptors can only be addressed through the generation of double knockout mouse or human cell line models. Previously, we have tried to generate such a *Gpr56-/-Gpr97-/-* mouse model by CRISPR/Cas9 methodology but were unsuccessful, likely due to embryonic lethality. Future studies aim to understand the individual roles of these receptors during HSC development by generating an in vivo conditional knockout across both genes and comparing effects with single knockout and/or individual rescue of Gpr56 and Gpr97.

5 THE ROLE OF GPR56 GAIN OF FUNCTION IN HUMAN HEMATOPOIESIS

5.1 Introduction

De novo generation of adult transplantable hematopoietic stem cells (HSCs) remains a key approach within regenerative medicine in the management of the blood-related disorders. Strategies to derive HSCs from undifferentiated embryonic stem cells (ESCs) have been guided by the understanding of the complex networks that orchestrate the emergence of HSC in embryos. These networks consist of a fine controlled regulation of a variety of intrinsic and extrinsic signals. Their dysregulation impairs the onset of HSCs in embryos and correlates with leukemic stem cell (LSC) signature in adults. Our laboratory identified *Gpr56* as novel regulator of the HSC onset in zebrafish and mouse (Solaimani Kartalaei, Yamada-Inagawa et al. 2015). Gpr56 is expressed in HSC as they are embryonically generated, and it remains expressed in bone marrow (BM) HSC population in adult mice. We functionally demonstrated that *Gpr56* loss-of-function profoundly alters the HSC biology quantitatively and qualitatively. In zebrafish, the downregulation of *Gpr56* abrogates the embryonic generation of HSPC population (Solaimani Kartalaei, Yamada-Inagawa et al. 2015), whereas in mouse we found that its absence affects the HSC quality (Maglitto A., Mariani S.A., 2020, under review). Upon *Gpr56* deletion, murine foetal liver derived HSCs displayed a reduced self-renewal capacity and hold a clonal bias toward myeloid differentiation both *in vitro* and *in vivo.*

Conversely, Gpr56 overexpression is frequently associated with patients affected by acute myeloid leukaemia (AML) (Daria, Kirsten et al. 2016, Pabst, Bergeron et al. 2016, Jentzsch, Bill et al. 2020). These patients suffer an abnormal proliferation and differentiation of myeloid stem cells. Although around 60% of AML patients achieve a complete remission (CR) from the induction therapy (chemotherapy), the remaining 40% relapse (De Kouchkovsky and Abdul-Hay 2016). This event is caused by few aggressive LSCs that resist and persist after the standard therapy. A recent study found

GPR56 as part of 17 biomarkers prognostic tool (LSC17) that define relapsing patients with aggressive LSCs (Ng, Mitchell et al. 2016). Another study demonstrated that *GPR56* expression defines a subgroup of LSCs with higher *in vivo* engraftment potential (Pabst, Bergeron et al. 2016, Daga, Rosenberger et al. 2019). Altogether, these findings indicate that the controlled regulation of *GPR56* plays a critical role in steady-state HSC biology. However, the abnormal expression of GPR56 confers enhanced "stemness properties" to those aggressive LSCs, so that gives them an unknown biological advantage to elude cancer therapies. Understanding the functional role of human GPR56 in normal and malignant hematopoiesis will benefit the development of effective strategies for *de novo* HSC generation and the identification of new intracellular targets to eradicate LSCs.

This chapter examines the biological function of aberrant *GPR56* expression in a human *in vitro* haematopoiesis differentiation model. To address this aim, I establish a novel human *GPR56* inducible reporter iPSC line which is *in vitro* differentiated to generate hematopoietic progenitor cells (HPCs). After the activation of GPR56 signalling pathway during the differentiation process. I evaluate the frequency of the *in vitro* derived HPCs, test their hematopoietic potential and examine characteristics that may be indicative of stemness.

5.2 Establishment of an inducible human *GPR56* iPSC line

5.2.1 Generation of the *hGPR56* reporter cassettes

To study the role of GPR56 in human haematopoiesis, I functionally test the hematopoietic potential of HPCs that overexpress *hGPR56*. To investigate the GPR56 *gain-of-function* in human hematopoiesis, it is necessary to establish a stable engineered human PSC line that overexpresses GPR56 during *in vitro* hematopoietic differentiation. The presence of a fluorescent reporter protein facilitates the *in vitro* tracing of those cells that upregulate the ectopic GPR56. To this aim, I generate a custom cassette that simultaneously expresses *GPR56* and *mCherry* reporter genes.

GPR56 (*ADGRG1*) has 14 exons and is locates on chromosome 16 (16q21) of the human genome. The *GPR56* sequence is predicted to produce a 693 amino acid protein characterized by different domains. The first 25 aminoacids encode a small consensus sequence called signal peptide (*SP*), which membrane proteins require to enter the secretory pathway. Membrane proteins that contain *SP* can transit through the cellular organelles, like ER and Golgi to undergo post-translational modifications that are necessary for the final maturation. Although the *SP* sequence is lost after protein maturation, its presence is required for the correct protein maturation, whereas its absence impairs their final destination onto the cell membrane. Upon maturation and insertion in the membrane, GPR56 can undergo autoproteolytic cleavage that divides the receptor in two different domains non-covalently associated: the extracellular N-terminus (from 26 to 382aa) and the C-terminus (from 383 to 693aa) **(Figure 5.1 A).** To produce a continuous *open-reading-frame* (ORF), I generated a novel cassette using the full length *GPR56* sequence assembled with the *mCherry* fluorescent reporter gene. Of note, several points need to be considered regarding the order of these two fragments. In the ideal set up, *GPR56* and *mCherry* should be co-expressed at equal amount. To produce equimolar levels of a bicistronic transcript, a "self-cleaving" 2A peptide (*p2a*) will be located between the two sequences. The self-cleavage occurs between the last two residues of this 22aa-long peptide. This means that the sequence cloned upstream the *p2a* sequence will have additional residues that might compromise protein folding and function (Kim, Lee et al. 2011) . To avoid that *p2a* residues will affect GPR56 downstream signalling activation, the *mCherry*

sequence will be cloned upstream *GPR56*. The same approach is used to generate other 2 similar *mCherry-p2a-hGPR56* cassettes that will overcome some biological and technical limitations. The first, *mCherry-p2a-his-hGPR56*, will include an *his-tag* between the *SP* and the *hGPR56* sequence. This additional sequence will facilitate the detection of GPR56 protein to validate the final cassette, as good reliable antibodies against GPR56 were not commercially available. The other cassette, *mCherry-p2a-hGPR56CA* consists of a *hGPR56* sequence that lacks the N-terminus end. Previous studies demonstrated that the deletion of the N-terminus end triggers the activation of *GPR56* cellular signalling cascade (Paavola, Stephenson et al. 2011). This construct will be further used to establish the final stable *hGPR56* hPSC line, where the GPR56 downstream signalling pathway can be activated without the requirement of any external ligand. To summarize, three different cassettes were generated:

- *mCherry-p2a-hGPR56* full length (SP + N-terminus + C-terminus)
- *mCherry-p2a-SP-his-hGPR56* (SP + his + N-terminus + C-terminus)
- *mCherry-p2a-SP-hGPRCA* (Constitutively Active form, SP + C-terminus)

5.2.1.1 Strategy to assemble the different fragments.

To make the custom cassettes, the Gibson assembly will be adopted as suitable cloning strategy to generate seamlessly ORFs. I PCR amplify *hGPR56* full length, *hGPR56CA*, *mCherry* and *SP+His* sequences using a set of primers that contains at their 5'ends a short (22nt) sequence shared with the adjacent fragments (**Figure 5.1 B and C**). The resulting PCR amplicons were eluted and purified from the agarose gel and the adjacent fragments were ligated together using the Gibson reaction mix to generate the desired ORF cassettes (**Figure 5.1 D**, primers listed in **Table 2.2**)

Afterwards, each resulting cassette was cloned into *pcDNA3.1* mammalian expression vector, whose backbone contains all the mammalian gene expression regulatory elements and the bacterial ampicillin resistance. The ampicillin resistance will select those bacteria that have been positively transfected with the custom plasmids.

Figures 5.1 E, F, G show the bacteria clones that have been PCR screened for each single cassette. The bands indicate those clones that are positive for the custom cassettes. Of note, the efficiency of the Gibson cloning varies according to the number

and the length of the fragments that have been assembled. The plasmids isolated from positive bacteria were sequenced to ensure that no mutations occurred within the *ORF* cassettes (see **Appendix B**). I select the correct cassettes to validate *in vitro* the expression of GPR56.

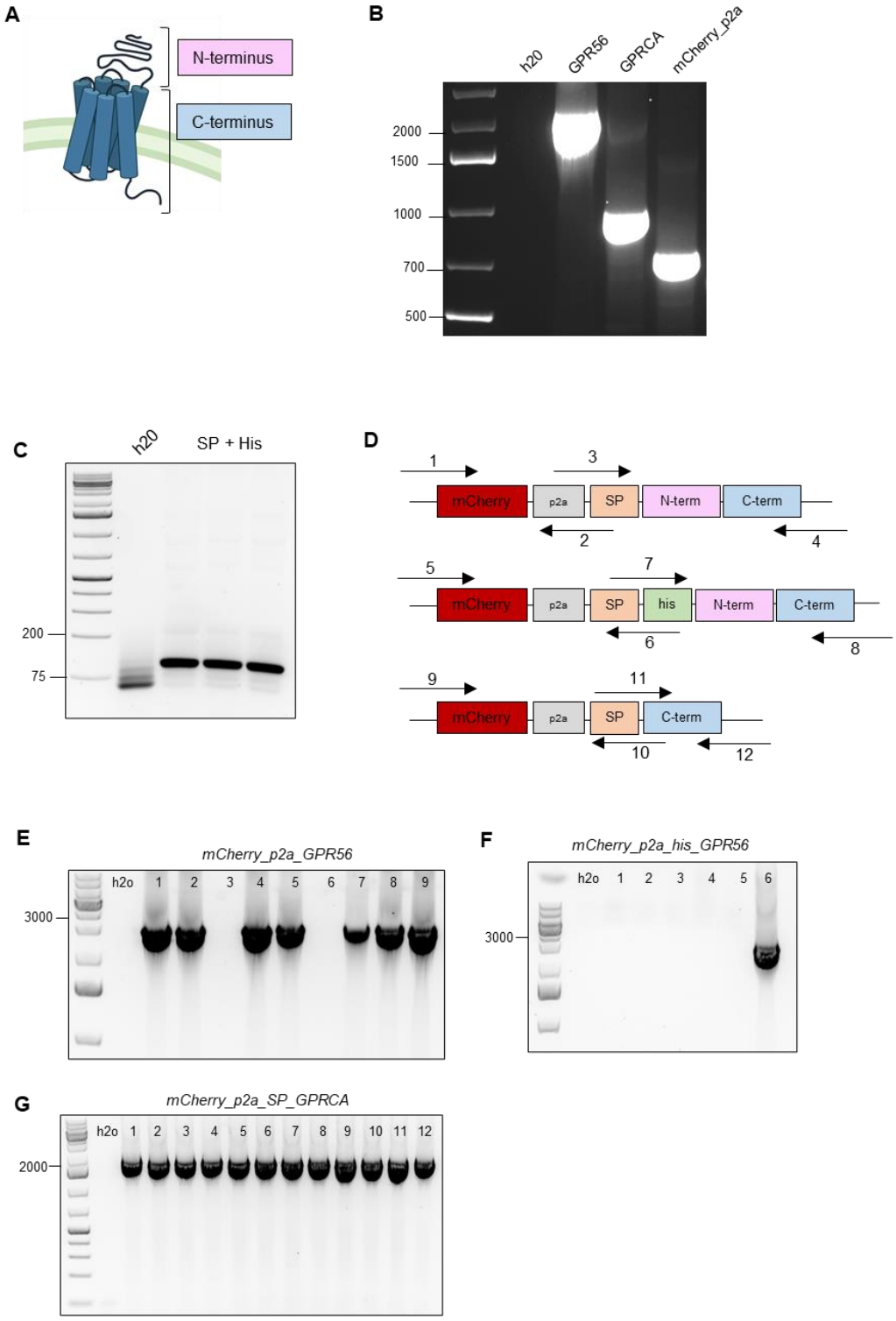

Figure 5.1 Generation of three *mCherry-GPR56* cassettes.

(A) Protein structure of human GPR56. The different colours indicate the protein domains: N-terminus (pink), C-terminus (blue) **(B)** PCR amplification of each single fragments: *hGPR56* (2082bp), *hGPR56CA* (950bp), *mCherry_p2a* (711bp) **(C)** PCR amplification of the SP-His tag fragment (110bp) **(D)** Schematic representation of the Gibson assembly strategy for the

three different cassettes: *mCherry-p2a-hGR56 full length* (2886bp, top), *mCherry-p2a-SP-his-hGPR56* (2928bp, middle), *mCherry-p2a-SP-hGPR56CA* (1815bp, bottom).. **(E, F, G)** Screening of bacteria cells transformed with the Gibson ligation products. The bands show the bacteria clones that are positive for **(E)** *mCherry-p2a-hGPR56* (2886bp), **(F)** *mCherry-p2a-SP-his-hGPR56* (2928bp) and **(G)** *mCherry-p2a-hGPRCA* (1815bp). See Appendix B for the sequencing data.

5.2.1.2 Validation of the resulting cassettes

After the custom cassettes have been generated and sequenced, it remains to establish whether *mCherry* and *GPP56* are transcribed and whether GPR56 protein properly matures to be expressed in the cell surface membrane. To address these points, the *pcDNA3.1 mCherry-p2a-his-hGPR56* is validated *in vitro* using 293HEK cells. Due to time-related and technical limitations, such as GPR56 antibody availability for protein detection, the *mCherry-p2a-his-hGPR56* is the suitable plasmid to perform different *in vitro* assays. As this plasmid shares the same structure with the other custom plasmids, I am confident that conclusions made from these results could be reasonably extended to the other plasmids.

293HEK cells were transfected with pcDNA3*.1 mCherry-p2a-his-hGPR56* alongside with control conditions: 293HEK untransfected (UT) and transfected with *pcDNA3.1* empty vector (EV). 48 hours post-transfection, 293HEK cells were observed under fluorescent microscope and FACS analysed to estimate the frequency of *mCherry* expressing cells. **Figures 5.2 A** and **B** demonstrate that almost 80% of 293HEK cells transfected with *mCherry-p2a-his-hGPR56* are *mCherry*+. RT-qPCR gene expression analysis demonstrates that *GPR56* transcript levels in these cells is upregulated as compared to the control counterparts (**Figure 5.2 C**). At the protein level, western blotting analysis confirms that in *mCherry-p2a-his-hGPR56* transfected cells the amount of GPR56 protein is higher than the controls. Finally, the immunostaining using an antibody against the *His-tag* confirms that GPR56 reaches the cell membrane. Indeed, **Figure 5.3** shows that the majority of *mCherry* positive cells (red dots) express GPR56 (green) on their surface membrane.

The validation of the *mCherry-p2a-his-hGPR56* vector confirms that it possible to trace those cells that are expressing ectopic GPR56. Although only *mCherry-p2a-his-hGPR56* has been tested at the protein level, *mCherry-p2a-hGPRCA* was employed to establish the inducible engineered hPSC reporter cell line. The engineered line allows to examine the effect of GPR56 *gain-of-function* on HPCs during human *in vitro* hematopoiesis.

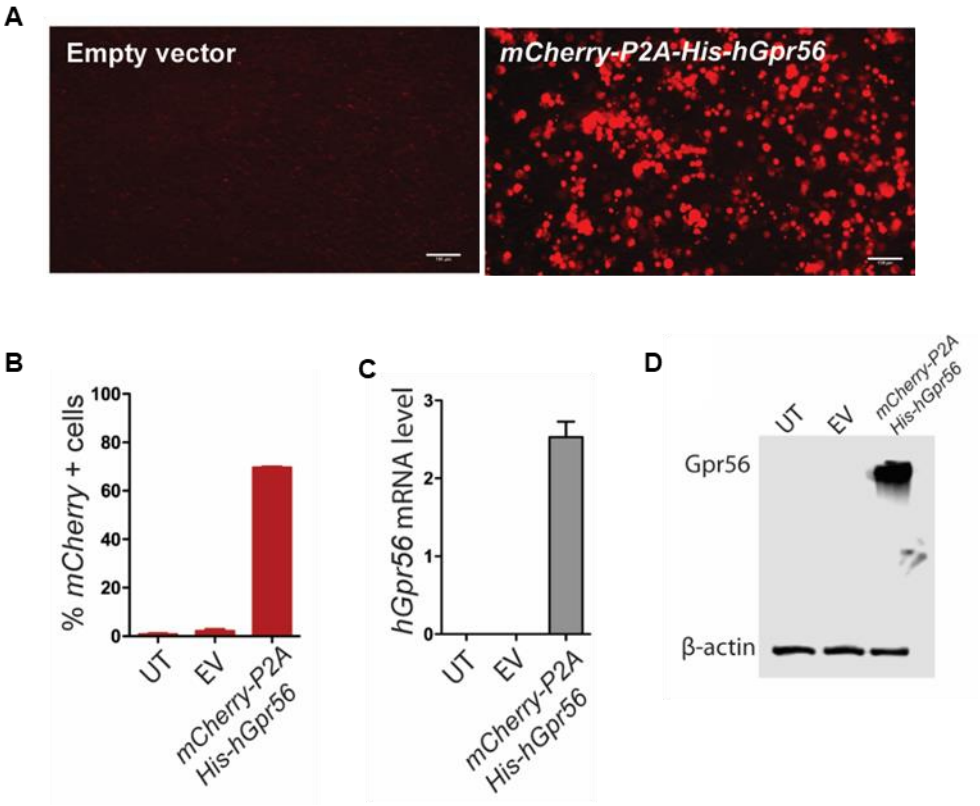

Figure 5.2 Validation of the *mCherry-p2a-his-hGPR56* cassette.

(A) Microscopy pictures of 293HEK cells transfected with an empty vector (left panel) and *mCherry-p2a-his-hGPR56* (right panel). The red dots represent the cells that are expressing *mCherry* fluorescent protein 48 hours post transfection. Scale bar=100 um **(B)** The bar graph shows the percentage of 293HEK expressing *mCherry* after FACS analysis. 293HEK cells were transfected with *mCherry-p2ac-his-hGpr56* plasmid. 48 hours post transfection, the cells were analysed and compared with 293HEK untransfected (UT) and transfected cells with an empty vector (EV) n=2. **(C)** Quantitative PCR analysis of *hGPR56* mRNA level from 293HEK mCherry positive cells 48 hours post-transfection. 293HEK untransfected (UT) and transfected with an empty vector (EV) are used as controls. The *hGpr56* expression levels were normalized to the *β-actin* reference gene. **(D)** Western blot of hGPR56 full-length (75kDa) protein on 293HEK cells untransfected and transfected with an empty vector or *mCherry-p2a-hGPR56. β-actin* was used as reference control.

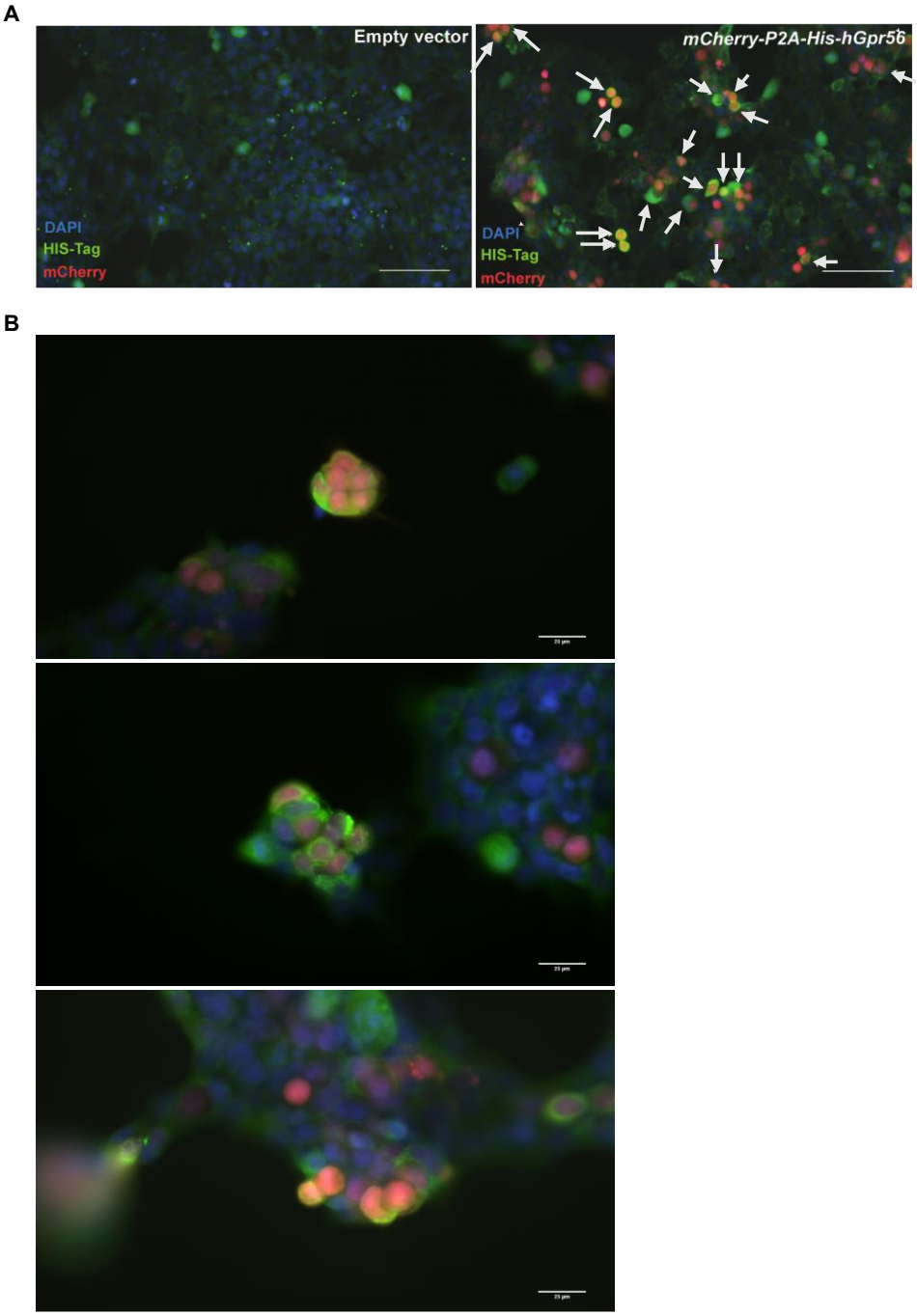

Figure 5.3 GPR56 is properly expressed in the cell membrane.

(A) Immunofluorescent staining of 293HEK cells 24 hours post transfection. The cells were transfected with an empty vector (left panel) and with *mCherry-p2a-his-hGPR56* plasmid (right panel). The blue dots represent the nuclei (DAPI), the red cells are expressing *mCherry*. The cells that show both red and green (*his-tag*) stains are those that are expressing *hGPR56* (indicated by the small white arrows) n=1. The left panel (Empty vector) shows some degree of green auto fluorescent in the background. Scale bar=100um **(B)** High magnification of 293HEK cells transfected with *mCherry-p2a-his-hGPR56* (24 hours of transfection). Blue dots are the nuclei (DAPI), red cells are expressing *mCherry* and the green stain (*his-tag)* shows GPR56 expressed around the cell membrane. n=2, scale bar=25um.

5.2.2 Targeting a human iPSC line with an inducible *hGPR56* vector

5.2.2.1 The Tet-On system as an eligible inducible system

The modulation of gene expression is an experimental approach that scientists broadly use to study the function of relevant genes. This has been achieved using different conditional methods such as the *Cre-Lox*, the *Flp-FRT*, the *Cre-Estrogen Receptor* (ER) and the tetracycline-inducible (*Tet*) system. Whilst the *Cre-Lox* and the *Flp-FRT* systems alter the gene expression permanently, the *Cre-ER* and *Tet* approaches can reversibly manipulate the expression of a gene of interest (GOI) by the external administration of a drug. For this reason, *Cre-ER* and *Tet* are widely employed in developmental studies, where gene expression is spatial and temporal restricted. Although *Cre-ER* and *Tet* systems function similarly, the *Tet* system gives an optimal and rapid control of the *hGPR56* expression.

The *Tet* inducible system relies on a group of proteins and regulatory elements (known as operon *Tn10*) that bacteria developed to resist tetracycline. *Tn10* consists of three elements: the tetracycline-responsive repressor protein (TetR), the operator sequences (*TetO*) and its downstream tetracycline-resistant gene (*TetA*). In the steady state, TetR is constitutively expressed and binds *TetO* with high affinity, repressing *TetA* expression. Conversely, the presence of tetracycline changes TetR protein conformation so that it dissociates the bond to *TetO*, inducing the expression of TetA. This configuration is called *Tet-Off* (Meier, Wray et al. 1988). In 1995 Gossen and colleagues modified and improved the *Tet-Off* system to modulate the expression of eukaryotic genes. They developed a novel *Tet-On* system, which consists of a reverse tetracycline-transactivator (rtTA), a GOI and *TetO*. The GOI is located downstream of a stretch of *TetO* repeats that are fused with a minimal eukaryotic promoter (*TRE*). In the *Tet-On* system, the rtTA is constitutively expressed but is unable to bind the *TRE* (**Figure 5.4 A**). The presence of the doxycycline (a tetracycline analogue) modifies rtTA conformation, allowing its binding with the *TRE* region, which results in the transcription of the GOI (Gossen, Freundlieb et al. 1995) (**Figure 5.4 B**). However, drug toxicity in the host cells remains the major drawback of the inducible systems (Zhou, Vink et al. 2006). In addition, conventional *Tet-On* systems carry *rtTA*, *TetO*

and *GOI* in different plasmids. This leads to tedious and time-consuming rounds of transfection, expansion and selection of positive clones.

These limitations have been overcome using a novel modified version of the commercially available *Tet-On3G.* The new system (*all-in-one-Tet-On*) improves the sensitivity of the rtTA to lower doses of doxycycline and lacks background activity (Zhou, Vink et al. 2006). Importantly, it holds all the *Tet-On* elements in one single vector, optimising the time to generate a *Tet-On* inducible transgenic cell lines. **Figure 5.5 A** illustrates the structure of the custom *all-in-one-Tet-On* vector (for more details, see **Appendix C**). *TRE* sequence locates at the 5' end followed by the GOI, whereas the *rtTA* element is at the 3' end followed by the *EF-1a* promoter, which induce its constitutive activation. The presence of a *polyA* signal at the 3' end of *rtTA* avoids the unforeseen expression of the *GOI*. When doxycycline is added, rtTA increases its affinity for the *TRE* and promotes the transcription of the *GOI*. I will insert the newly formed *mCherry-p2a-hGPR56/his/CA* cassettes into the *all-in-one-Tet-On* vector to establish an inducible *mCherry-p2a-hGPR56/his/CA knock-in* vectors. To deliver these vectors into the human genome, it is important to develop a safe and efficient targeting strategy to insert them into the iPSC genome.

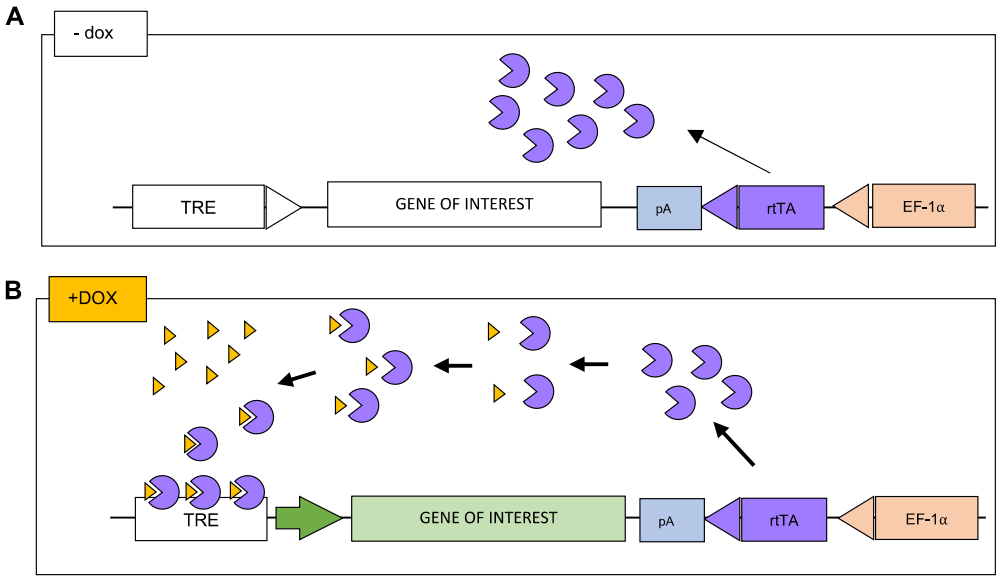

Figure 5.4 Schematic illustration of the *Tet-On* inducible system.

(A) In the absence of doxycycline, the transcriptional activator (rtTA) is constitutively expressed but unable to bind the TetO elements. **(B)** The doxycycline changes the rtTA's conformation al-lowing to bind the TetO sequence. This event triggers the expression of the Gene-Of-Interest (GOI).

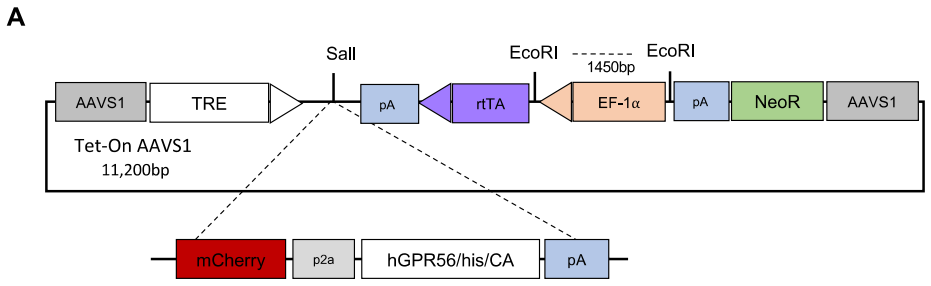

Figure 5.5 Scheme of the *all-in-one-Tet-On* donor vectors.

(A) The *all-in-one-Tet-ON AAVS1* donor vector (11,200bp) contains different elements: the Tet-On regulatory sequences (*TetO*, *rtTA*), *AAVS1* homology arms (HA), neomycin and puromycin (not shown) resistances. The plasmid includes a SalI restriction site and two EcoRI sites. The SalI site will receive the newly formed *mCherry-p2a_hGPR56/his/CA* cassettes, whereas the EcoRI sites will be used for a diagnostic digestion.

5.2.2.2 Strategy to integrate *hGPR56* cassettes into the human genome.

Gene editing technologies are powerful tools to study the function of a gene in vivo and in vitro, which include downregulation, knock-out and knock-in (Gaj, Gersbach et al. 2013). The latter approach consists of the integration of a transgene into a host genome. Historically, the insertion of a transgene into host cells was achieved using the physiological cell homologous recombination (HR), although this approach resulted time consuming and inefficient. Interestingly, scientists found that genomic double breaks (DSBs) activate the homology directed repair (HDR) pathway, which accepts homologous sequences as donor templates to repair genomic damages (Cannan and Pederson 2016). Molecular biologists took advantage of this system to increase the efficiency of the gene knock-in by co-delivering enzymes that generate genomic nicks (endonucleases) and donor vectors that contain host genomic homologous sequences, called homology arms, *HAs* (Moehle, Rock et al. 2007). This approach will be used to perform *Tet-On-hGPR56* knock-in into human iPSC line. To generate DSBs, I use the Zinc Fingers Nucleases (ZFNs). Such ZFNs are chimeric nucleases resulted from the fusion of the FokI non-specific restriction endonuclease domain with zinc-finger DNA-binding proteins. These are 30 amino-acids long synthetic proteins that recognise a contiguous 18 bp DNA sequence with high specificity (Liu, Segal et al. 1997). The ZFNs need to be carefully designed to target the specific genomic location where the donor vector will be integrated. Therefore, the choice of the host genomic locus is crucial to guarantee the proper transgene expression.

An ideal gene *knock-in* strategy should ensure the stable expression of the transgene without altering the cell physiological processes. Conventional *knock-in* approaches employed gamma-retroviral and lentiviral particles as vectors to integrate and express a transgene. However, the viral delivery systems present limitations that affect the expression of the transgene and host endogenous genes. As viral genomic integration occurs randomly, the transgene can dysregulate the expression of important host genes, causing the activation of oncogenes or the mutation of oncosuppressors. The alteration of these two classes of genes frequently leads to an aberrant cell clonal expansion or malignant transformation. Another limitation is the silencing of the transgene. This

event takes place when the transgene integrates within an intronic or heterochromatic portion of the genome. Moreover, changes in the chromatin conformation often occur during *in vitro* differentiation protocols. During the differentiation process, PSCs undergo progressive and continuous variations in their epigenetic architecture that might cause the silencing of the transgene. To avoid these drawbacks, studies identified three suitable human *loci* to accommodate the integration of the transgene: the *chemokine receptor 5* (*CCR5*), the human ortholog of the mouse *Rosa26* locus and the *adeno-associated virus site 1* (AAVS1) located in chromosome 19. The *AAVS1* is a well-studied locus that is ubiquitously expressed in multiple cell types. A transgene delivered in this genomic locus preserves a good expression without interfering with host regulatory elements (Lombardo, Cesana et al. 2011). For this reason, the *AAVS1* locus is consider the *safe acceptor* locus that will ensure a robust transgene expression during iPSC *in vitro* differentiation (Papapetrou and Schambach 2016).

To integrate the *Tet-On-hGPR56* cassettes into the *AAVS1* locus, the donor plasmid brings two externals left (HLA, 528bp) and right (HRA, 762bp) homology arms that enable the homologous recombination with the locus (**Figure 5.5 A**) (Yang, Ma et al. 2017). Moreover, to increase the targeting efficiency, ZNFs have been specifically designed to perform genomic nicks in the *AAVS1* locus. The simultaneous transfection of the *AAVS1*-specific ZFNs with the *AAVS1-Tet-On-hGPR56* donor vector ensures the site-specific integration of the *hGPR56* transgene in the human *AAVS1 safe harbour*, ready to be activated during the *in vitro* differentiation.

5.2.2.3 Generation of the *AAVS1-Tet-On-hGPR56* donor vectors

Molecular cloning approaches were used to generate three different *AAVS1-Tet-On* donor vectors: *AAVS1-Tet-On-hGPR56, AAVS1-Tet-On-his-hGPR56* and *AAVS1-Tet-On-hGPR56CA.* Firstly, the *AAVS1-TetOn* plasmid was digested with SalI and EcoRI. EcoRI has been used to perform a diagnostic digestion of the donor backbone, while SalI enzyme cuts out the sequence previously cloned into the *AAVS1-Tet-On* backbone. The resulting agarose gel restriction fragment separation confirmed the *in silico* prediction of the *AAVS1-Tet-On* plasmid map. EcoRI generated a band of ~1450 bp (**Figure 5.6 A**), whereas SalI gave three fragments (**Figure 5.6 B**). The middle band (~9kbp) corresponds to the linearized backbone, the bottom band (~7kb) represents the insert that was previously cloned into the donor backbone, whilst the upper band likely resembles the uncut plasmid. The linearized *AAVS1-Tet-On* plasmid (middle band) was purified from the agarose gel and stored for further application.

To prepare the *hGPR56* transgenes, I PCR-amplified the *mChery-p2a-hGPR56* (3230bp), *mCherry-p2a-hGPR56CA* (2159bp) and *mCherry-p2a-his-hGPR56* (3254bp) cassettes that have been previously cloned into *pcDNA3.1* plasmid (**Figure 5.6 C**). Each cassette includes also the *polyA* sequences at their 3'ends. The *polyA* signal is fundamental to ensure the correct mRNA nuclear export, stabilisation and translation. The set of primers designed for the cassettes contains the SalI RE sequences at their 5' and 3' ends. This will be useful to generate the sticky overhangs required for the ligation of the cassettes into the *AAVS1-Tet-ON* backbone. The three different resulting amplicons were resolved on agarose gel, eluted and digested with SalI. Then, each cassette was ligated into SalI digested *AAVS1-Tet-On* backbones and transformed into E.coli competent cells. Viable bacteria colonies were PCR screened using a set of primers that amplify the entire *mCherry-p2a-hGPR56* cassette (**Figure 5.7 A**). The positive bands indicate the bacteria that have the correct plasmid. Among all the bacteria screened, the agarose gels show that only 6, 1, and 2 bacteria have successfully ligated *AAVS1-Tet-On-mCherry-p2a-hGPR56, AAVS1-Tet-On-mCherry-p2a-his-hGPR56* and *AAVS1-Tet-On-mCherry-p2a-hGPR56CA* cassettes respectively (**Figure 5.7 B, C, D**). However, the use of a single restriction enzyme does not ensure the correct orientation of the *hGPR56* cassettes. **Figures 5.8 A** and **B** summarise the

strategy adopted to establish cassette orientation. Therefore, a set of primers was specifically designed to establish the orientation of the cassettes in the positive plasmids. A forward primer anneals the 3' end of *hGPR56*, while the revers is complementary with the *rtTA* sequence. The *hGPR56* correct orientation produce an amplicon of ~2900bp (**Figures 5.8 A**), whereas a ~1200bp fragment indicates the wrong orientation (**Figures 5.8 B**). Correct orientations are found in donor vectors coming from colony #83 (*mCherry-p2a-hGPR56*), #16 (*mCherry-p2a-his-hGPR56*) and #8 & #9 (*mCherry-p2a-hGPR56CA*) (for more details about the sequencing, see **Appendix D**).

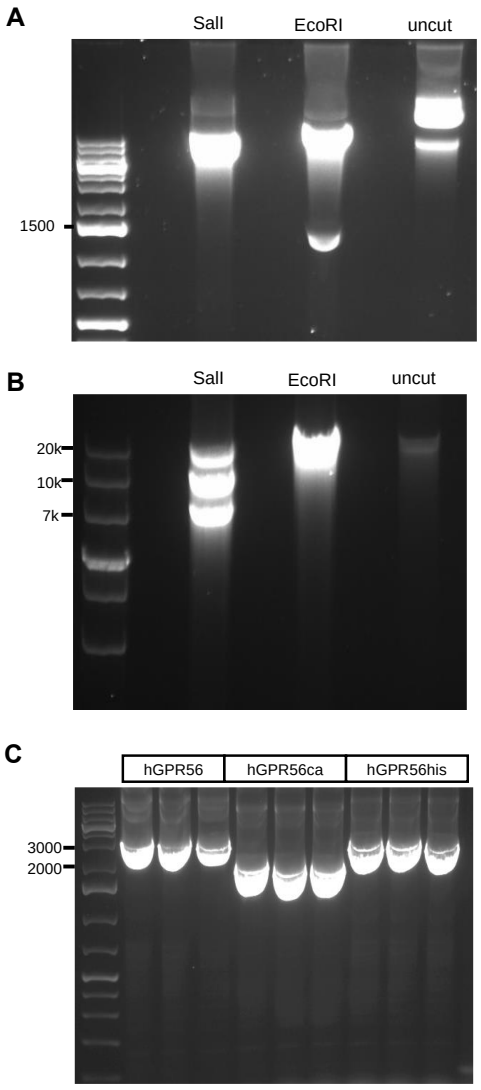

Figure 5.6 Preparation of the donor vector and amplicons.

(A) Diagnostic digestion of the *Tet-On-AAVS1* vector with SalI, EcoRI and uncut plasmid. The EcoRI digestion results in a band of 1450bp and undigested plasmid (upper band). **(B)** The SalI cut resulted in three different bands. The upper band (~20kbp) likely corresponds to the uncut plasmid, whereas the middle band (~10kbp) is the linearized conformation. The bottom band (~7kbp) correspond to the human RUNX1c gene and other regulatory sequences that were previously cloned into the *Tet-On-AAVS1* plasmid. **(C)** The agarose shows the *mCherry_p2a_hGPR56* (~3200bp), *mCherry_p2a_hGPR56ca* (~2100bp) and *the mCherry_p2a_his_hGPR56* (~3200bp) amplicons with the additional polyA sequence.

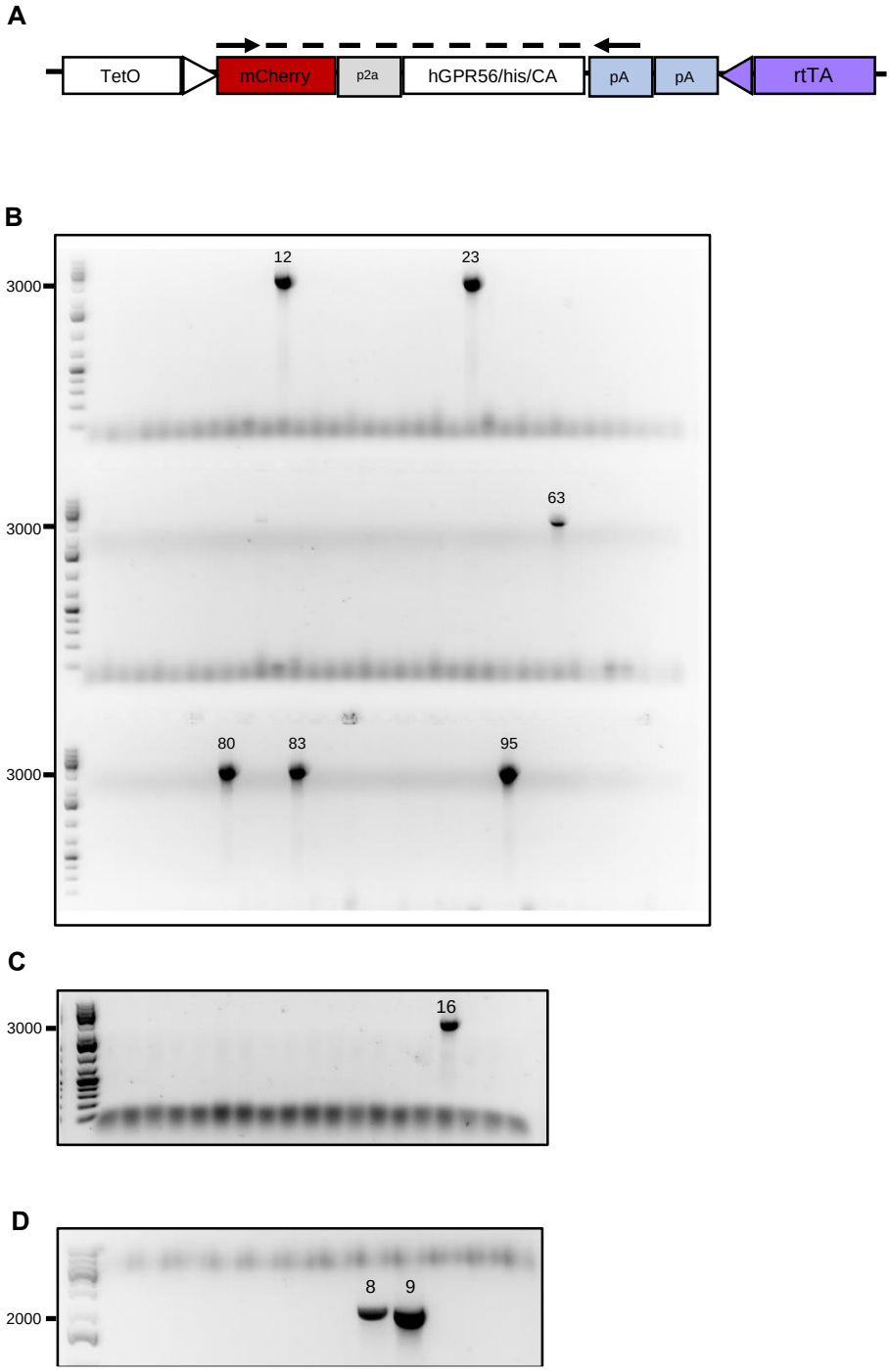

Figure 5.7 Screening of *AAVS1-Tet-On-hGPR56/his/CA* transformed bacteria.

(A) Schematic representation of the PCR screening strategy. **(B)** The bands indicate the number of bacteria that ligated successfully *mCherry-p2a-hGPR56* (~3200bp), **(C)** *mCherry-p2a-his-hGPR56* (~3200bp), **(D)** *mCherry-p2a-hGPR56CA* (~2100bp) into the *AAVS1-Tet-On* backbone.

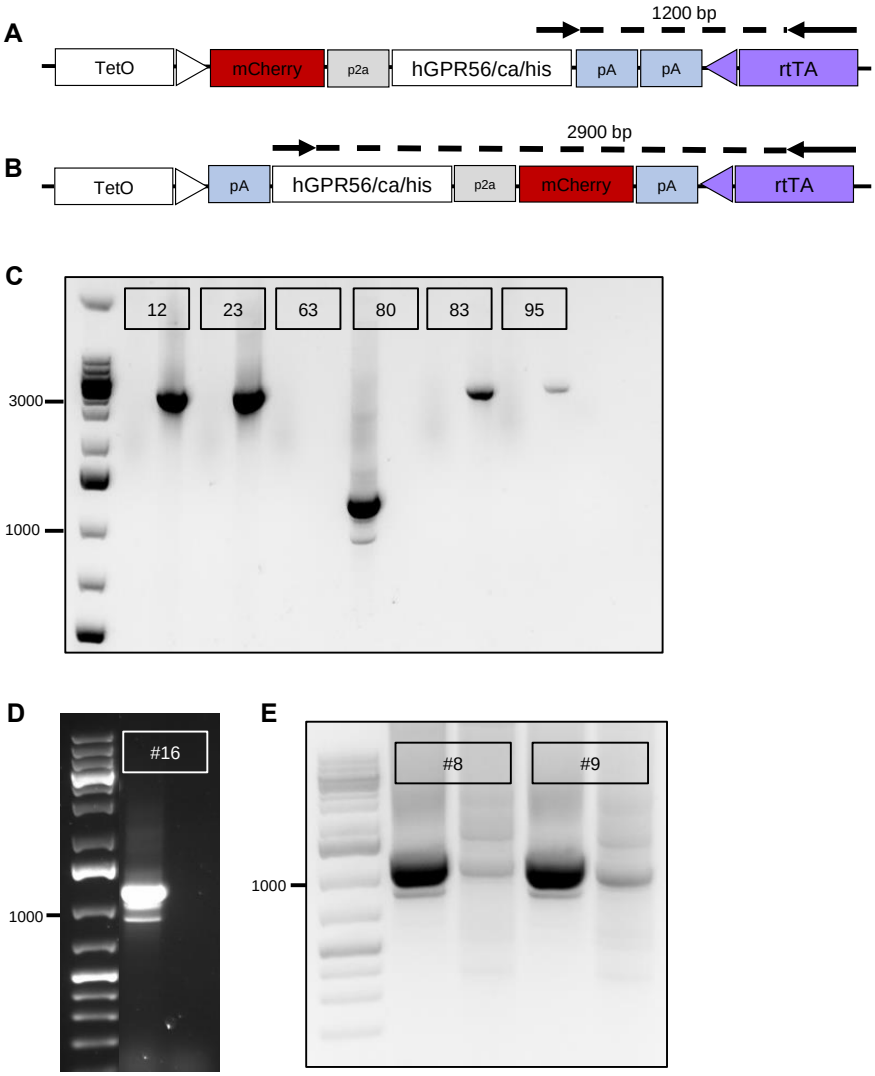

Figure 5.8 Directionally screening to establish the correct cassette's orientation.

Different length of amplicons establishes whether the cassette is ligated in the correct (1200bp) **(A)** or wrong (2900) **(B)** direction. The following agarose gels show the results of the directional screening of positive bacteria clones for *mCherry_p2a_hGPR56* **(C)** *mCherry_p2a_his_hGPR56* **(D)** and *mCherry_p2a_hGPR56ca*. The bottom extra band represents non-specific amplicons **(E)** Clones #83 **(C)**, #16 **(D)** and #8 & #9 **(E)** have the correct orientation of the cassettes. To ensure the correct orientation of the cassette, each sample was PCR amplified in duplicate using the same PCR reagents but different PCR polymerization times (elongation step): 1.5 minutes (loaded in the left lane) and 4 minutes (loaded in the right lane). The band showed in the left line confirms that the cassette has the correct orientation. Gene Ruler 1kb Plus (Thermo Scientific cat# 11511635) was used as DNA ladder in the agarose gels.

5.2.2.4 Establishment and validation of the *i55GPR56CA* human iPSC line

SFCi55 was transfected with *AAVS1-Tet-On-mCherry-p2a-hGPR56CA* (Constitutively Active form) donor vector by electroporation. To select positive clones, electroporated cells were cultured in maintenance medium supplemented with neomycin. Afterwards, 18 viable clones were picked, and PCR screened. The screening consists in two rounds of amplification using two different set of primers. The first set amplifies the *mCherry-p2a-hGPR56CA* cassette (1782bp), whereas the second, amplifies a fragment that spans the vector portion and the *AAVS1* host locus (2045bp). This resulting amplicon confirms that the donor vector has been integrated correctly in the *AAVS1* locus (**Figure 5.10 A**). The clones that show positive bands in both PCRs are those that have integrated correctly the *AAVS1-Tet-On-mCherry-p2a-hGPR56CA* donor vector. The clones that do not show both bands simultaneously, most likely, have integrated the cassette in a different location of the genome. This random integration could cause the silencing of the transgene or alter cell functions leading to abnormal cellular behaviour. Of the 18 viable clones selected by neomycin, 14 are positive for *mCherry-p2a-hGPR56CA* (**Figure 5.10 B**) Among them, 8 clones (clone #B, D, M, N, O, P, Q, V) resulted positive for the second PCR amplification (**Figure 5.10 C**). The PCR amplicons confirm that the *AAVS1-Tet-On-mCherry-p2a-hGPR56CA* donor vector has been properly integrated into the AAVS1 locus of clones #B, D, M, N, O, P, Q, V. Most likely, the other bands on the bottom of the agarose gel are the amplification of unwanted non-specific genomic products. Among the positive clones, I validate clone #M and use it to perform functional hematopoietic analyses. From now onwards, I refer to it as *i55GPR56CA*. Karyotype on the newly generated *i55GPR56CA* iPSC line needs to be performed to exclude genomic anomalies.

To validate the inducible reporter gene activation, undifferentiated and differentiating *i55GPR56CA* were tested in the presence or the absence of doxycycline. 24 hours after been exposed to doxycycline, undifferentiated cells activate the reporter *mCherry* gene (**Figure 5.11 A** and **B**). Similarly, day 6 (D6) differentiating *i55GPR56CA* embryoid bodies (EBs) were *mCherry* positive after the doxycycline has been added into the culture media at D4 (**Figure 5.12 A**). The same EBs were harvested and FACS analysed to evaluate the frequency of the mCherry expressing cells. Around 32% of single live cells are mCherry expressing (**Figure 5.12 B**). To assess whether mCherry+

fraction expresses *hGPR56CA*, D6 *i55GPR56CA* EBs were FACS sorted into mCherry+ and mCherry- fractions. RT-qPCR analysis shows that h*GPR56CA* transcript is exclusively expressed by the mCherry+ as compared to mCherry- cells (**Figure 5.12 C**). The validation of the established *i55GPR56CA* cell line reported that, upon doxycycline, mCherry+ cells overexpress *hGPR56CA* during *in vitro* differentiation. This novel *i55GPR56CA* iPSC line will be used to investigate the hematopoietic output of HPCs after *hGPR56CA* overexpression.

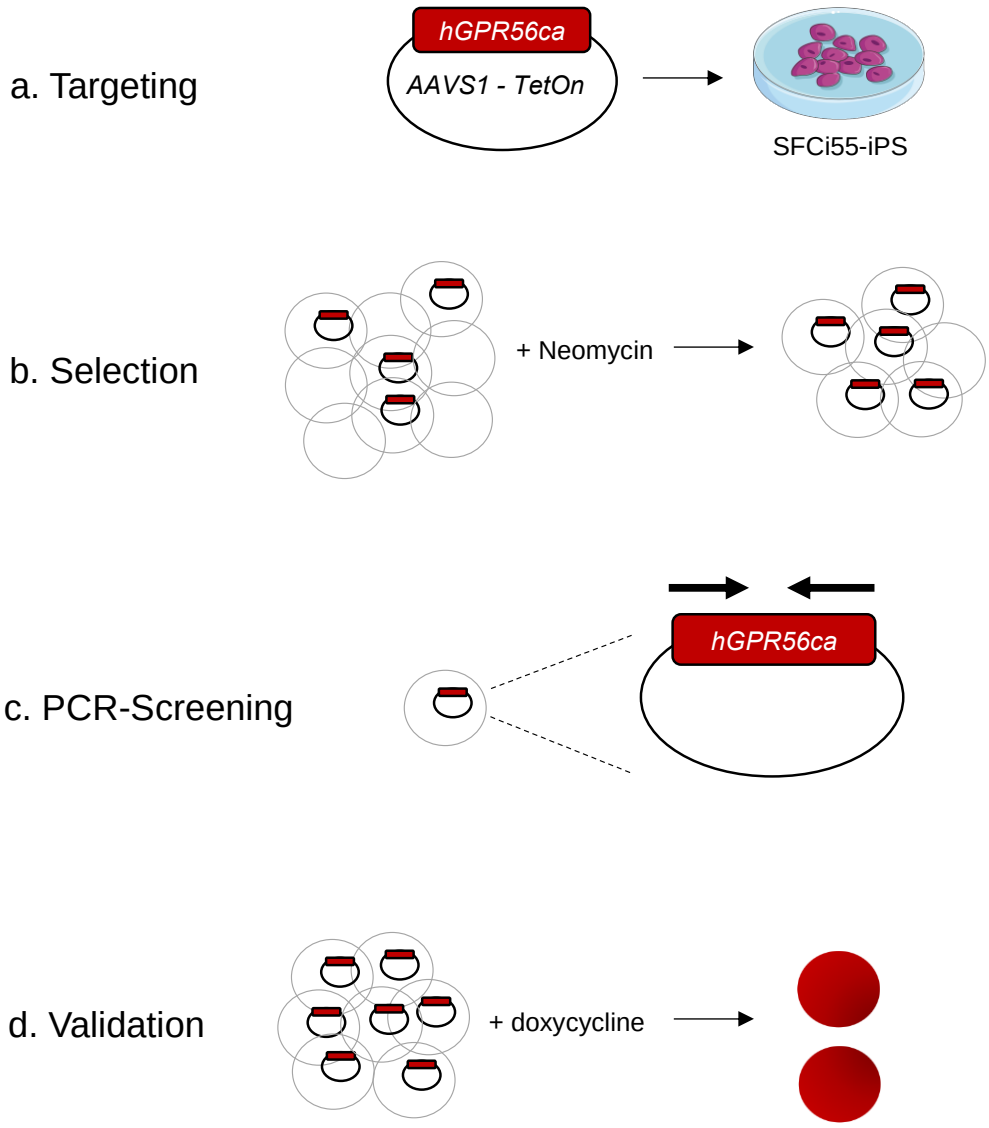

Figure 5.9 Workflow to establish the *i55GPR56CA* iPSC line.

(A) SFCi55 cell line has been targeted with *AAVS1-TetOn-hGPR56ca*. **(B)** The neomycin supplemented in the medium selects the clones that have integrated the *AAVS1-TetOn-hGPR56ca* donor vector. **(C)** PCR screening of neomycin resistant clones to assess the proper integration of the *AAVS1-TetOn-hGPR56ca* in the AAVS1 locus. **(D)** The selected clone has been validated adding the doxycycline in the medium to activate the transgene.

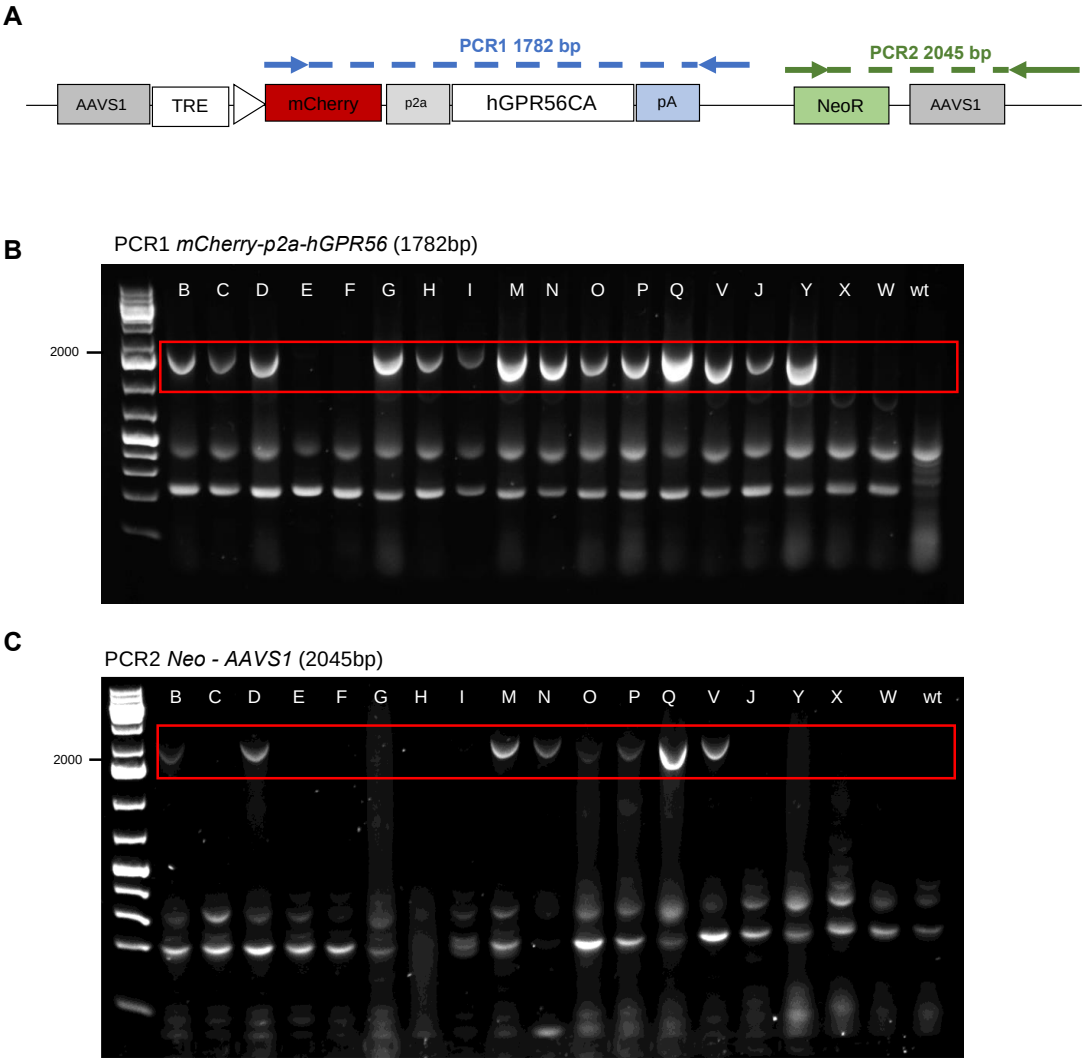

Figure 5.10 Screening of viable SFCi55-after neomycin selection

(A) Strategy to assess the correct targeting of the *AAVS1-Tet-On-hGPR56CA* donor vector. The PCR1 amplifies the *mCherry-p2a-hGPR56CA* (1782bp) cassette, while PCR2 amplicon (2045bp) confirms that the donor vector locates in the *AAVS1* locus. **(B)** Screening of 18 viable clones for the PCR1. 14 of them are positive for *mCherry-p2a-hGPR56CA*. **(C)** Screening of the same 18 clones for the PCR2 (*Neo-AAVS1*). Only 8 of them resulted positive. Correct bands are indicated within the red squares.

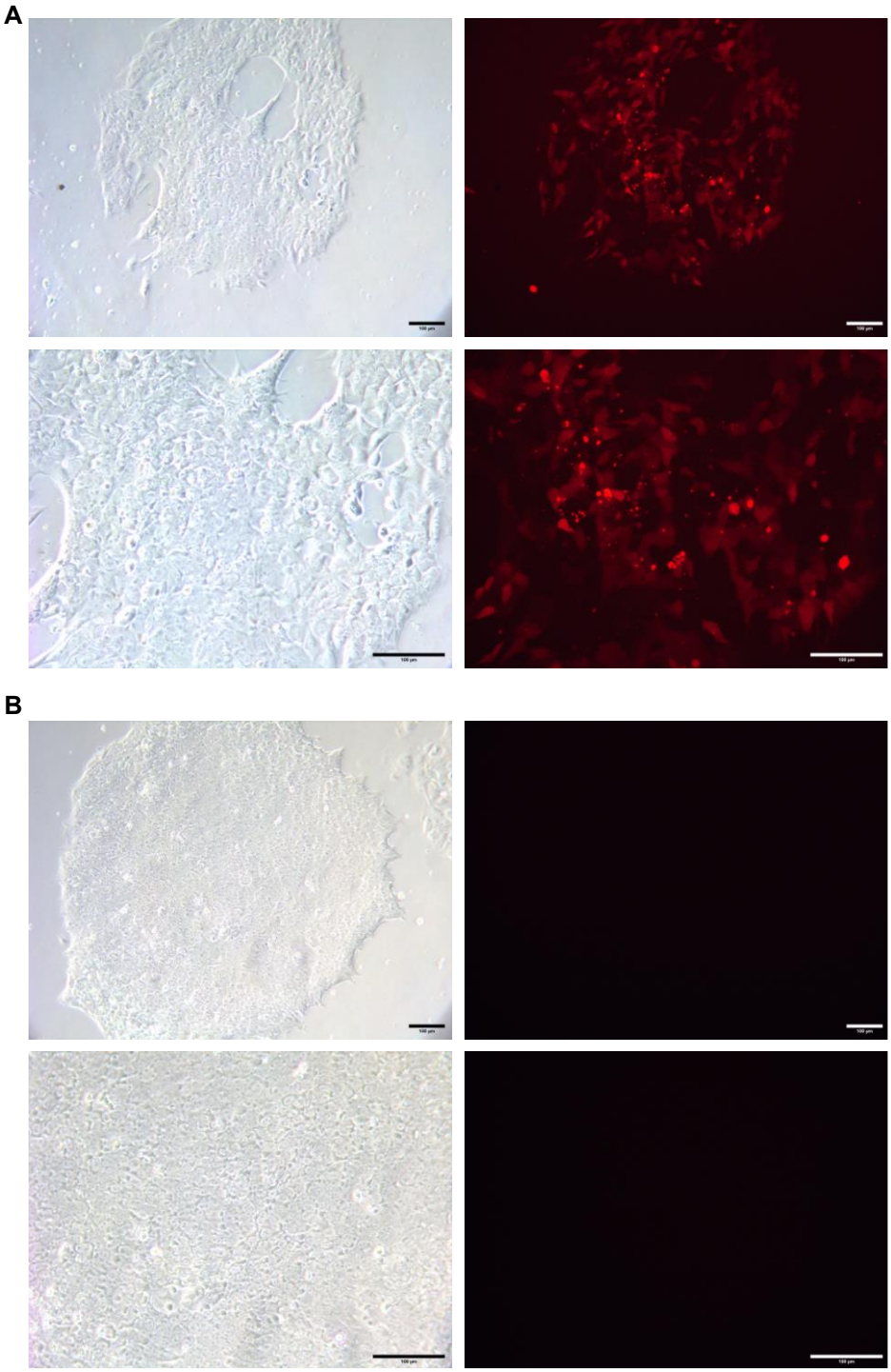

Figure 5.11 Assessment of successful *Tet-On-AAVS1-hGPR56CA* targeting.

Undifferentiated *i55-hGPR56CA* #M cells were tested in the presence **(A)** or absence **(B)** of doxycycline. On the left I show the bright field channels; on the right, the red channels. Each figure shows an example of a *i55-hGPR56CA* #M colony at 10x (top) and 20x (bottom) magnification, n=2. Scale bar=100um.

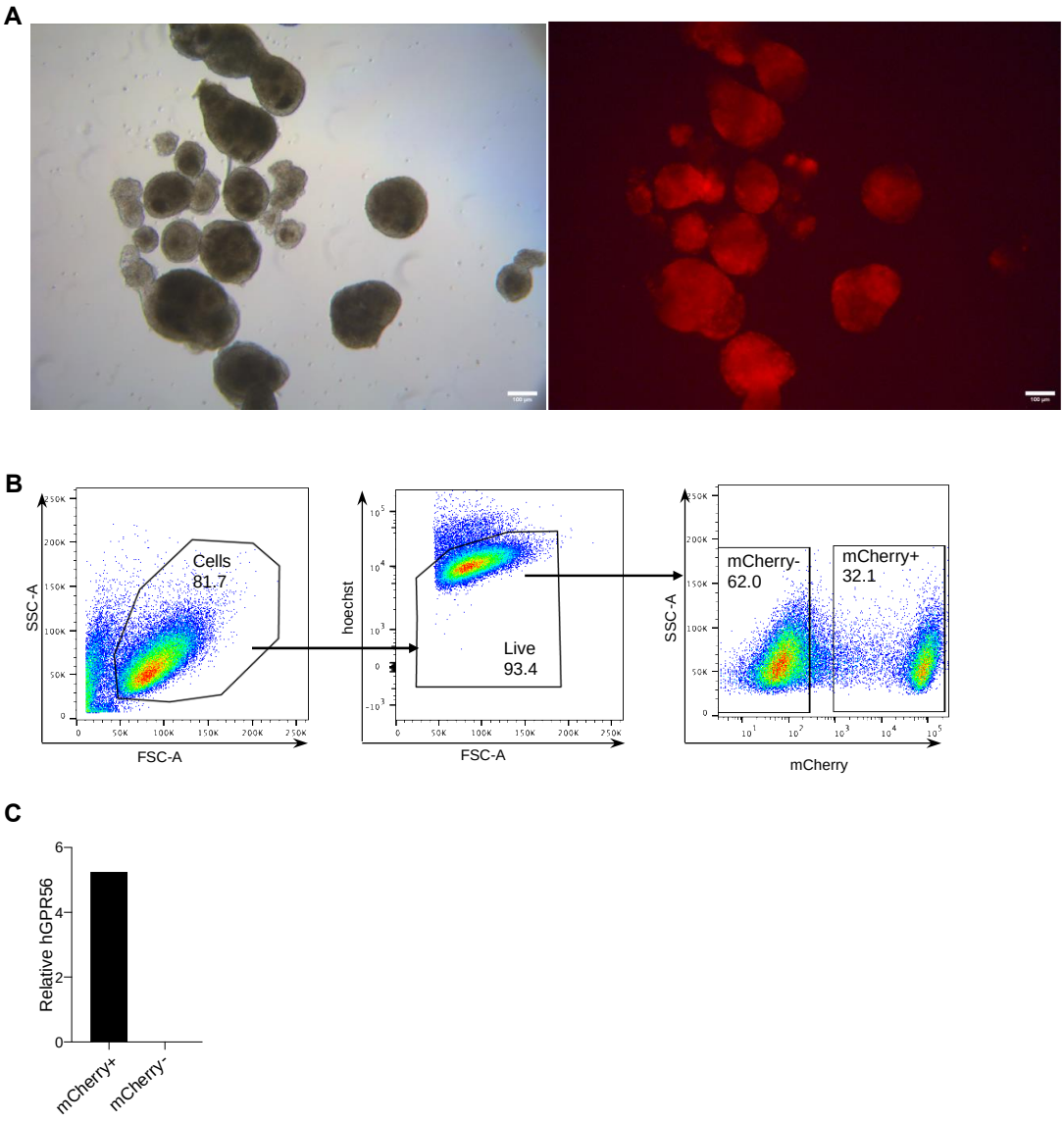

Figure 5.12 Evaluation of *hGPR56* transcript's expression within the *mCherry* populations.

To activate mCherry-hGPR56CA, doxycycline was added in the culture medium at day (d)4 of hematopoietic differentiation. **(A)** Day (d)6 EBs. Bright channel on the left red channel on the right. Scale bar=100um **(B)** D6 dox-activated EBs were collected and FACS analysed. Viable cells were resolved for mCherry signal; mCherry+ and mCherry- population were FACS sorted **(C)** Relative mRNA expression of hGPR56 sequence in FACS-sorted mCherry+ and mCherry- populations. Beta-actin was used as reference gene.

5.2.3 Functional role of GPR56 overexpression in iPSC-derived HPCs

To investigate the hematopoietic output after the overexpression of GPR56, the *i55GPR56CA* was *in vitro* differentiated towards the hematopoietic lineage. Taking advantage of the *mCherry* fluorescent reporter, it is possible to trace the cells that overexpress GPR56 and evaluate their contribution on generating hematopoietic progenitor cells (HPCs). To differentiate *i55GPR56CA*, I developed a modified version of the well-established *in vitro* embryoid bodies (EB) based hematopoietic differentiation protocol, described by the Keller group (Kennedy, Awong et al. 2012). Similarly to the previous protocol adopted by Kennedy and colleagues, the new method takes advantage of the three-dimensional aggregates called embryoid bodies (EBs). However, it no longer necessitates to incubate human undifferentiated iPSC lines for 8 days under hypoxic condition to generate EBs. Along the differentiation, we discriminate three different stages: EB induction (EI) from day (D) 0 to D4, hematopoietic cell specification (HS) from D6 to D8 and hematopoietic maturation (HM) from D8 to D11 (**Figure 5.13 A**). In all these different stages, I supplemented the basal serum-free culture medium with different cytokine compositions. During the EI, the undifferentiated iPSCs were primed to induce EB formation and differentiated into mesodermal lineage using BMP4, SCL and VEGF cytokines. In the HS and HM phases, the basal medium was supplemented with different cytokine combinations that are required to commit the cells into the hematopoietic fate. *In vitro* human early HPCs begin to be detected by D9 and their frequency gradually increase over time to peak at D11. From D11 onwards, they decline and are no longer detectable by D15 (Vodyanik, Thomson et al. 2006, Timmermans, Velghe et al. 2009, Kennedy, Awong et al. 2012). The frequency of D11 *i55GPR56CA* derived HPCs (CD38-CD34+) was assessed in the presence or in the absence of doxycycline.

To induce the constitutive GPR56 activation, doxycycline was supplemented in the culture medium from D4 onwards, every other day (D6, 8, 10). D11 EBs were FACS analysed to evaluate viable cells and the frequency of the HPCs. The analysis showed that there is no significant difference between the percentage of viable (Hoechst-) dox-induced versus dox-non-induced (**Figure 5.13 B**).

To explore the functional effect of GPR56CA overexpression on HPCs, we analysed the frequency of D11-derived HPCs in the presence or absence of doxycycline (**Figure 5.13 C, D**). *GPR56CA* dox-induced cells significantly increased the frequency of the phenotypic HPCs (CD38-CD34+) by a factor of 3.2 (±1.7) as compared to the non-induced counterpart (**Figure 5.13 E**). To test the hematopoietic potential, D11 CD38-CD34+ HPCs were FACS sorted and plated into methylcellulose. CFU-C colony types have been scored based on their morphology after 10 days of expansion. Our preliminary data (n=2) demonstrated that the hematopoietic potential is selectively restricted to the dox-induced HPC population as compared to the CD38-CD34+ dox-non-induced counterpart (**Figure 5.13 F**). Thus, induced-GPR56CA expressing cells showed an increase in the total number of CFUCs when compared to the dox-non-induced (n=2).

Afterwards, I assessed the frequency of GPR56CA expressing cells in the dox-induced population. Less than 40% of the viable dox-induced cells express GPR56CA (**Figure 5.14 A**). However, this percentage was surprisingly sufficient to generate significant increases in the CD38-CD34+ population. Since the *i55GPR56CA* is a mixed population which contains up to 40% of *GPR56CA* expressing cells, I wanted to determine the origin of the CD38-CD34+ cells, whether they differentiate from mCherry+ or mCherry- subpopulations. I analysed the frequency of mCherry+/- cells within the dox-induced *i55GPR56CA* derived HPC population (**Figure 5.14 B** and **C**). Interestingly, all of single experiments revealed that ~60% of HPCs derived from the mCherry- fraction (**Figure 5.14 D, E**). I investigated whether the mCherry- HPCs possess an increased *in vitro* hematopoietic potential. The hematopoietic potential of D11 dox-induced mCherry+ and mCherry- derived HPCs was tested in CFU-C assay. Surprisingly, the CFU colony number of the dox-induced mCherry- fraction was higher when compared to mCherry+ counterpart (**Figure 5.14 F**). Altogether, these preliminary results lead to the hypothesis that the overexpression of GPR56CA increases the frequency of the *in vitro* derived HPCs likely by the simultaneous contribution of two unknown mechanisms: direct and indirect. However, few other hypotheses need to be considered. The simultaneous increase of mCherry- and the decrease of mCherry+ derived CFU-C could be caused by a toxic effect of GPR56 overexpression or perhaps due to different protein stability between mCherry and

GPR56. To confirm these hypotheses, a wild-type SCFi55 (not-engineered) needs to be included in the experimental set-up. This control would rule out any survival effect induced by doxycycline when added into the culture media.

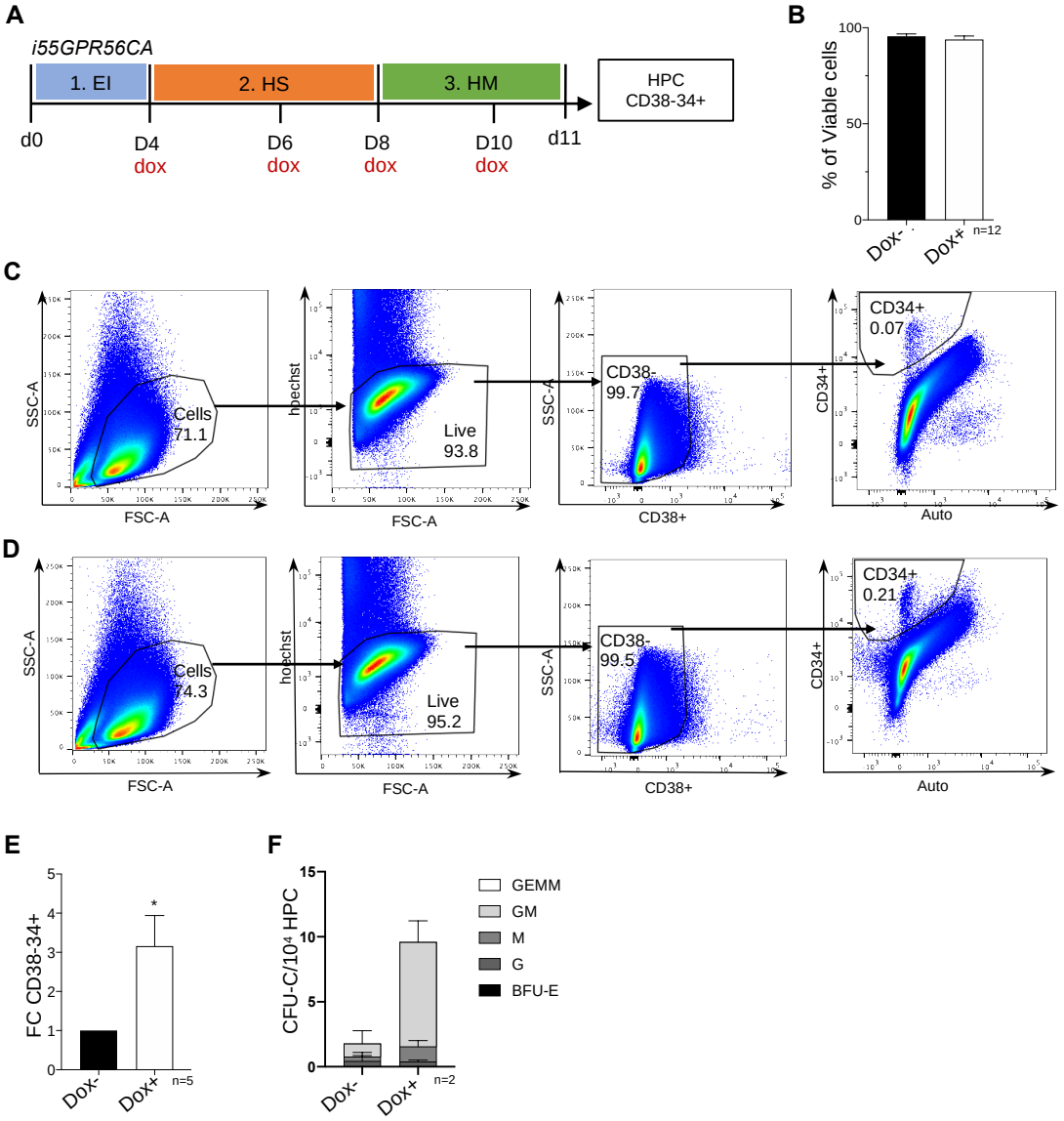

Figure 5.13 *In vitro* functional analysis of *i55GPR56CA* line.

(A) Illustration of the *in vitro* human haematopoietic differentiation. The protocol consists of three different stages: embryoid bodies induction (EI), haematopoietic specification (HS) and haematopoietic maturation (HM). From d4 onwards, doxycyline was added every other day. At d11, the embryoid bodies (EBs) were collected, dissociated and FACS-analyzed to assess the frequency of the haematopoietic progenitors (CD38-CD34+). **(B)** Percentage of viable cells in dox- and dox+ i55-hGPR56ca (n=12). Viable cells are defined as hoechst negative (Ho-). FACS analysis of day 11 haemtopoietic progenitors (HPCs) in doxycycline's absence **(C)** or presence **(D)** n=5, mean +/- SEM, *p<0.05. **(E)** Fold change of Dox-/+ i55-hGPR56ca-derived HPCs (n=5). **(F)** CFU-C haematopoietic colony output from Dox-/+ FACS sorted

HPCs (CD38CD34+) plated into methylcellulose, n=2, mean of no Dox CFU-G 0.5, CFU-M 0.5, CFU-C GM 1.5. Mean Dox CFU-G 1.15, CFU-M 2.5, CFU-GM 9.8

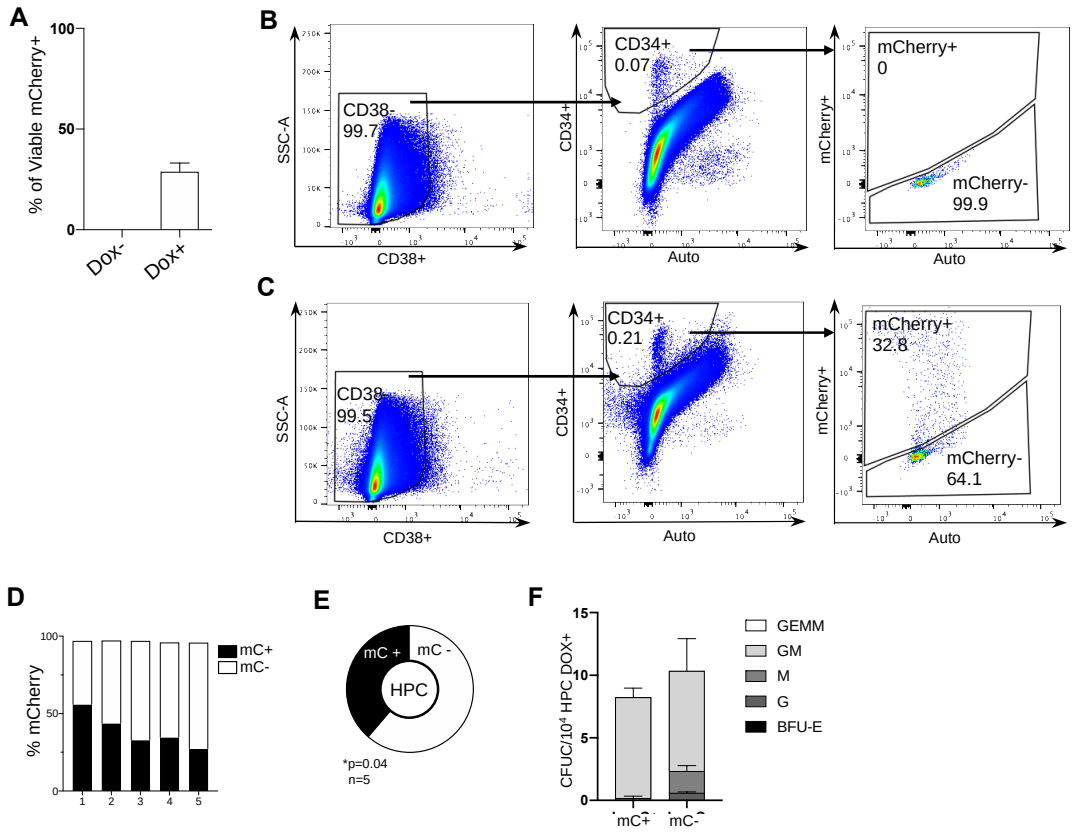

Figure 5.14 *In vitro* Dox-derived HPCs arise from a non mCherry-reporter expressing i*55GPR56CA* subfraction.

(A) Percentage of viable mCherry+ *hGPR56ca* expressing cells within the Dox activated *i55-hGPR56* cell line. FACS analysis of the dox- **(B)** and dox+ **(C)** HPCs. CD38-CD34+ were resolved for mCherry signal. **(D)** Percentage of mCherry+/- derived HPCs. Each column represents a single experiment. **(E)** The pie chart displays the contribution of mCherry + and mCherry- supopulation in generating HPCs. n=5, *p<0.05. **(F)** CFU-C colonies derived from mCherry+ and mCherry- HPCs after being seeded in methylcellulose. n=2, mean.

5.3 Discussion

The controlled expression of Gpr56 is required for mouse embryonic HSC generation and for their maintenance in the adult BM (Saito, Kaneda et al. 2013, Rao, Marks-Bluth et al. 2015, Solaimani Kartalaei, Yamada-Inagawa et al. 2015). Nevertheless, the effects of GPR56 aberrant expression in normal hematopoietic cells and its role in LSCs remain unexplored. In this chapter, I elucidated the biological effect of the aberrant human GPR56 expression in *in vitro* hematopoiesis. By generating a novel human inducible GPR56 reporter iPSC line (*i55GPR56CA*), I overexpressed GPR56 during the hematopoietic differentiation, which resulted in enhanced HPC generation.

To ensure GPR56 activation, I expressed a truncated GPR56 form, which is known to trigger the ligand-independent constitutive activation of the GPR56 downstream signalling pathway (Paavola, Stephenson et al. 2011). GPR56 activation remains an important limitation as ligands and downstream effectors are tissue dependent. Few studies demonstrated that GPR56 is constitutively activated in a ligand-independent mechanism. This has been achieved through exposing the *Stachel* domain by deletion of the *n-terminal* portion of the receptor (Paavola, Stephenson et al. 2011). However, this chapter did not provide direct evidence of the GPR56 downstream signalling activation. Additional experiments are required to assess the activation of downstream effectors, such as RhoA and ROCK phosphorylation or the activation of GPR56-related transcription factors.

The data highlighted that the majority of the HPCs are generated from a subset of cells that do not express mCherry. Few hypotheses might be formulated to explain this event. The first, it refers to the different protein stability between mCherry and GPR56. Cells that no longer express mCherry could still express constitutively active GPR56 in the cell membrane. Or it could be possible that mCherry- HPCs benefit from a paracrine effect by mCheery+ dox-induced cells. This GPR56-dependent paracrine effect focuses attention on a novel regulatory mechanism that has not yet been described. Previous works conducted in melanoma reported that GPR56 overexpression increases IL-6 secretion (Chiang, Peng et al. 2017). Another study demonstrated that AML blasts activate the STAT3 pro-proliferative pathway by high IL-6 secretion levels (Schuringa, Jonk et al. 2000). However, further experiments are

required to investigate the link between GPR56 dependent IL-6 secretion and the constitutive expression of the STAT3 pathway.

The lower frequency of mCherry+ expressing cells is another limitation to be addressed. To test GPR56 overexpression, an dox-inducible GPR56 vector was delivered into the human *AAVS1* locus. This strategy is known to overcomes the main drawbacks brought by lentiviral particles, such us random integration and unforeseen mutation of host's important genes (Ellis 2005). Targeting the *AAVS1* locus is supposed to avoid the transgene silencing due to epigenetic changes that occur along *in vitro* differentiation. However, recent findings reported that the *AAVS1* locus shouldn't be considered as an accurate safe harbour (Bhagwan, Collins et al. 2019). The expression of a transgene integrated in the *AAVS1* locus varies between clones and it showed a clone-dependent degree of silencing towards hematopoietic and cardiomyocyte differentiation (Bhagwan, Collins et al. 2019). This drawback might justify the lower mCherry+ cell fraction obtained in targeted cells. It is also unknown whether *AAVS1* engineered cells will silence the transgene overtime after several hematopoietic differentiations. Thus, the ectopic expression of GPR56 in the newly engineered cell line could be affected over time by this unforeseen clone-dependent silencing.

Although some limitations remain to be addressed, collectively, the data show that the overexpression of GPR56CA generates higher frequency of HPC population that holds an enhanced hematopoietic potential. These findings raised further questions on their origin, whether they result from an increased number of endothelial cells that undergo EHT or whether GPR56 expression activates an internal feedback mechanism that promotes hematopoietic progenitor cell proliferation.

To conclude, a better understanding of GPR56 in human haematopoiesis will contribute to develop new strategies to improve the current cancer therapies. The over-expression and activation of GPR56 during *in vitro* differentiation, could contribute to improve well-establish protocols for *de novo* generation of HSC or to develop new therapeutic strategies to target GPR56-dependent malignant molecular pathways. Also, the relevant *in vitro* expansion of HPCs upon GPR56 over-expression might be used as a tool to try to expand HSCs *ex vivo.* However, further *in vitro* and *in vivo*

functional examinations are required to assess the function and the long-term effects of these HPCs.

6 DISCUSSION AND FUTURE DIRECTIONS

To date, two groups attempted to study Gpr56 loss of function in adult hematopoiesis (Saito, Kaneda et al. 2013; Rao, Marks-Bluth et al. 2015). However, those studies revealed discrepancies in their results as the mouse model adopted failed to truly knock-out *Gpr56* (Saito, Kaneda et al. 2013; Rao, Marks-Bluth et al. 2015). This thesis aims to investigate the effect of Gpr56 *loss-of-function* and *gain-of-function* in the HSPC population using novel animal models and *in vitro* approaches.

The embryonic downregulation of Gpr56 decreases YS-derived HPC frequency and their hematopoietic potential, whereas Gpr56 is dispensable for bulk FL-derived HSCs. Single cells transplantation of Gpr56 conditional knockout (cKO) FL-derived HSCs showed that Gpr56 is required to maintain HSC self-renewal capacity and their balanced hematopoietic output. Moreover, Gpr56 cKO FL-HSCs are myeloid-biased, as preferentially differentiate into myeloid blood cells when transplanted into recipient mice. These findings were confirmed also *in vitro* using mESC. The differentiation of mouse *G2V.56*^{KO} ESCs generate HPCs with enhanced myeloid potential. Interestingly, Gpr56-cKO FL-HSCs and *G2V.56*^{KO} derived HPCs upregulate another GPCR, *Gpr97*, which resides within the *Gpr56* locus. Functional analyses performed in *gpr56* MO zebrafish larvae demonstrate that Gpr97 rescues the generation of HSPCs. The concomitant deletion of *Gpr97* and *Gpr56* in mESCs impairs HPC generation, indicating that both receptors are required for *in vitro* hematopoiesis. These data suggest that Gpr97 might compensate for the absence of Gpr56 in FL-derived HSPCs and *G2V.56*^{KO} HPCs, possibly driving their differentiation into myeloid cells.

6.1 Gpr97 as putative receptor that functionally compensates for Gpr56 deletion.

Similar to Gpr56, Gpr97 (Adgrg3) belongs to the adhesion GPCRs. It has a long extracellular domain (ECD), a *stachel* domain and a 7 transmembrane domain (7TM), which joins with an intracellular domain to trigger the signalling cascade upon receptor

activation (Stoveken, Hajduczok et al. 2015). The protein comparison of Gpr97 with Gpr56 confirmed that these domains are very similar and mostly conserved. Few studies have described the biological importance of Gpr97 in immune cells. Hsiao and colleagues provided insights into the role of aGPCRs along haematopoietic differentiation. The aGPCRs expression profile in human cord blood and BM confirmed that *Gpr56* is highly expressed in HSPCs and cytotoxic lymphocytes, whereas *Gpr97* is abundantly upregulated in polymorphonuclear cells (PMNs) (Hsiao, Chu et al. 2018). In PMNs, full length Gpr97 activates cAMP signalling and inhibits the NF-kB pathway. Like Gpr56, Gpr97 is activated by the detachment of the extracellular N-fragment (NTF) from the main protein. The exposition of the encrypted tethered agonist *stachel* domain, activates the receptor signalling. Thanks to *in vitro* cellular assays, the authors investigated the downstream pathways using Gpr97 full length and Gpr97 constitutively active form, which lack the N-terminus end. When compared to the full length, Gpr97 constitutively active form increased the levels of intracellular SRE and NF-kB, with a significant reduction of CREB (cAMP responsive element-binding protein) (Hsiao, Chu et al. 2018). Another study reported that Gpr97 regulates the motility of lymphatic endothelial cell (LECs) by modulating the equilibrium between Cdc42 and RhoA downstream pathways (Valtcheva, Primorac et al. 2013). Valtcheva and colleagues showed that after Gpr97 KD, LECs activate Cdc42 followed by cytoskeleton rearrangement that led to an improved cell migration and reduced cell adhesion (Valtcheva, Primorac et al. 2013). Collectively, these data provide preliminary evidences that Gpr97 could compensate for Gpr56 absence in hematopoiesis. It would be interesting to perform additional *in vitro* experiments with Gpr97 overexpression to rescue the HPC generation in *G2V.56*^{KO}*97*^{KO}cell line. This would be a key experiment to confirm Gpr97 functional compensatory mechanism in mouse *G2V.56*^{KO} ESCs.

6.2 To understand the molecular mechanism that regulates the interplay between Gpr56 and Gpr97.

Although Gpr56 and Gpr97 share a similar structure and downstream pathway, the molecular mechanism that governs this potential compensatory mechanism remains to be explored. Future experiments are required to explain whether these two genes are

regulated at transcriptional and/or post-translational level. Importantly, it is unclear whether they share the same promoter and/or regulatory regions. As Gpr56 and Gpr97 proteins share high homology domains and mechanism of activation, it would be important to ascertain whether they also share intracellular signalling pathways or extracellular ligands.

Another important point to consider is the different microenvironments that HSPCs are exposed to at different developmental stages. The niche plays a crucial role in HSC commitment, specification and support during adult life (reviewed in Crisan and Dzierzak 2016, Gao, Xu et al. 2018). It would be interesting to understand the higher expression of *Gpr97* in *Gpr56*$^{-/-}$ FL-HSCs but not in *Gpr56*$^{-/-}$ BM-HSCs. To compensate for Gpr56 downregulation, the BM niche may provide extracellular signals to the HSPC population, so that they do not require to overexpress *Gpr97*. This could be interrogated by characterizing the transcriptomic profile of BM and FL microenvironments in *Gpr56*$^{-/-}$ mouse models.

The most unexpected results came from the *G2V.56*^{KO}*97*^{KO} double knock out mES cell line. Very few HPCs were produced after *in vitro* hematopoietic differentiation. This prompted us to investigate the concomitant deletion of Gpr56 and Gpr97 *in vivo*. The generation of a double knock-out mouse model could not be easy to achieve, as the generation of a Gpr56 and Gpr97 KO germline might result in embryonic lethality. Currently, we are generating a floxed mouse model that would locate 2 loxP sites spanning *Gpr56* and *Gpr97* genomic sequences. To investigate the role of Gpr56 and Gpr97 deletion in *in vivo* haematopoiesis, the newly generated floxed mice will be crossed with the *VAV*- and *VEC-Cre* mouse models to generate *Gpr56/97* conditionally double KO embryos. Using these mouse embryos, we will evaluate the effect of Gpr56 and Gpr97 *loss-of-function* in the generation of HSCs *in vivo.*

6.3 To study the reduction of self-renewal in Gpr56$^{-/-}$HSCs

The transplantation of few FL-HSCs revealed that Gpr56-/- FL-HSCs gradually reduce their repopulation activity after serial transplantations, which resembles the phenotype of aged HSCs. It would be interesting to compare the proliferation rates of young and aged BM derived *Gpr56*$^{-/-}$ HSCs versus WT counterparts. Moreover, it would be also

interesting to assess whether *Gpr56*$^{-/-}$ HSCs are unable to maintain their quiescent state, with enhanced differentiation rate compared to the WT. Additionally, transcriptomic analysis as well as ATAC sequencing may reveal important features of the genetic/epigenetic changes related to Gpr56 function and/or aging.

Mobilization and homing are also important features for HSCs. As part of adhesion G-protein coupled receptors, Gpr56 might be involved in the regulation of HSC motility. The lower engraftment capacity of *Gpr56*$^{-/-}$ HSCs in recipient mice might be explained by their reduced ability in homing or adhesion capacities after transplantation into host BM. Future experiments with high resolution microscopy would be beneficial to visualize the localisation of *Gpr56*$^{-/-}$ HSCs in the BM of recipient mice.

6.4 To determine the signalling pathways regulated by Gpr56.

Further experiments are also required to understand the signalling pathways regulated by the activation of Gpr56. In our preliminary experiments (data not shown), the addition of Col3A to the *G2V* mES differentiation culture media activates RhoA-ROCK effectors. Further experiments are required to confirm these preliminary findings. Nevertheless, to identify pathways that are modulated by Gpr56, the mouse *G2V* cell line offers a great opportunity to profile the transcriptome of *G2V.56*^{KO} as compared to *G2V.WT*.

Gpr56 activation may be promoted also by external mechanical forces, a process that involves changes in the cytoskeleton architecture (Iguchi, Sakata et al. 2008, Ohashi, Fujiwara et al. 2017). The pathway that involves cytoskeleton changes is the Hippo pathway, which is regulated by cell-cell interaction, cell polarity and actin cytoskeleton remodelling (reviewed in (Yu and Guan 2013, Johnson and Halder 2014). This pathway is involved in the regulation of organ size and tumorigenesis by modulating cell survival, proliferation and differentiation (reviewed in Davis and Tapon 2019). Different GPCRs have been found to modulate Hippo pathway activation. Interestingly, the activation of Hippo effectors, YAP/TAZ is dependent on GPCRs coupled with Galpha12/13 and protein kinases Rho GTPases (Yu, Zhao et al. 2012, Yu and Guan 2013). Investigating the relationship between Gpr56 and

YAP/TAZ activation during embryonic HSPC generation would represent a novel Gpr56-regulated downstream pathway that has not been described yet.

6.5 GPR56 *gain-of-function* enhances the generation of HPCs.

Although several studies characterised Gpr56 *loss-of-function*, few studies focused on investigating the Gpr56 *gain-of-function* in hematopoiesis (Piao, Hill et al. 2004, Ng, Mitchell et al. 2016, Pabst, Bergeron et al. 2016, Huang and Lin 2018). To overexpress GPR56 during human hematopoiesis, we established a novel inducible constitutively active GPR56 reporter human iPSC line and differentiated it towards HPCs. The engineered iPSC line ectopically expresses active GPR56 upon the addition of doxycycline into culture medium. Thanks to the expression of *mCherry* fluorescent reporter protein, we were able to origin-trace these HPCs. The enforced GPR56 activation on human EBs from D4 onwards results in a 3-fold change in HPC expansion. HPCs mainly derived from the mCherry- fraction within doxy-activated cells. There are few reasons that can explain this event. It could be possible that the majority of the mCherrry+ cells undergo to cell death due to the cellular toxicity caused by the prolonged GPR56 overexpression. Another explanation might be found in the different protein stability between mCherry and GPR56, or it could be reasonable to think that some soluble factors or cytokines secreted by mCherry+ cells might activate some mitogenic pathway in the mCherry- cells.

Interestingly, previous studies observed that the activation of GPR56 with CG4 mAb promotes the secretion of the pro-inflammatory cytokine IL-6 (Chiang, Peng et al. 2017). IL-6 has been described to play different roles at different stages of melanoma development: at early stages it suppresses cell growth, whereas in later stages, it stimulates the expansion of the metastasis (Hoejberg, Bastholt et al. 2012). Other studies reported high IL-6 expression in malignant metastatic melanoma patients who respond poorly to therapy (Heikkila, Ebrahim et al. 2008, Hoejberg, Bastholt et al. 2012).

Cytokine dysregulation is known to contribute to the pathogenesis of AML. The aberrant expression of pro-inflammatory cytokines has been associated with

proliferation, blast survival, LSC resistance to chemotherapy and long-term prognosis (Tsimberidou, Estey et al. 2008). Sanchez-Correa and colleagues profiled pro and anti/-inflammatory cytokines in the plasma of AML patients and found that increased IL-6 correlated with poor survival in patients with AML (Sanchez-Correa, Bergua et al. 2013). These findings are supported by another clinical study performed on a cohort of 45 paediatric patients affected by AML. The study explained the role of IL-6 BM-derived secretion in conferring LSCs long-term survival after chemotherapy (Stevens, Miller et al. 2017). IL-6 has been reported as one of the ligands that activates the STAT3 pathway. When the pathway is active, phospho-STAT3 proteins dimerise and migrate into the nucleus to promote the transcription of pro-survival genes that support aggressive LSCs (Bromberg, Wrzeszczynska et al. 1999, Redell, Ruiz et al. 2013). IL-6 activates STAT3 pathway in LSCs, which acquire resistance to chemotherapy and lead to disease progression (Stevens, Miller et al. 2017). In addition, relapsing LSCs maintain a higher level of IL-6-induced STAT3 activation than the same LSCs at diagnosis (Stevens, Ruiz et al. 2015), perhaps offering LSCs an advantage to promote expansion. Thus, it may be interesting to understand whether GPR56-induced IL-6 is the putative pro-inflammatory cytokine that promotes higher frequency of HPCs in *in vitro* hematopoiesis.

The results presented in Chapter 5 suffers from few technical limitations. Although it was demonstrated by previous studies (Paavola, Stephenson et al. 2011), GPR56 signalling activation needs to be confirmed in the newly generated *i55GPR56CA* iPSC line. Equally, an additional set of wild type iPSCs needs to be integrated in the experimental set up to rule out the possibility that higher frequency of HPCs are merely caused by the doxycycline treatment. Another limitation is the low frequency of mCherry+ cells. This might be caused by gene silencing, as recent studies demonstrated that the *AAVS1* locus is not truly considered as the *"safe harbour"* of the human genome (Bhagwan, Collins et al. 2019). It could be interesting to investigate the effect of GPR56 overexpression in the HPC generation using a pure of GPR56-transduced iPSC line and pulse GPR56 activation at different time-points of in vitro hematopoiesis.

6.6 To characterize the biology of GPR56-activated HPCs

The *in vitro* forced overexpression of *GPR56* in human hematopoiesis generated HPC expansion, which may resemble the phenotypic behaviour of aggressive LSCs with an enhanced engraftment and proliferation potential (Pabst, Bergeron et al. 2016). The higher frequency of *GPR56*-activated HPCs may be due to the contribution of two different biological events: an increased cellular growth and an inhibition of apoptosis. Further *in vitro* cellular assays would be required to assess the proliferation and apoptotic rates of doxycycline-activated cells, particularly among the mCherry+/- populations. Furthermore, the transplantation of doxycycline derived HPCs would determine the engraftment potential of *GPR56*-activated HPCs. To evaluate any *in vivo* leukemic behaviour of GPR56-activated cells, doxycycline activated mCherry+ and mCherry- fractions could be injected into immunocompromised mice and compared with the doxycycline negative and wild-type counterparts.

It would be interesting to investigate the haematopoietic potential of human iPSC derived HPCs in the absence of GPR56. *In vivo* and *in vitro* data demonstrated that murine *Gpr56*$^{-/-}$ HSPCs decrease their self-renewal capacity, possess a myeloid-biased output and, simultaneously, upregulate Gpr97. The establishment of a novel human iPSC *GPR56KO* will provide a great opportunity to test whether these biological events occur in human hematopoiesis. *GPR56KO* derived HPCs could be examined to evaluate their proliferation capacity and hematopoietic bias together with gene expression analysis to confirm *GPR97* upregulation. The deletion of *GPR56* could be also performed on patient derived LSCs. It would be interesting to observe the effects of *GPR56* deletion and *GPR97* expression on AML blasts.

The identification of aberrant pathways activated by *GPR56* may be useful to distinguish healthy from malignant HSPCs. The above-mentioned studies direct our focus on understanding the GPR56-IL-6-STAT3 axis. Further experiments will be required to examine whether GPR56 activation is associated with increased IL-6 secretion in doxycycline activated mCherry+ cells. It would be interesting to assess whether doxycycline activated mCherry- cells are responsive to IL-6 secretion by activating STAT3 pathway. These speculations would be validated using antibodies or

small molecules that prevent the binding between IL-6 and its receptor or inhibiting the activation of the STAT3 pathway.

Finally, the ectopic and controlled expression of GPR56 may be useful as a tool to expand HSCs *ex vivo* or improve the efficiency of established protocols to generate HPCs *in vitro*. The controlled regulation of Gpr56 during *in vitro* differentiation might unlock some epigenetic patterns that could favour the generation of transplantable HSCs or increase HPCs yield.

7 CONCLUSION

In conclusion, this thesis research provided new insights into the role of Gpr56 in mammalian hematopoiesis. Using *in vitro* and *in vivo* models, our study demonstrated that the loss of Gpr56 reduced the HSPC self-renewal and shifted their hematopoietic output towards myeloid cells. In these HSPCs, the reduced expression of Gpr56 is followed by Gpr97 upregulation. Experiments performed in zebrafish revealed that Gpr97 can rescue the generation of HSPC in *gpr56* MO larvae. Our work tested the effect of GPR56 overexpression in human *in vitro* hematopoietic differentiation. The forced GPR56 expression from D4 onwards of differentiation led to an HPC expansion. Together, these findings advance the efficiency and promise of protocols to *de novo* generate human HSCs.

8 REFERENCES

Ackerman, S. D., C. Garcia, X. Piao, D. H. Gutmann and K. R. Monk (2015). "The adhesion GPCR Gpr56 regulates oligodendrocyte development via interactions with Galpha12/13 and RhoA." Nat Commun **6**: 6122.

Ackerman, S. D., R. Luo, Y. Poitelon, A. Mogha, B. L. Harty, M. D'Rozario, N. E. Sanchez, A. K. K. Lakkaraju, P. Gamble, J. Li, J. Qu, M. R. MacEwan, W. Z. Ray, A. Aguzzi, M. L. Feltri, X. Piao and K. R. Monk (2018). "GPR56/ADGRG1 regulates development and maintenance of peripheral myelin." J Exp Med **215**(3): 941-961.

Akashi, K., D. Traver, T. Miyamoto and I. L. Weissman (2000). "A clonogenic common myeloid progenitor that gives rise to all myeloid lineages." Nature **404**(6774): 193-197.

Amabile, G., R. S. Welner, C. Nombela-Arrieta, A. M. D'Alise, A. Di Ruscio, A. K. Ebralidze, Y. Kraytsberg, M. Ye, O. Kocher, D. S. Neuberg, K. Khrapko, L. E. Silberstein and D. G. Tenen (2013). "In vivo generation of transplantable human hematopoietic cells from induced pluripotent stem cells." Blood **121**(8): 1255-1264.

Arac, D., A. A. Boucard, M. F. Bolliger, J. Nguyen, S. M. Soltis, T. C. Sudhof and A. T. Brunger (2012). "A novel evolutionarily conserved domain of cell-adhesion GPCRs mediates autoproteolysis." EMBO J **31**(6): 1364-1378.

Barjesteh van Waalwijk van Doorn-Khosrovani, S., C. Erpelinck, W. L. van Putten, P. J. Valk, S. van der Poel-van de Luytgaarde, R. Hack, R. Slater, E. M. Smit, H. B. Beverloo, G. Verhoef, L. F. Verdonck, G. J. Ossenkoppele, P. Sonneveld, G. E. de Greef, B. Lowenberg and R. Delwel (2003). "High EVI1 expression predicts poor survival in acute myeloid leukemia: a study of 319 de novo AML patients." Blood **101**(3): 837-845.

Batsivari, A., S. Rybtsov, C. Souilhol, A. Binagui-Casas, D. Hills, S. Zhao, P. Travers and A. Medvinsky (2017). "Understanding Hematopoietic Stem Cell Development through Functional Correlation of Their Proliferative Status with the Intra-aortic Cluster Architecture." Stem Cell Reports **8**(6): 1549-1562.

Batta, K., M. Florkowska, V. Kouskoff and G. Lacaud (2014). "Direct reprogramming of murine fibroblasts to hematopoietic progenitor cells." Cell Rep **9**(5): 1871-1884.

Benveniste, P., C. Frelin, S. Janmohamed, M. Barbara, R. Herrington, D. Hyam and N. N. Iscove (2010). "Intermediate-term hematopoietic stem cells with extended but time-limited reconstitution potential." Cell Stem Cell **6**(1): 48-58.

Benz, C., M. R. Copley, D. G. Kent, S. Wohrer, A. Cortes, N. Aghaeepour, E. Ma, H. Mader, K. Rowe, C. Day, D. Treloar, R. R. Brinkman and C. J. Eaves (2012). "Hematopoietic stem cell subtypes expand differentially during development and display distinct lymphopoietic programs." Cell Stem Cell **10**(3): 273-283.

Bhagwan, J. R., E. Collins, D. Mosqueira, M. Bakar, B. B. Johnson, A. Thompson, J. G. W. Smith and C. Denning (2019). "Variable expression and silencing of CRISPR-Cas9 targeted transgenes identifies the AAVS1 locus as not an entirely safe harbour." F1000Res **8**: 1911.

Boisset, J. C., W. van Cappellen, C. Andrieu-Soler, N. Galjart, E. Dzierzak and C. Robin (2010). "In vivo imaging of haematopoietic cells emerging from the mouse aortic endothelium." Nature **464**(7285): 116-120.

Bresnick, E. H., H. Y. Lee, T. Fujiwara, K. D. Johnson and S. Keles (2010). "GATA switches as developmental drivers." J Biol Chem **285**(41): 31087-31093.

Bromberg, J. F., M. H. Wrzeszczynska, G. Devgan, Y. Zhao, R. G. Pestell, C. Albanese and J. E. Darnell, Jr. (1999). "Stat3 as an oncogene." Cell **98**(3): 295-303.

Bussmann, J., F. L. Bos, A. Urasaki, K. Kawakami, H. J. Duckers and S. Schulte-Merker (2010). "Arteries provide essential guidance cues for lymphatic endothelial cells in the zebrafish trunk." Development **137**(16): 2653-2657.

Cai, Z., M. de Bruijn, X. Ma, B. Dortland, T. Luteijn, R. J. Downing and E. Dzierzak (2000). "Haploinsufficiency of AML1 affects the temporal and spatial generation of hematopoietic stem cells in the mouse embryo." Immunity **13**(4): 423-431.

Cannan, W. J. and D. S. Pederson (2016). "Mechanisms and Consequences of Double-Strand DNA Break Formation in Chromatin." J Cell Physiol **231**(1): 3-14.

Carrelha, J., Y. Meng, L. M. Kettyle, T. C. Luis, R. Norfo, V. Alcolea, H. Boukarabila, F. Grasso, A. Gambardella, A. Grover, K. Hogstrand, A. M. Lord, A. Sanjuan-Pla, P. S. Woll, C. Nerlov and S. E. W. Jacobsen (2018). "Hierarchically related lineage-restricted fates of multipotent haematopoietic stem cells." Nature **554**(7690): 106-111.

Cauley, E. S., A. Hamed, I. N. Mohamed, M. Elseed, S. Martinez, A. Yahia, F. Abozar, R. Abubakr, M. Koko, L. Elsayed, X. Piao, M. A. Salih and M. C. Manzini (2019). "Overlap of polymicrogyria, hydrocephalus, and Joubert syndrome in a family with novel truncating mutations in ADGRG1/GPR56 and KIAA0556." Neurogenetics **20**(2): 91-98.

Cerletti, M., M. J. Molloy, K. K. Tomczak, S. Yoon, M. F. Ramoni, A. T. Kho, A. H. Beggs and E. Gussoni (2006). "Melanoma cell adhesion molecule is a novel marker for human fetal myogenic cells and affects myoblast fusion." J Cell Sci **119**(Pt 15): 3117-3127.

Chang, G. W., C. C. Hsiao, Y. M. Peng, F. A. Vieira Braga, N. A. Kragten, E. B. Remmerswaal, M. D. van de Garde, R. Straussberg, G. M. Konig, E. Kostenis, V. Knauper, L. Meyaard, R. A. van Lier, K. P. van Gisbergen, H. H. Lin and J. Hamann (2016). "The Adhesion G Protein-Coupled Receptor GPR56/ADGRG1 Is an Inhibitory Receptor on Human NK Cells." Cell Rep **15**(8): 1757-1770.

Chen, M. J., T. Yokomizo, B. M. Zeigler, E. Dzierzak and N. A. Speck (2009). "Runx1 is required for the endothelial to haematopoietic cell transition but not thereafter." Nature **457**(7231): 887-891.

Chiang, N. Y., Y. M. Peng, H. H. Juang, T. C. Chen, H. L. Pan, G. W. Chang and H. H. Lin (2017). "GPR56/ADGRG1 Activation Promotes Melanoma Cell Migration via NTF Dissociation and CTF-Mediated Galpha12/13/RhoA Signaling." J Invest Dermatol **137**(3): 727-736.

Cho, R. H., H. B. Sieburg and C. E. Muller-Sieburg (2008). "A new mechanism for the aging of hematopoietic stem cells: aging changes the clonal composition of the stem cell compartment but not individual stem cells." Blood **111**(12): 5553-5561.

Choi, K. (1998). "Hemangioblast development and regulation." Biochem Cell Biol **76**(6): 947-956.

Crisan, M. and E. Dzierzak (2016). "The many faces of hematopoietic stem cell heterogeneity." Development **143**(24): 4571-4581.

Crisan, M., P. S. Kartalaei, C. S. Vink, T. Yamada-Inagawa, K. Bollerot, I. W. van, R. van der Linden, S. M. de Sousa Lopes, R. Monteiro, C. Mummery and E. Dzierzak (2015). "BMP signalling differentially regulates distinct haematopoietic stem cell types." Nat Commun **6**: 8040.

Daga, S., A. Rosenberger, F. Quehenberger, N. Krisper, B. Prietl, A. Reinisch, A. Zebisch, H. Sill and A. Wolfler (2019). "High GPR56 surface expression correlates with a leukemic stem cell gene signature in CD34-positive AML." Cancer Med **8**(4): 1771-1778.

Daria, D., N. Kirsten, A. Muranyi, M. Mulaw, S. Ihme, A. Kechter, M. Hollnagel, L. Bullinger, K. Dohner, H. Dohner, M. Feuring-Buske and C. Buske (2016). "GPR56 contributes to the development of acute myeloid leukemia in mice." Leukemia **30**(8): 1734-1741.

Davis, J. R. and N. Tapon (2019). "Hippo signalling during development." Development **146**(18).

de Bruijn, M. F., X. Ma, C. Robin, K. Ottersbach, M. J. Sanchez and E. Dzierzak (2002). "Hematopoietic stem cells localize to the endothelial cell layer in the midgestation mouse aorta." Immunity **16**(5): 673-683.

de Bruijn, M. F., N. A. Speck, M. C. Peeters and E. Dzierzak (2000). "Definitive hematopoietic stem cells first develop within the major arterial regions of the mouse embryo." EMBO J **19**(11): 2465-2474.

De Kouchkovsky, I. and M. Abdul-Hay (2016). "'Acute myeloid leukemia: a comprehensive review and 2016 update'." Blood Cancer J **6**(7): e441.

de Pater, E., P. Kaimakis, C. S. Vink, T. Yokomizo, T. Yamada-Inagawa, R. van der Linden, P. S. Kartalaei, S. A. Camper, N. Speck and E. Dzierzak (2013). "Gata2 is required for HSC generation and survival." J Exp Med **210**(13): 2843-2850.

Dieterlen-Lievre, F. (1975). "On the origin of haemopoietic stem cells in the avian embryo: an experimental approach." J Embryol Exp Morphol **33**(3): 607-619.

Ditadi, A., C. M. Sturgeon, J. Tober, G. Awong, M. Kennedy, A. D. Yzaguirre, L. Azzola, E. S. Ng, E. G. Stanley, D. L. French, X. Cheng, P. Gadue, N. A. Speck, A. G. Elefanty and G. Keller (2015). "Human definitive haemogenic endothelium and arterial vascular endothelium represent distinct lineages." Nat Cell Biol **17**(5): 580-591.

Doulatov, S., L. T. Vo, S. S. Chou, P. G. Kim, N. Arora, H. Li, B. K. Hadland, I. D. Bernstein, J. J. Collins, L. I. Zon and G. Q. Daley (2013). "Induction of multipotential hematopoietic progenitors from human pluripotent stem cells via respecification of lineage-restricted precursors." Cell Stem Cell **13**(4): 459-470.

Dykstra, B., D. Kent, M. Bowie, L. McCaffrey, M. Hamilton, K. Lyons, S. J. Lee, R. Brinkman and C. Eaves (2007). "Long-term propagation of distinct hematopoietic differentiation programs in vivo." Cell Stem Cell **1**(2): 218-229.

Dzierzak, E. and A. Bigas (2018). "Blood Development: Hematopoietic Stem Cell Dependence and Independence." Cell Stem Cell **22**(5): 639-651.

Dzierzak, E. and N. A. Speck (2008). "Of lineage and legacy: the development of mammalian hematopoietic stem cells." Nat Immunol **9**(2): 129-136.

Elcheva, I., V. Brok-Volchanskaya, A. Kumar, P. Liu, J. H. Lee, L. Tong, M. Vodyanik, S. Swanson, R. Stewart, M. Kyba, E. Yakubov, J. Cooke, J. A. Thomson and I. Slukvin (2014). "Direct induction of haematoendothelial programs in human pluripotent stem cells by transcriptional regulators." Nat Commun **5**: 4372.

Ellis, J. (2005). "Silencing and variegation of gammaretrovirus and lentivirus vectors." Hum Gene Ther **16**(11): 1241-1246.

Ferkowicz, M. J. and M. C. Yoder (2005). "Blood island formation: longstanding observations and modern interpretations." Exp Hematol **33**(9): 1041-1047.

Fong, C. Y., O. Gilan, E. Y. Lam, A. F. Rubin, S. Ftouni, D. Tyler, K. Stanley, D. Sinha, P. Yeh, J. Morison, G. Giotopoulos, D. Lugo, P. Jeffrey, S. C. Lee, C. Carpenter, R. Gregory, R. G. Ramsay, S. W. Lane, O. Abdel-Wahab, T. Kouzarides, R. W. Johnstone, S. J. Dawson, B. J. Huntly, R. K. Prinjha, A. T. Papenfuss and M. A. Dawson (2015). "BET inhibitor resistance emerges from leukaemia stem cells." Nature **525**(7570): 538-542.

Ford, C. E., J. L. Hamerton, D. W. Barnes and J. F. Loutit (1956). "Cytological identification of radiation-chimaeras." Nature **177**(4506): 452-454.

Fredriksson, R., M. C. Lagerstrom, L. G. Lundin and H. B. Schioth (2003). "The G-protein-coupled receptors in the human genome form five main families. Phylogenetic analysis, paralogon groups, and fingerprints." Mol Pharmacol **63**(6): 1256-1272.

Gaj, T., C. A. Gersbach and C. F. Barbas, 3rd (2013). "ZFN, TALEN, and CRISPR/Cas-based methods for genome engineering." Trends Biotechnol **31**(7): 397-405.

Ganuza, M., T. Hall, D. Finkelstein, A. Chabot, G. Kang and S. McKinney-Freeman (2017). "Lifelong haematopoiesis is established by hundreds of precursors throughout mammalian ontogeny." Nat Cell Biol **19**(10): 1153-1163.

Gao, X., T. Wu, K. D. Johnson, J. L. Lahvic, E. A. Ranheim, L. I. Zon and E. H. Bresnick (2016). "GATA Factor-G-Protein-Coupled Receptor Circuit Suppresses Hematopoiesis." Stem Cell Reports **6**(3): 368-382.

Gao, X., C. Xu, N. Asada and P. S. Frenette (2018). "The hematopoietic stem cell niche: from embryo to adult." Development **145**(2).

Geiger, H., G. de Haan and M. C. Florian (2013). "The ageing haematopoietic stem cell compartment." Nat Rev Immunol **13**(5): 376-389.

Gibson, D. G., L. Young, R. Y. Chuang, J. C. Venter, C. A. Hutchison, 3rd and H. O. Smith (2009). "Enzymatic assembly of DNA molecules up to several hundred kilobases." Nat Methods **6**(5): 343-345.

Giera, S., Y. Deng, R. Luo, S. D. Ackerman, A. Mogha, K. R. Monk, Y. Ying, S. J. Jeong, M. Makinodan, A. R. Bialas, B. S. Chang, B. Stevens, G. Corfas and X. Piao (2015). "The adhesion G protein-coupled receptor GPR56 is a cell-autonomous regulator of oligodendrocyte development." Nat Commun **6**: 6121.

Gossen, M., S. Freundlieb, G. Bender, G. Muller, W. Hillen and H. Bujard (1995). "Transcriptional activation by tetracyclines in mammalian cells." Science **268**(5218): 1766-1769.

Groschel, S., M. A. Sanders, R. Hoogenboezem, E. de Wit, B. A. M. Bouwman, C. Erpelinck, V. H. J. van der Velden, M. Havermans, R. Avellino, K. van Lom, E. J. Rombouts, M. van Duin, K. Dohner, H. B. Beverloo, J. E. Bradner, H. Dohner, B. Lowenberg, P. J. M. Valk, E. M. J. Bindels, W. de Laat and R. Delwel (2014). "A single oncogenic enhancer rearrangement causes concomitant EVI1 and GATA2 deregulation in leukemia." Cell **157**(2): 369-381.

Hall, A. (2012). "Rho family GTPases." Biochem Soc Trans **40**(6): 1378-1382.

Heikkila, K., S. Ebrahim and D. A. Lawlor (2008). "Systematic review of the association between circulating interleukin-6 (IL-6) and cancer." Eur J Cancer **44**(7): 937-945.

Helgason, C. D., G. Sauvageau, H. J. Lawrence, C. Largman and R. K. Humphries (1996). "Overexpression of HOXB4 enhances the hematopoietic potential of embryonic stem cells differentiated in vitro." Blood **87**(7): 2740-2749.

Hoejberg, L., L. Bastholt, J. S. Johansen, I. J. Christensen, J. Gehl and H. Schmidt (2012). "Serum interleukin-6 as a prognostic biomarker in patients with metastatic melanoma." Melanoma Res **22**(4): 287-293.

Hsiao, C. C., T. Y. Chu, C. J. Wu, M. van den Biggelaar, C. Pabst, J. Hebert, T. W. Kuijpers, B. P. Scicluna, K. Y. I, T. C. Chen, I. Liebscher, J. Hamann and H. H. Lin (2018). "The Adhesion G Protein-Coupled Receptor GPR97/ADGRG3 Is Expressed in Human Granulocytes and Triggers Antimicrobial Effector Functions." Front Immunol **9**: 2830.

Huang, K. Y. and H. H. Lin (2018). "The Activation and Signaling Mechanisms of GPR56/ADGRG1 in Melanoma Cell." Front Oncol **8**: 304.

Iguchi, T., K. Sakata, K. Yoshizaki, K. Tago, N. Mizuno and H. Itoh (2008). "Orphan G protein-coupled receptor GPR56 regulates neural progenitor cell migration via a G alpha 12/13 and Rho pathway." J Biol Chem **283**(21): 14469-14478.

Ihara, K., S. Muraguchi, M. Kato, T. Shimizu, M. Shirakawa, S. Kuroda, K. Kaibuchi and T. Hakoshima (1998). "Crystal structure of human RhoA in a dominantly active form complexed with a GTP analogue." J Biol Chem **273**(16): 9656-9666.

Ikuta, K., T. Kina, I. MacNeil, N. Uchida, B. Peault, Y. H. Chien and I. L. Weissman (1990). "A developmental switch in thymic lymphocyte maturation potential occurs at the level of hematopoietic stem cells." Cell **62**(5): 863-874.

Ikuta, K. and I. L. Weissman (1992). "Evidence that hematopoietic stem cells express mouse c-kit but do not depend on steel factor for their generation." Proc Natl Acad Sci U S A **89**(4): 1502-1506.

Jackson, M., A. Fidanza, A. H. Taylor, S. Rybtsov, R. Axton, M. Kydonaki, S. Meek, T. Burdon, A. Medvinsky and L. M. Forrester (2020). "Modulation of Aplnr signaling is required during the development and maintenance of the hematopoietic system." bioRxiv: 2020.2006.2015.145649.

Jacobson, L. O., E. L. Simmons, E. K. Marks and J. H. Eldredge (1951). "Recovery from radiation injury." Science **113**(2940): 510-511.

Jaffe, A. B. and A. Hall (2005). "Rho GTPases: biochemistry and biology." Annu Rev Cell Dev Biol **21**: 247-269.

Jaffredo, T., K. Bollerot, D. Sugiyama, R. Gautier and C. Drevon (2005). "Tracing the hemangioblast during embryogenesis: developmental relationships between endothelial and hematopoietic cells." Int J Dev Biol **49**(2-3): 269-277.

Jentzsch, M., M. Bill, J. Grimm, J. Schulz, L. Schuhmann, D. Brauer, K. Goldmann, F. Wilke, G. N. Franke, G. Behre, W. Ponisch, V. Vucinic, D. Niederwieser, U. Platzbecker and S. Schwind (2020). "High expression of the stem cell marker GPR56 at diagnosis identifies acute myeloid leukemia patients at higher relapse risk after allogeneic stem cell transplantation in context with the CD34+/CD38- population." Haematologica.

Johnson, R. and G. Halder (2014). "The two faces of Hippo: targeting the Hippo pathway for regenerative medicine and cancer treatment." Nat Rev Drug Discov **13**(1): 63-79.

Kaimakis, P., E. de Pater, C. Eich, P. Solaimani Kartalaei, M. L. Kauts, C. S. Vink, R. van der Linden, M. Jaegle, T. Yokomizo, D. Meijer and E. Dzierzak (2016). "Functional and molecular characterization of mouse Gata2-independent hematopoietic progenitors." Blood **127**(11): 1426-1437.

Kauts, M. L., B. De Leo, C. Rodriguez-Seoane, R. Ronn, F. Glykofrydis, A. Maglitto, P. Kaimakis, M. Basi, H. Taylor, L. Forrester, A. C. Wilkinson, B. Gottgens, P. Saunders and E. Dzierzak (2018). "Rapid Mast Cell Generation from Gata2 Reporter Pluripotent Stem Cells." Stem Cell Reports **11**(4): 1009-1020.

Kauts, M. L., C. Rodriguez-Seoane, P. Kaimakis, S. C. Mendes, X. Cortes-Lavaud, U. Hill and E. Dzierzak (2017). "In Vitro Differentiation of Gata2 and Ly6a Reporter Embryonic Stem Cells Corresponds to In Vivo Waves of Hematopoietic Cell Generation." Stem Cell Reports.

Ke, N., H. Ma, G. Diedrich, J. Chionis, G. Liu, D. H. Yu, F. Wong-Staal and Q. X. Li (2008). "Biochemical characterization of genetic mutations of GPR56 in patients with bilateral frontoparietal polymicrogyria (BFPP)." Biochem Biophys Res Commun **366**(2): 314-320.

Ke, N., R. Sundaram, G. Liu, J. Chionis, W. Fan, C. Rogers, T. Awad, M. Grifman, D. Yu, F. Wong-Staal and Q. X. Li (2007). "Orphan G protein-coupled receptor GPR56 plays a role in cell transformation and tumorigenesis involving the cell adhesion pathway." Mol Cancer Ther **6**(6): 1840-1850.

Kennedy, M., G. Awong, C. M. Sturgeon, A. Ditadi, R. LaMotte-Mohs, J. C. Zuniga-Pflucker and G. Keller (2012). "T lymphocyte potential marks the emergence of definitive hematopoietic progenitors in human pluripotent stem cell differentiation cultures." Cell Rep **2**(6): 1722-1735.

Kennedy, M., S. L. D'Souza, M. Lynch-Kattman, S. Schwantz and G. Keller (2007). "Development of the hemangioblast defines the onset of hematopoiesis in human ES cell differentiation cultures." Blood **109**(7): 2679-2687.

Kim, J. H., S. R. Lee, L. H. Li, H. J. Park, J. H. Park, K. Y. Lee, M. K. Kim, B. A. Shin and S. Y. Choi (2011). "High cleavage efficiency of a 2A peptide derived from porcine teschovirus-1 in human cell lines, zebrafish and mice." PLoS One **6**(4): e18556.

Kishore, A., R. H. Purcell, Z. Nassiri-Toosi and R. A. Hall (2016). "Stalk-dependent and Stalk-independent Signaling by the Adhesion G Protein-coupled Receptors GPR56 (ADGRG1) and BAI1 (ADGRB1)." J Biol Chem **291**(7): 3385-3394.

Kissa, K. and P. Herbomel (2010). "Blood stem cells emerge from aortic endothelium by a novel type of cell transition." Nature **464**(7285): 112-115.

Kobayashi-Osaki, M., O. Ohneda, N. Suzuki, N. Minegishi, T. Yokomizo, S. Takahashi, K. C. Lim, J. D. Engel and M. Yamamoto (2005). "GATA motifs regulate early hematopoietic lineage-specific expression of the Gata2 gene." Mol Cell Biol **25**(16): 7005-7020.

Kondo, M., I. L. Weissman and K. Akashi (1997). "Identification of clonogenic common lymphoid progenitors in mouse bone marrow." Cell **91**(5): 661-672.

Kreso, A. and J. E. Dick (2014). "Evolution of the cancer stem cell model." Cell Stem Cell **14**(3): 275-291.

Kumaravelu, P., L. Hook, A. M. Morrison, J. Ure, S. Zhao, S. Zuyev, J. Ansell and A. Medvinsky (2002). "Quantitative developmental anatomy of definitive haematopoietic stem cells/long-term repopulating units (HSC/RUs): role of the aorta-gonad-mesonephros (AGM) region and the yolk sac in colonisation of the mouse embryonic liver." Development **129**(21): 4891-4899.

Kyba, M., R. C. Perlingeiro and G. Q. Daley (2002). "HoxB4 confers definitive lymphoid-myeloid engraftment potential on embryonic stem cell and yolk sac hematopoietic progenitors." Cell **109**(1): 29-37.

Langenhan, T., G. Aust and J. Hamann (2013). "Sticky signaling--adhesion class G protein-coupled receptors take the stage." Sci Signal **6**(276): re3.

Langenhan, T., X. Piao and K. R. Monk (2016). "Adhesion G protein-coupled receptors in nervous system development and disease." Nat Rev Neurosci **17**(9): 550-561.

Liebscher, I., J. Schon, S. C. Petersen, L. Fischer, N. Auerbach, L. M. Demberg, A. Mogha, M. Coster, K. U. Simon, S. Rothemund, K. R. Monk and T. Schoneberg (2014). "A tethered agonist within the ectodomain activates the adhesion G protein-coupled receptors GPR126 and GPR133." Cell Rep **9**(6): 2018-2026.

Lim, K. C., G. Lakshmanan, S. E. Crawford, Y. Gu, F. Grosveld and J. D. Engel (2000). "Gata3 loss leads to embryonic lethality due to noradrenaline deficiency of the sympathetic nervous system." Nat Genet **25**(2): 209-212.

Lin, H. F., D. Traver, H. Zhu, K. Dooley, B. H. Paw, L. I. Zon and R. I. Handin (2005). "Analysis of thrombocyte development in CD41-GFP transgenic zebrafish." Blood **106**(12): 3803-3810.

Lin, H. H., G. W. Chang, J. Q. Davies, M. Stacey, J. Harris and S. Gordon (2004). "Autocatalytic cleavage of the EMR2 receptor occurs at a conserved G protein-coupled receptor proteolytic site motif." J Biol Chem **279**(30): 31823-31832.

Lis, R., C. C. Karrasch, M. G. Poulos, B. Kunar, D. Redmond, J. G. B. Duran, C. R. Badwe, W. Schachterle, M. Ginsberg, J. Xiang, A. R. Tabrizi, K. Shido, Z. Rosenwaks, O. Elemento, N. A. Speck, J. M. Butler, J. M. Scandura and S. Rafii (2017). "Conversion of adult endothelium to immunocompetent haematopoietic stem cells." Nature.

Liu, Q., D. J. Segal, J. B. Ghiara and C. F. Barbas, 3rd (1997). "Design of polydactyl zinc-finger proteins for unique addressing within complex genomes." Proc Natl Acad Sci U S A **94**(11): 5525-5530.

Liu, Z., Z. Huang, W. Yang, Z. Li, S. Xing, H. Li, B. Hu and P. Li (2017). "Expression of orphan GPR56 correlates with tumor progression in human epithelial ovarian cancer." Neoplasma **64**(1): 32-39.

Lombardo, A., D. Cesana, P. Genovese, B. Di Stefano, E. Provasi, D. F. Colombo, M. Neri, Z. Magnani, A. Cantore, P. Lo Riso, M. Damo, O. M. Pello, M. C. Holmes, P. D. Gregory, A. Gritti, V. Broccoli, C. Bonini and L. Naldini (2011). "Site-specific integration and tailoring of cassette design for sustainable gene transfer." Nat Methods **8**(10): 861-869.

Lorenz, E., D. Uphoff, T. R. Reid and E. Shelton (1951). "Modification of irradiation injury in mice and guinea pigs by bone marrow injections." J Natl Cancer Inst **12**(1): 197-201.

Luo, R., S. J. Jeong, Z. Jin, N. Strokes, S. Li and X. Piao (2011). "G protein-coupled receptor 56 and collagen III, a receptor-ligand pair, regulates cortical development and lamination." Proc Natl Acad Sci U S A **108**(31): 12925-12930.

Luo, R., S. J. Jeong, A. Yang, M. Wen, D. E. Saslowsky, W. I. Lencer, D. Arac and X. Piao (2014). "Mechanism for adhesion G protein-coupled receptor GPR56-mediated RhoA activation induced by collagen III stimulation." PLoS One **9**(6): e100043.

Ma, X., C. Robin, K. Ottersbach and E. Dzierzak (2002). "The Ly-6A (Sca-1) GFP transgene is expressed in all adult mouse hematopoietic stem cells." Stem Cells **20**(6): 514-521.

Manwani, D. and J. J. Bieker (2008). "The erythroblastic island." Curr Top Dev Biol **82**: 23-53.

Manz, M. G., T. Miyamoto, K. Akashi and I. L. Weissman (2002). "Prospective isolation of human clonogenic common myeloid progenitors." Proc Natl Acad Sci U S A **99**(18): 11872-11877.

McCulloch, E. A. and J. E. Till (1960). "The radiation sensitivity of normal mouse bone marrow cells, determined by quantitative marrow transplantation into irradiated mice." Radiat Res **13**: 115-125.

McGrath, K. E., J. M. Frame, K. H. Fegan, J. R. Bowen, S. J. Conway, S. C. Catherman, P. D. Kingsley, A. D. Koniski and J. Palis (2015). "Distinct Sources of Hematopoietic Progenitors Emerge before HSCs and Provide Functional Blood Cells in the Mammalian Embryo." Cell Rep **11**(12): 1892-1904.

McGrath, K. E., A. D. Koniski, J. Malik and J. Palis (2003). "Circulation is established in a stepwise pattern in the mammalian embryo." Blood **101**(5): 1669-1676.

Medvinsky, A. and E. Dzierzak (1996). "Definitive hematopoiesis is autonomously initiated by the AGM region." Cell **86**(6): 897-906.

Meier, I., L. V. Wray and W. Hillen (1988). "Differential regulation of the Tn10-encoded tetracycline resistance genes tetA and tetR by the tandem tet operators O1 and O2." EMBO J **7**(2): 567-572.

Moehle, E. A., J. M. Rock, Y. L. Lee, Y. Jouvenot, R. C. DeKelver, P. D. Gregory, F. D. Urnov and M. C. Holmes (2007). "Targeted gene addition into a specified location in the human genome using designed zinc finger nucleases." Proc Natl Acad Sci U S A **104**(9): 3055-3060.

Moore, M. A. and D. Metcalf (1970). "Ontogeny of the haemopoietic system: yolk sac origin of in vivo and in vitro colony forming cells in the developing mouse embryo." Br J Haematol **18**(3): 279-296.

Moore, M. A. and J. J. Owen (1965). "Chromosome marker studies on the development of the haemopoietic system in the chick embryo." Nature **208**(5014): 956 passim.

Moore, M. A. and J. J. Owen (1967). "Chromosome marker studies in the irradiated chick embryo." Nature **215**(5105): 1081-1082.

Morrison, S. J., N. Uchida and I. L. Weissman (1995). "The biology of hematopoietic stem cells." Annu Rev Cell Dev Biol **11**: 35-71.

Morrison, S. J., A. M. Wandycz, H. D. Hemmati, D. E. Wright and I. L. Weissman (1997). "Identification of a lineage of multipotent hematopoietic progenitors." Development **124**(10): 1929-1939.

Muller-Sieburg, C. E., R. H. Cho, M. Thoman, B. Adkins and H. B. Sieburg (2002). "Deterministic regulation of hematopoietic stem cell self-renewal and differentiation." Blood **100**(4): 1302-1309.

Ng, S. W., A. Mitchell, J. A. Kennedy, W. C. Chen, J. McLeod, N. Ibrahimova, A. Arruda, A. Popescu, V. Gupta, A. D. Schimmer, A. C. Schuh, K. W. Yee, L. Bullinger, T. Herold, D. Gorlich, T. Buchner, W. Hiddemann, W. E. Berdel, B. Wormann, M. Cheok, C. Preudhomme, H. Dombret, K. Metzeler, C. Buske, B. Lowenberg, P. J. Valk, P. W. Zandstra, M. D. Minden, J. E. Dick and J. C. Wang (2016). "A 17-gene stemness score for rapid determination of risk in acute leukaemia." Nature **540**(7633): 433-437.

North, T., T. L. Gu, T. Stacy, Q. Wang, L. Howard, M. Binder, M. Marin-Padilla and N. A. Speck (1999). "Cbfa2 is required for the formation of intra-aortic hematopoietic clusters." Development **126**(11): 2563-2575.

Ogilvy, S., D. Metcalf, L. Gibson, M. L. Bath, A. W. Harris and J. M. Adams (1999). "Promoter elements of vav drive transgene expression in vivo throughout the hematopoietic compartment." Blood **94**(6): 1855-1863.

Ohashi, K., S. Fujiwara and K. Mizuno (2017). "Roles of the cytoskeleton, cell adhesion and rho signalling in mechanosensing and mechanotransduction." J Biochem **161**(3): 245-254.

Okuda, T., J. van Deursen, S. W. Hiebert, G. Grosveld and J. R. Downing (1996). "AML1, the target of multiple chromosomal translocations in human leukemia, is essential for normal fetal liver hematopoiesis." Cell **84**(2): 321-330.

Olaniru, O. E., A. Pingitore, S. Giera, X. Piao, R. Castanera Gonzalez, P. M. Jones and S. J. Persaud (2018). "The adhesion receptor GPR56 is activated by extracellular matrix collagen III to improve beta-cell function." Cell Mol Life Sci **75**(21): 4007-4019.

Paavola, K. J., J. R. Stephenson, S. L. Ritter, S. P. Alter and R. A. Hall (2011). "The N terminus of the adhesion G protein-coupled receptor GPR56 controls receptor signaling activity." J Biol Chem **286**(33): 28914-28921.

Pabst, C., A. Bergeron, V. P. Lavallee, J. Yeh, P. Gendron, G. L. Norddahl, J. Krosl, I. Boivin, E. Deneault, J. Simard, S. Imren, G. Boucher, K. Eppert, T. Herold, S. K. Bohlander, K. Humphries, S. Lemieux, J. Hebert, G. Sauvageau and F. Barabe (2016). "GPR56 identifies primary human acute myeloid leukemia cells with high repopulating potential in vivo." Blood **127**(16): 2018-2027.

Palis, J., S. Robertson, M. Kennedy, C. Wall and G. Keller (1999). "Development of erythroid and myeloid progenitors in the yolk sac and embryo proper of the mouse." Development **126**(22): 5073-5084.

Papapetrou, E. P. and A. Schambach (2016). "Gene Insertion Into Genomic Safe Harbors for Human Gene Therapy." Mol Ther **24**(4): 678-684.

Pereira, C. F., B. Chang, J. J. Qiu, X. H. Niu, D. Papatsenko, C. E. Hendry, N. R. Clark, A. Nomura-Kitabayashi, J. C. Kovacic, A. Ma'ayan, C. Schaniel, I. R. Lemischka and K. Moore (2013). "Induction of a Hemogenic Program in Mouse Fibroblasts." Cell Stem Cell **13**(2): 205-218.

Piao, X., R. S. Hill, A. Bodell, B. S. Chang, L. Basel-Vanagaite, R. Straussberg, W. B. Dobyns, B. Qasrawi, R. M. Winter, A. M. Innes, T. Voit, M. E. Ross, J. L. Michaud, J. C. Descarie, A. J. Barkovich and C. A. Walsh (2004). "G protein-coupled receptor-dependent development of human frontal cortex." Science **303**(5666): 2033-2036.

Pietras, E. M., D. Reynaud, Y. A. Kang, D. Carlin, F. J. Calero-Nieto, A. D. Leavitt, J. M. Stuart, B. Gottgens and E. Passegue (2015). "Functionally Distinct Subsets of Lineage-Biased Multipotent Progenitors Control Blood Production in Normal and Regenerative Conditions." Cell Stem Cell **17**(1): 35-46.

Porcheri, C., O. Golan, F. J. Calero-Nieto, R. Thambyrajah, C. Ruiz-Herguido, X. Wang, F. Catto, Y. Guillen, R. Sinha, J. Gonzalez, S. J. Kinston, S. A. Mariani, A. Maglitto, C. S. Vink, E. Dzierzak, P. Charbord, B. Gottgens, L. Espinosa, D. Sprinzak and A. Bigas (2020). "Notch ligand Dll4 impairs cell recruitment to aortic clusters and limits blood stem cell generation." EMBO J: e104270.

Ran, F. A., P. D. Hsu, J. Wright, V. Agarwala, D. A. Scott and F. Zhang (2013). "Genome engineering using the CRISPR-Cas9 system." Nat Protoc **8**(11): 2281-2308.

Rao, T. N., J. Marks-Bluth, J. Sullivan, M. K. Gupta, V. Chandrakanthan, S. R. Fitch, K. Ottersbach, Y. C. Jang, X. Piao, R. N. Kulkarni, T. Serwold, J. E. Pimanda and A. J. Wagers (2015). "High-level Gpr56 expression is dispensable for the maintenance and function of hematopoietic stem and progenitor cells in mice." Stem Cell Res **14**(3): 307-322.

Redell, M. S., M. J. Ruiz, R. B. Gerbing, T. A. Alonzo, B. J. Lange, D. J. Tweardy, S. Meshinchi and G. Children's Oncology (2013). "FACS analysis of Stat3/5 signaling reveals sensitivity to G-CSF and IL-6 as a significant prognostic factor in pediatric AML: a Children's Oncology Group report." Blood **121**(7): 1083-1093.

Riddell, J., R. Gazit, B. S. Garrison, G. Guo, A. Saadatpour, P. K. Mandal, W. Ebina, P. Volchkov, G. C. Yuan, S. H. Orkin and D. J. Rossi (2014). "Reprogramming committed murine blood cells to induced hematopoietic stem cells with defined factors." Cell **157**(3): 549-564.

Robb, L., I. Lyons, R. Li, L. Hartley, F. Kontgen, R. P. Harvey, D. Metcalf and C. G. Begley (1995). "Absence of yolk sac hematopoiesis from mice with a targeted disruption of the scl gene." Proc Natl Acad Sci U S A **92**(15): 7075-7079.

Rybtsov, S., A. Batsivari, K. Bilotkach, D. Paruzina, J. Senserrich, O. Nerushev and A. Medvinsky (2014). "Tracing the origin of the HSC hierarchy reveals an SCF-dependent, IL-3-independent CD43(-) embryonic precursor." Stem Cell Reports **3**(3): 489-501.

Rybtsov, S., M. Sobiesiak, S. Taoudi, C. Souilhol, J. Senserrich, A. Liakhovitskaia, A. Ivanovs, J. Frampton, S. Zhao and A. Medvinsky (2011). "Hierarchical organization and early hematopoietic specification of the developing HSC lineage in the AGM region." J Exp Med **208**(6): 1305-1315.

Saito, Y., K. Kaneda, A. Suekane, E. Ichihara, S. Nakahata, N. Yamakawa, K. Nagai, N. Mizuno, K. Kogawa, I. Miura, H. Itoh and K. Morishita (2013). "Maintenance of the hematopoietic stem cell pool in bone marrow niches by EVI1-regulated GPR56." Leukemia **27**(8): 1637-1649.

Sanchez-Correa, B., J. M. Bergua, C. Campos, I. Gayoso, M. J. Arcos, H. Banas, S. Morgado, J. G. Casado, R. Solana and R. Tarazona (2013). "Cytokine profiles in acute myeloid leukemia patients at

diagnosis: survival is inversely correlated with IL-6 and directly correlated with IL-10 levels." Cytokine **61**(3): 885-891.

Sandler, V. M., R. Lis, Y. Liu, A. Kedem, D. James, O. Elemento, J. M. Butler, J. M. Scandura and S. Rafii (2014). "Reprogramming human endothelial cells to haematopoietic cells requires vascular induction." Nature **511**(7509): 312-318.

Sanjuan-Pla, A., I. C. Macaulay, C. T. Jensen, P. S. Woll, T. C. Luis, A. Mead, S. Moore, C. Carella, S. Matsuoka, T. Bouriez Jones, O. Chowdhury, L. Stenson, M. Lutteropp, J. C. Green, R. Facchini, H. Boukarabila, A. Grover, A. Gambardella, S. Thongjuea, J. Carrelha, P. Tarrant, D. Atkinson, S. A. Clark, C. Nerlov and S. E. Jacobsen (2013). "Platelet-biased stem cells reside at the apex of the haematopoietic stem-cell hierarchy." Nature **502**(7470): 232-236.

Santos-Silva, R., A. Passas, C. Rocha, R. Figueiredo, J. Mendes-Ribeiro, S. Fernandes, S. Biskup and M. Leao (2015). "Bilateral frontoparietal polymicrogyria: a novel GPR56 mutation and an unusual phenotype." Neuropediatrics **46**(2): 134-138.

Sauvageau, G., P. M. Lansdorp, C. J. Eaves, D. E. Hogge, W. H. Dragowska, D. S. Reid, C. Largman, H. J. Lawrence and R. K. Humphries (1994). "Differential expression of homeobox genes in functionally distinct CD34+ subpopulations of human bone marrow cells." Proc Natl Acad Sci U S A **91**(25): 12223-12227.

Schioth, H. B. and R. Fredriksson (2005). "The GRAFS classification system of G-protein coupled receptors in comparative perspective." Gen Comp Endocrinol **142**(1-2): 94-101.

Schuringa, J. J., L. J. Jonk, W. H. Dokter, E. Vellenga and W. Kruijer (2000). "Interleukin-6-induced STAT3 transactivation and Ser727 phosphorylation involves Vav, Rac-1 and the kinase SEK-1/MKK-4 as signal transduction components." Biochem J **347 Pt 1**: 89-96.

Shashidhar, S., G. Lorente, U. Nagavarapu, A. Nelson, J. Kuo, J. Cummins, K. Nikolich, R. Urfer and E. D. Foehr (2005). "GPR56 is a GPCR that is overexpressed in gliomas and functions in tumor cell adhesion." Oncogene **24**(10): 1673-1682.

Shima, Y. and I. Kitabayashi (2011). "Deregulated transcription factors in leukemia." Int J Hematol **94**(2): 134-141.

Shivdasani, R. A., E. L. Mayer and S. H. Orkin (1995). "Absence of blood formation in mice lacking the T-cell leukaemia oncoprotein tal-1/SCL." Nature **373**(6513): 432-434.

Sieburg, H. B., R. H. Cho, B. Dykstra, N. Uchida, C. J. Eaves and C. E. Muller-Sieburg (2006). "The hematopoietic stem compartment consists of a limited number of discrete stem cell subsets." Blood **107**(6): 2311-2316.

Solaimani Kartalaei, P., T. Yamada-Inagawa, C. S. Vink, E. de Pater, R. van der Linden, J. Marks-Bluth, A. van der Sloot, M. van den Hout, T. Yokomizo, M. L. van Schaick-Solerno, R. Delwel, J. E. Pimanda, I. W. F. van and E. Dzierzak (2015). "Whole-transcriptome analysis of endothelial to hematopoietic stem cell transition reveals a requirement for Gpr56 in HSC generation." J Exp Med **212**(1): 93-106.

Spangrude, G. J., S. Heimfeld and I. L. Weissman (1988). "Purification and characterization of mouse hematopoietic stem cells." Science **241**(4861): 58-62.

Stadtfeld, M. and T. Graf (2005). "Assessing the role of hematopoietic plasticity for endothelial and hepatocyte development by non-invasive lineage tracing." Development **132**(1): 203-213.

Stevens, A. M., J. M. Miller, J. O. Munoz, A. S. Gaikwad and M. S. Redell (2017). "Interleukin-6 levels predict event-free survival in pediatric AML and suggest a mechanism of chemotherapy resistance." Blood Adv **1**(18): 1387-1397.

Stevens, A. M., M. J. Ruiz, R. B. Gerbing, T. A. Alonzo, A. S. Gamis and M. S. Redell (2015). "Ligand-induced STAT3 signaling increases at relapse and is associated with outcome in pediatric acute myeloid leukemia: a report from the Children's Oncology Group." Haematologica **100**(12): e496-500.

Stoveken, H. M., A. G. Hajduczok, L. Xu and G. G. Tall (2015). "Adhesion G protein-coupled receptors are activated by exposure of a cryptic tethered agonist." Proc Natl Acad Sci U S A **112**(19): 6194-6199.

Sugimura, R., D. K. Jha, A. Han, C. Soria-Valles, E. L. da Rocha, Y. F. Lu, J. A. Goettel, E. Serrao, R. G. Rowe, M. Malleshaiah, I. Wong, P. Sousa, T. N. Zhu, A. Ditadi, G. Keller, A. N. Engelman, S. B. Snapper, S. Doulatov and G. Q. Daley (2017). "Haematopoietic stem and progenitor cells from human pluripotent stem cells." Nature **545**(7655): 432-438.

Suzuki, N., S. Yamazaki, T. Yamaguchi, M. Okabe, H. Masaki, S. Takaki, M. Otsu and H. Nakauchi (2013). "Generation of engraftable hematopoietic stem cells from induced pluripotent stem cells by way of teratoma formation." Mol Ther **21**(7): 1424-1431.

Takahashi, K. and S. Yamanaka (2006). "Induction of pluripotent stem cells from mouse embryonic and adult fibroblast cultures by defined factors." Cell **126**(4): 663-676.

Taoudi, S., C. Gonneau, K. Moore, J. M. Sheridan, C. C. Blackburn, E. Taylor and A. Medvinsky (2008). "Extensive hematopoietic stem cell generation in the AGM region via maturation of VE-cadherin+CD45+ pre-definitive HSCs." Cell Stem Cell **3**(1): 99-108.

Till, J. E. and C. E. Mc (1961). "A direct measurement of the radiation sensitivity of normal mouse bone marrow cells." Radiat Res **14**: 213-222.

Timmermans, F., I. Velghe, L. Vanwalleghem, M. De Smedt, S. Van Coppernolle, T. Taghon, H. D. Moore, G. Leclercq, A. W. Langerak, T. Kerre, J. Plum and B. Vandekerckhove (2009). "Generation of T cells from human embryonic stem cell-derived hematopoietic zones." J Immunol **182**(11): 6879-6888.

Tsai, F. Y., G. Keller, F. C. Kuo, M. Weiss, J. Chen, M. Rosenblatt, F. W. Alt and S. H. Orkin (1994). "An early haematopoietic defect in mice lacking the transcription factor GATA-2." Nature **371**(6494): 221-226.

Tsai, S. F., D. I. Martin, L. I. Zon, A. D. D'Andrea, G. G. Wong and S. H. Orkin (1989). "Cloning of cDNA for the major DNA-binding protein of the erythroid lineage through expression in mammalian cells." Nature **339**(6224): 446-451.

Tsimberidou, A. M., E. Estey, S. Wen, S. Pierce, H. Kantarjian, M. Albitar and R. Kurzrock (2008). "The prognostic significance of cytokine levels in newly diagnosed acute myeloid leukemia and high-risk myelodysplastic syndromes." Cancer **113**(7): 1605-1613.

Ueno, H. and I. L. Weissman (2006). "Clonal analysis of mouse development reveals a polyclonal origin for yolk sac blood islands." Dev Cell **11**(4): 519-533.

Valtcheva, N., A. Primorac, G. Jurisic, M. Hollmen and M. Detmar (2013). "The orphan adhesion G protein-coupled receptor GPR97 regulates migration of lymphatic endothelial cells via the small GTPases RhoA and Cdc42." J Biol Chem **288**(50): 35736-35748.

Verovskaya, E., M. J. Broekhuis, E. Zwart, M. Ritsema, R. van Os, G. de Haan and L. V. Bystrykh (2013). "Heterogeneity of young and aged murine hematopoietic stem cells revealed by quantitative clonal analysis using cellular barcoding." Blood **122**(4): 523-532.

Vo, L. T. and G. Q. Daley (2015). "De novo generation of HSCs from somatic and pluripotent stem cell sources." Blood **125**(17): 2641-2648.

Vodyanik, M. A., J. A. Thomson and Slukvin, II (2006). "Leukosialin (CD43) defines hematopoietic progenitors in human embryonic stem cell differentiation cultures." Blood **108**(6): 2095-2105.

Wang, Y. and N. Nakayama (2009). "WNT and BMP signaling are both required for hematopoietic cell development from human ES cells." Stem Cell Res **3**(2-3): 113-125.

Warren, A. J., W. H. Colledge, M. B. Carlton, M. J. Evans, A. J. Smith and T. H. Rabbitts (1994). "The oncogenic cysteine-rich LIM domain protein rbtn2 is essential for erythroid development." Cell **78**(1): 45-57.

White, J. P., C. D. Wrann, R. R. Rao, S. K. Nair, M. P. Jedrychowski, J. S. You, V. Martinez-Redondo, S. P. Gygi, J. L. Ruas, T. A. Hornberger, Z. Wu, D. J. Glass, X. Piao and B. M. Spiegelman (2014). "G protein-coupled receptor 56 regulates mechanical overload-induced muscle hypertrophy." Proc Natl Acad Sci U S A **111**(44): 15756-15761.

Wilkinson, A. C., R. Ishida, M. Kikuchi, K. Sudo, M. Morita, R. V. Crisostomo, R. Yamamoto, K. M. Loh, Y. Nakamura, M. Watanabe, H. Nakauchi and S. Yamazaki (2019). "Long-term ex vivo haematopoietic-stem-cell expansion allows nonconditioned transplantation." Nature **571**(7763): 117-121.

Wilson, A., E. Laurenti, G. Oser, R. C. van der Wath, W. Blanco-Bose, M. Jaworski, S. Offner, C. F. Dunant, L. Eshkind, E. Bockamp, P. Lio, H. R. Macdonald and A. Trumpp (2008). "Hematopoietic stem cells reversibly switch from dormancy to self-renewal during homeostasis and repair." Cell **135**(6): 1118-1129.

Wilson, N. K., F. J. Calero-Nieto, R. Ferreira and B. Gottgens (2011). "Transcriptional regulation of haematopoietic transcription factors." Stem Cell Res Ther **2**(1): 6.

Wilson, N. K., S. D. Foster, X. Wang, K. Knezevic, J. Schutte, P. Kaimakis, P. M. Chilarska, S. Kinston, W. H. Ouwehand, E. Dzierzak, J. E. Pimanda, M. F. de Bruijn and B. Gottgens (2010). "Combinatorial transcriptional control in blood stem/progenitor cells: genome-wide analysis of ten major transcriptional regulators." Cell Stem Cell **7**(4): 532-544.

Wu, A. M., J. E. Till, L. Siminovitch and E. A. McCulloch (1967). "A cytological study of the capacity for differentiation of normal hemopoietic colony-forming cells." J Cell Physiol **69**(2): 177-184.

Wu, M. P., J. R. Doyle, B. Barry, A. Beauvais, A. Rozkalne, X. Piao, M. W. Lawlor, A. S. Kopin, C. A. Walsh and E. Gussoni (2013). "G-protein coupled receptor 56 promotes myoblast fusion through serum response factor- and nuclear factor of activated T-cell-mediated signalling but is not essential for muscle development in vivo." FEBS J **280**(23): 6097-6113.

Xu, L., S. Begum, J. D. Hearn and R. O. Hynes (2006). "GPR56, an atypical G protein-coupled receptor, binds tissue transglutaminase, TG2, and inhibits melanoma tumor growth and metastasis." Proc Natl Acad Sci U S A **103**(24): 9023-9028.

Yamada, Y., A. J. Warren, C. Dobson, A. Forster, R. Pannell and T. H. Rabbitts (1998). "The T cell leukemia LIM protein Lmo2 is necessary for adult mouse hematopoiesis." Proc Natl Acad Sci U S A **95**(7): 3890-3895.

Yamaguchi, T. P., D. J. Dumont, R. A. Conlon, M. L. Breitman and J. Rossant (1993). "flk-1, an flt-related receptor tyrosine kinase is an early marker for endothelial cell precursors." Development **118**(2): 489-498.

Yamamoto, R., Y. Morita, J. Ooehara, S. Hamanaka, M. Onodera, K. L. Rudolph, H. Ema and H. Nakauchi (2013). "Clonal analysis unveils self-renewing lineage-restricted progenitors generated directly from hematopoietic stem cells." Cell **154**(5): 1112-1126.

Yang, C. T., R. Ma, R. A. Axton, M. Jackson, A. H. Taylor, A. Fidanza, L. Marenah, J. Frayne, J. C. Mountford and L. M. Forrester (2017). "Activation of KLF1 Enhances the Differentiation and Maturation of Red Blood Cells from Human Pluripotent Stem Cells." Stem Cells **35**(4): 886-897.

Yang, L., D. Bryder, J. Adolfsson, J. Nygren, R. Mansson, M. Sigvardsson and S. E. Jacobsen (2005). "Identification of Lin(-)Sca1(+)kit(+)CD34(+)Flt3- short-term hematopoietic stem cells capable of rapidly reconstituting and rescuing myeloablated transplant recipients." Blood **105**(7): 2717-2723.

Yokomizo, T. and E. Dzierzak (2010). "Three-dimensional cartography of hematopoietic clusters in the vasculature of whole mouse embryos." Development **137**(21): 3651-3661.

Yokomizo, T., K. Hasegawa, H. Ishitobi, M. Osato, M. Ema, Y. Ito, M. Yamamoto and S. Takahashi (2008). "Runx1 is involved in primitive erythropoiesis in the mouse." Blood **111**(8): 4075-4080.

Yokomizo, T., M. Ogawa, M. Osato, T. Kanno, H. Yoshida, T. Fujimoto, S. Fraser, S. Nishikawa, H. Okada, M. Satake, T. Noda, S. Nishikawa and Y. Ito (2001). "Requirement of Runx1/AML1/PEBP2alphaB for the generation of haematopoietic cells from endothelial cells." Genes Cells **6**(1): 13-23.

Yoshimoto, M., P. Porayette, N. L. Glosson, S. J. Conway, N. Carlesso, A. A. Cardoso, M. H. Kaplan and M. C. Yoder (2012). "Autonomous murine T-cell progenitor production in the extra-embryonic yolk sac before HSC emergence." Blood **119**(24): 5706-5714.

Yu, F. X. and K. L. Guan (2013). "The Hippo pathway: regulators and regulations." Genes Dev **27**(4): 355-371.

Yu, F. X., B. Zhao, N. Panupinthu, J. L. Jewell, I. Lian, L. H. Wang, J. Zhao, H. Yuan, K. Tumaneng, H. Li, X. D. Fu, G. B. Mills and K. L. Guan (2012). "Regulation of the Hippo-YAP pathway by G-protein-coupled receptor signaling." Cell **150**(4): 780-791.

Yu, Q. C., C. E. Hirst, M. Costa, E. S. Ng, J. V. Schiesser, K. Gertow, E. G. Stanley and A. G. Elefanty (2012). "APELIN promotes hematopoiesis from human embryonic stem cells." Blood **119**(26): 6243-6254.

Yue, R., H. Li, H. Liu, Y. Li, B. Wei, G. Gao, Y. Jin, T. Liu, L. Wei, J. Du and G. Pei (2012). "Thrombin receptor regulates hematopoiesis and endothelial-to-hematopoietic transition." Dev Cell **22**(5): 1092-1100.

Zape, J. P., C. O. Lizama, K. M. Cautivo and A. C. Zovein (2017). "Cell cycle dynamics and complement expression distinguishes mature haematopoietic subsets arising from hemogenic endothelium." Cell Cycle **16**(19): 1835-1847.

Zhang, P., Q. He, D. Chen, W. Liu, L. Wang, C. Zhang, D. Ma, W. Li, B. Liu and F. Liu (2015). "G protein-coupled receptor 183 facilitates endothelial-to-hematopoietic transition via Notch1 inhibition." Cell Res **25**(10): 1093-1107.

Zhang, X. B., B. C. Beard, G. D. Trobridge, B. L. Wood, G. E. Sale, R. Sud, R. K. Humphries and H. P. Kiem (2008). "High incidence of leukemia in large animals after stem cell gene therapy with a HOXB4-expressing retroviral vector." J Clin Invest **118**(4): 1502-1510.

Zhou, X., M. Vink, B. Klaver, B. Berkhout and A. T. Das (2006). "Optimization of the Tet-On system for regulated gene expression through viral evolution." Gene Ther **13**(19): 1382-1390.

Zhu, B., R. Luo, P. Jin, T. Li, H. C. Oak, S. Giera, K. R. Monk, P. Lak, B. K. Shoichet and X. Piao (2019). "GAIN domain-mediated cleavage is required for activation of G protein-coupled receptor 56 (GPR56) by its natural ligands and a small-molecule agonist." J Biol Chem **294**(50): 19246-19254.

Zovein, A. C., J. J. Hofmann, M. Lynch, W. J. French, K. A. Turlo, Y. Yang, M. S. Becker, L. Zanetta, E. Dejana, J. C. Gasson, M. D. Tallquist and M. L. Iruela-Arispe (2008). "Fate tracing reveals the endothelial origin of hematopoietic stem cells." Cell Stem Cell **3**(6): 625-636.

9 APPENDICES

9.1 Appendix A

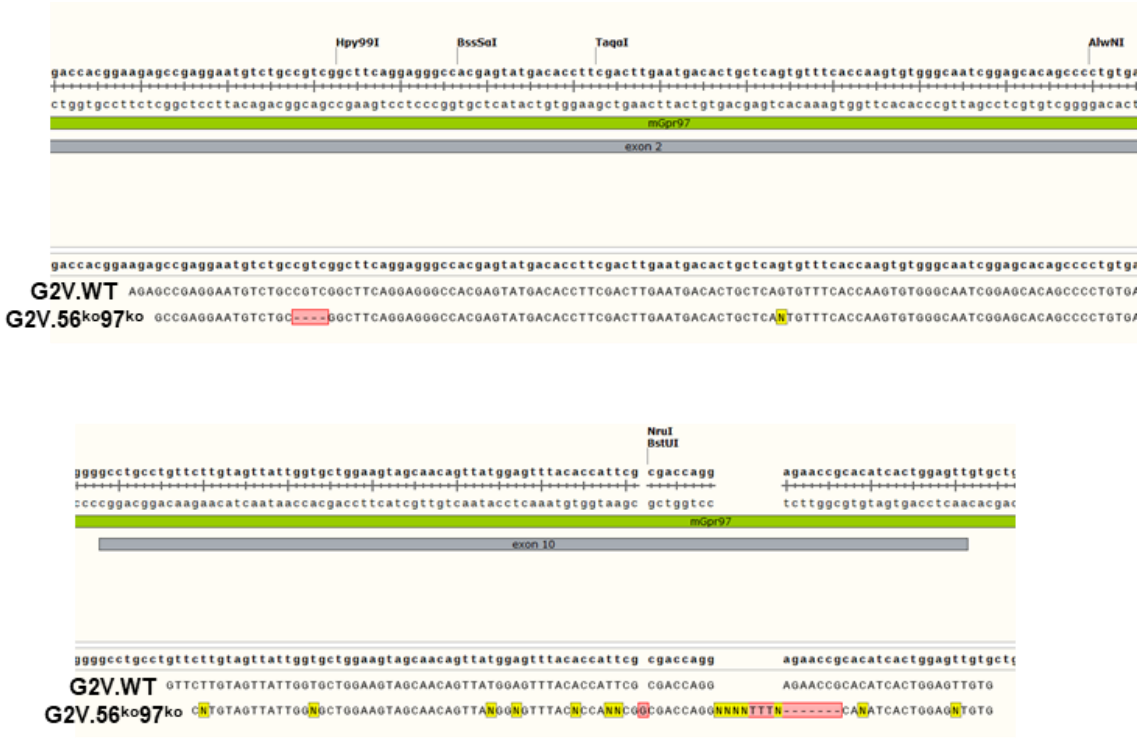

Sequencing of mouse genomic *Gpr97* exon 2 and exon 10. To assess indels caused by CRISPR/Cas9 genome editing. *G2V.WT and G2V.56^{ko}97^{ko}* reads are compared and mapped against the corresponding mouse reference genome. The genomic sequence is taken from Ensembl genome browser.

9.2 Appendix B

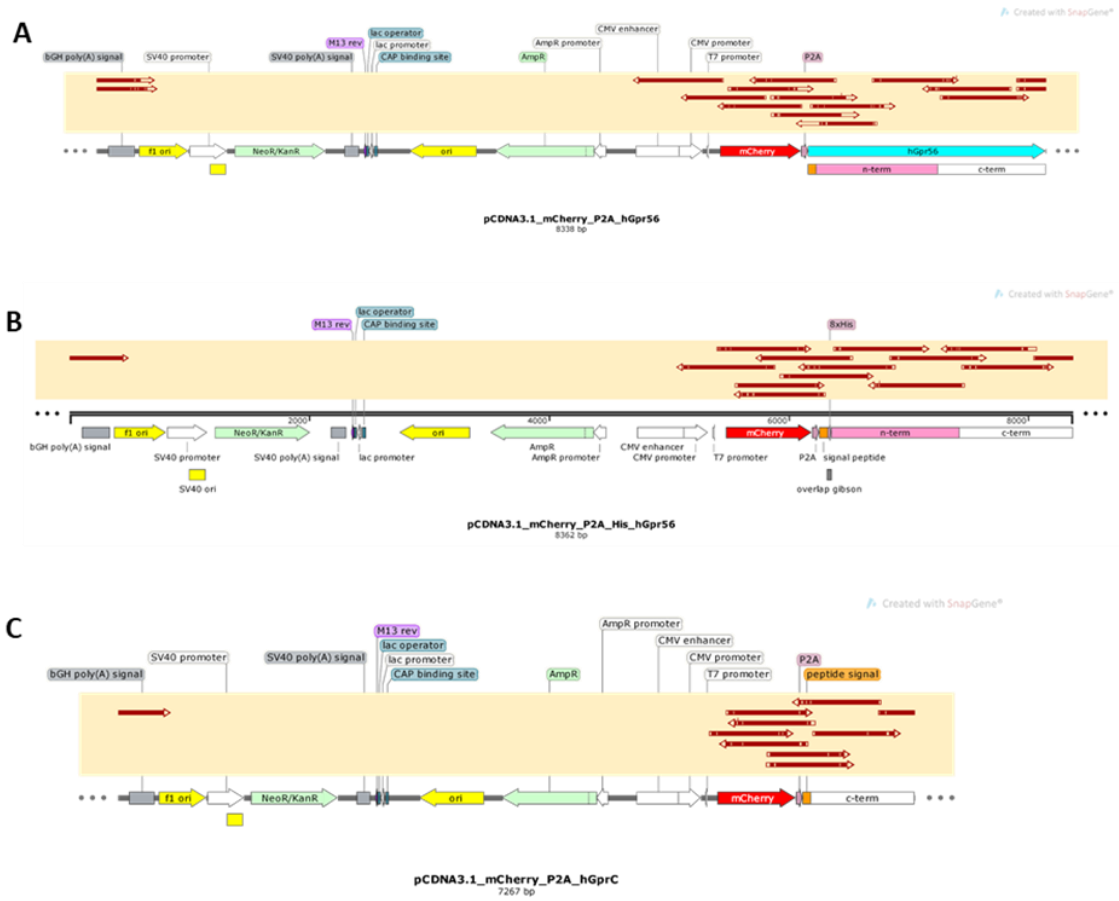

Plasmid maps and sequencing of **(A)** *mCherry_p2a_hGPR56*, **(B)** *mCherry_p2a_his_hGPR56* and **(C)** *mCherry_p2a_hGPRCA* cassettes cloned into *pCDNA3.1* backbones. The bolded arrows confirm the correct sequences. Overlapping reads were required to cover the entire length of the cassettes.

9.3 Appendix C

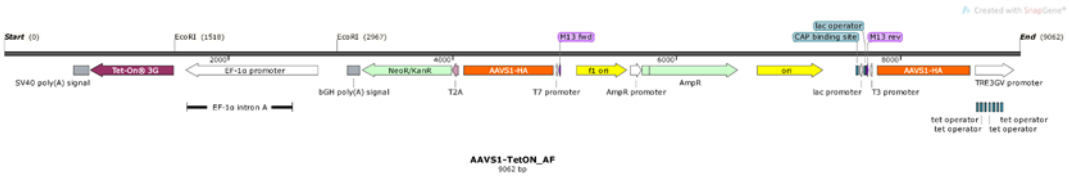

Plasmid map of *AAVS1-TetOn all-in* plasmid provided by Forrester Lab.

9.4 Appendix D

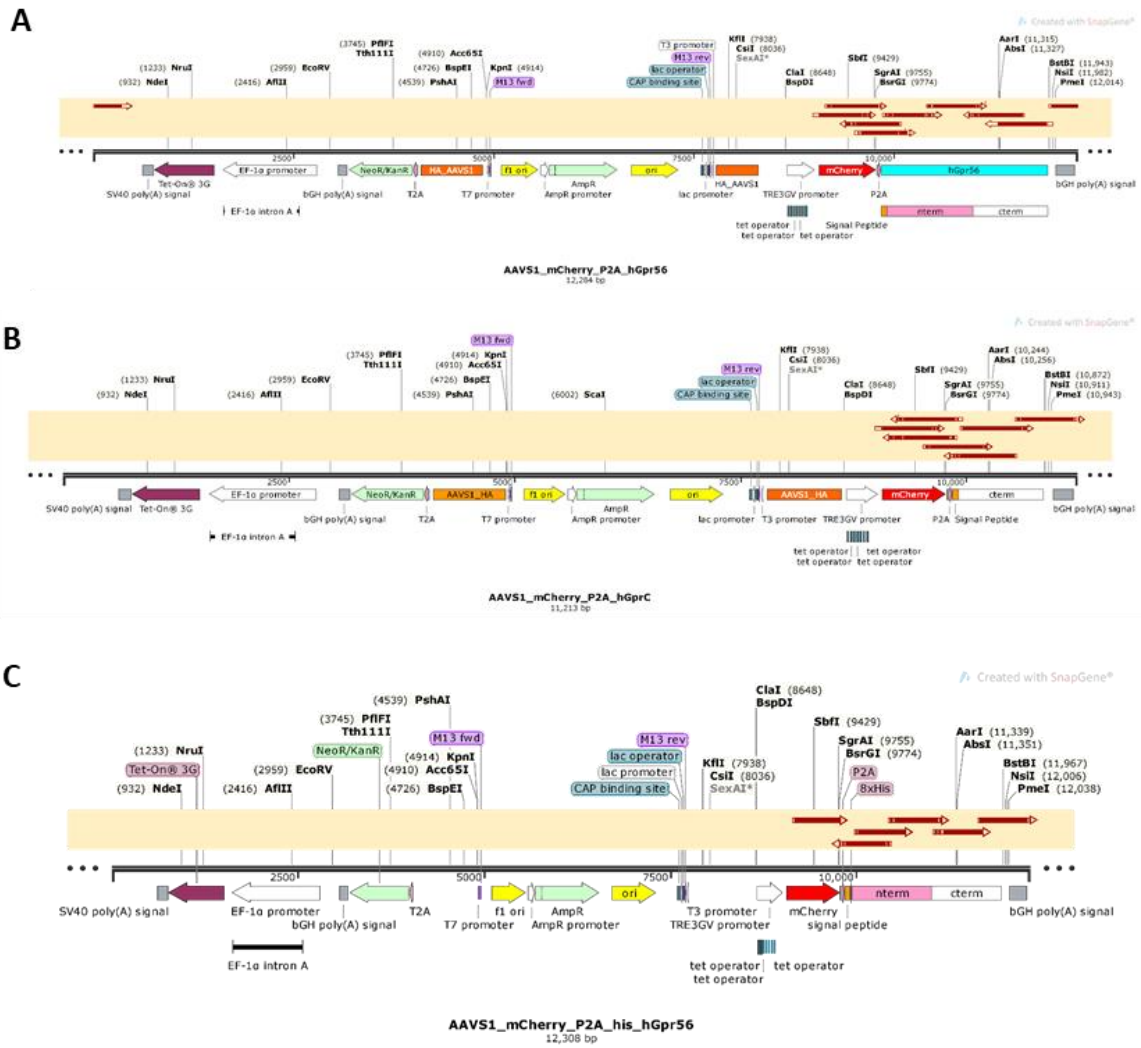

Plasmid maps and sequencing *of* **(A)** *mCherry_p2a_hGPR56,* **(B)** *mCherry_p2a_his_hGPR56* and **(C)** *mCherry_p2a_hGPRCA* cassettes cloned into *AAVS1-TetOn* backbones. The bolded arrows confirm the correct sequences. Overlapping reads were required to cover the entire length of the cassettes.